Dissertation

Gluconeogenesis in tumor-promoting macrophages

submitted by

Katharina Schindlmaier, BSc MSc

for the Academic Degree of

Doctor of Philosophy (PhD)

at the

Medical University of Graz

Division of Pharmacology

Otto Loewi Research Center

Austria

under the supervision of

Katharina Leithner, Ass.-Prof. Priv.-Doz. Dr.med.univ. PhD

2026

Statutory declaration

I hereby confirm that the present thesis is the result of my own independent scholarly work. I also confirm that in all cases, where material from the work of others (in books, articles, essays, dissertations, and on the internet) is acknowledged, quotations and paraphrases are clearly indicated. No material other than that cited in the reference list has been used. I have read and understood the Medical University's regulations and procedures concerning plagiarism. Furthermore, I hereby declare that if artificial intelligence (AI) tools were used for the generation and/or correction of certain text passages in the creation of this work, such employment was conducted in compliance with ethical principles, academic integrity, and the regulations of my university. Additionally, it was ensured that this usage was transparently disclosed and appropriately attributed.

Katharina Schindlmaier Graz, February 2026

Disclosures

Parts of this PhD thesis have been published in:

K. Schindlmaier, *et al.*, Metabolic adaptation of glucose-deprived macrophages involves partial gluconeogenesis. *Proceedings of the National Academy of Sciences of the United States of America* **122**, 44 (2025).

I confirm that all co-authors agreed to use their data published in Schindlmaier *et al.* (2025) (1) in my PhD thesis. All permissions needed have been obtained and all co-authors who contributed to the research in this thesis have agreed to the use of their data.

Parts of this thesis were adapted from my publication in PNAS (1). Figures that were adapted from the above-mentioned publication show the respective citation in the figure legends.

Additional publications during the course of my PhD:

Additionally, I contributed to the following publications:

J. Krstic *et al.*, Fasting improves therapeutic response in hepatocellular carcinoma through p53-dependent metabolic synergism. *Science advances* **8**, eabh2635 (2022).

J. Krstic, K. Schindlmaier, & A. Prokesch, Combination strategies to target metabolic flexibility in cancer. *International review of cell and molecular biology* **373**, 159–197 (2022).

T. Haitzmann*, K. Schindlmaier* *et al.*, Serine synthesis and catabolism in starved lung cancer and primary bronchial epithelial cells. *Cancer Metab* **12**, 9 (2024). *Equal contribution.

B. Konrad *et al.*, A shift in the cellular redox state redirects aspartate for export under glucose deprivation. *Cancer Metab.* Accepted for publication.

Co-authors who contributed to this thesis:

Theresa Haitzmann

Division of Pharmacology, Otto Loewi Research Center, Medical University of Graz, 8010 Graz, Austria.

Division of Pulmonology, Department of Internal Medicine, Medical University of Graz, 8036 Graz, Austria.

Visnja Bubalo

Division of Pulmonology, Department of Internal Medicine, Medical University of Graz, 8036 Graz, Austria.

Barbara Konrad

Division of Pulmonology, Department of Internal Medicine, Medical University of Graz, 8036 Graz, Austria.

Joseph Jelwan

Division of Pharmacology, Otto Loewi Research Center, Medical University of Graz, 8010 Graz, Austria.

Division of Pulmonology, Department of Internal Medicine, Medical University of Graz, 8036 Graz, Austria.

Gabriele Bluemel

Department of Biosciences and Medical Biology, Bioanalytical Research Labs, University of Salzburg, 5020 Salzburg, Austria.

Sonja Rittchen

Division of Immunology, Otto Loewi Research Center, Medical University of Graz, 8010 Graz, Austria.

Vanessa Jäger

Division of Oncology, Department of Internal Medicine, Medical University of Graz, 8036 Graz, Austria.

Michael A. Dengler

Division of Oncology, Department of Internal Medicine, Medical University of Graz, 8036 Graz, Austria.

Luka Brcic

Lung Research Cluster, Medical University of Graz, 8010 Graz, Austria.

Present address: Department of Pathology, Hospital Graz II, 8020 Graz, Austria.

Diagnostic and Research Institute of Pathology, Medical University of Graz, 8010 Graz, Austria.

Jörg Lindenmann

Lung Research Cluster, Medical University of Graz, 8010 Graz, Austria.

Division of Thoracic and Hyperbaric Surgery, Medical University of Graz, 8036 Graz, Austria.

Thomas O. Eichmann

Core Facility Mass Spectrometry, Medical University of Graz, 8010 Graz, Austria.

Martin Trötzmüller

Core Facility Mass Spectrometry, Medical University of Graz, 8010 Graz, Austria.

Leigh M. Marsh

Lung Research Cluster, Medical University of Graz, 8010 Graz, Austria.

Otto Loewi Research Center, Medical University of Graz, 8010 Graz, Austria.

Ludwig Boltzmann Institute for Lung Vascular Research, 8010 Graz, Austria.

BioTechMed-Graz, 8010 Graz, Austria.

Alexander Kirchmair

Biocenter, Institute of Bioinformatics, Medical University of Innsbruck, 6020 Innsbruck, Austria.

Zlatko Trajanoski

Biocenter, Institute of Bioinformatics, Medical University of Innsbruck, 6020 Innsbruck, Austria.

Julia Kargl

Division of Pharmacology, Otto Loewi Research Center, Medical University of Graz, 8010 Graz, Austria.

Cristina Muñoz-Pinedo

Preclinical and Experimental Research in Thoracic Tumors (PReTT), Bellvitge Biomedical Research Institute (IDIBELL), 08908 L'Hospitalet, Spain.

Katharina Leithner

Division of Pharmacology, Otto Loewi Research Center, Medical University of Graz, 8010 Graz, Austria.

Division of Pulmonology, Department of Internal Medicine, Medical University of Graz, 8036 Graz, Austria.

Lung Research Cluster, Medical University of Graz, 8010 Graz, Austria.

BioTechMed-Graz, 8010 Graz, Austria.

Acknowledgements

First and foremost, I would like to express my sincere gratitude to the Medical University of Graz and the PhD Program RESPImmun (Immune Modulation in Respiratory Diseases) for providing the academic framework and support for my PhD studies. I am deeply thankful to the Clinical Division of Pulmonology, where I first began my PhD journey, and to the Division of Pharmacology, Otto Loewi Research Center, where our workgroup later continued its research. Furthermore, I would like to thank all the funding sources that made this PhD project possible: doc.funds project grant (DOC129), a stand-alone project to Katharina Leithner (P 33508) by the Austrian Science Fund, funding to Katharina Schindlmaier by the European Molecular Biology Organization (EMBO, Scientific Exchange Grant 10661) and the Austrian Federal Ministry of Education, Science and Research (BMBWF, Marietta Blau Stipend MMC-2023-07001).

I would also like to thank Melanie Kienzl, Iris Red, and Marah Runtsch, Division of Pharmacology, Medical University of Graz, for supporting the isolation and analysis of macrophages and Stefan Spörk and Harald Köfeler for their support with mass spectrometry.

In addition, I would like to thank my thesis committee, Jelena Krstic, Jörg Lindenmann, and Cristina Muñoz-Pinedo, and my mentor Andreas Prokesch, for their valuable support along the PhD journey.

My heartfelt thanks go to my principal investigator, Katharina Leithner, for her continuous guidance, encouragement, and inspiring mentorship throughout this work. I am also very grateful to my entire workgroup for their collaboration and support, especially Theresa Haitzmann and Joseph Jelwan, for their help, motivation, and most importantly, their friendship along the way.

On a personal note, I would like to thank my parents and my sister for their unconditional love, understanding, and encouragement throughout all these years. As well, I would like to thank my best friend Selina for her continuous support. Finally, my deepest gratitude goes to my partner, Michi, for his endless support, patience, and belief in me.

Table of contents

Abbreviations

A.U.	arbitrary units
ACTB	β-actin
BRAF	B-Raf proto-oncogene, B-rapidly accelerated fibrosarcoma
BSA	bovine serum albumin
dGDP	deoxyguanosine diphosphate
EGFR	epidermal growth factor receptor
FCS	fetal calf serum
G3P	glycerol-3-phosphate
GC-MS	gas chromatography – mass spectrometry
HIF-1α	hypoxia-inducible factor 1 alpha
IFNγ	interferon-γ
IL-4	interleukin 4
KRAS	Kirsten rat sarcoma virus
LC-MS	liquid chromatography – mass spectrometry
LPS	lipopolysaccharide
MeOH	methanol
MDMs	monocyte-derived macrophages
MET	MET proto-oncogene
MTBE	methyl tert-butyl ether
MTBSTFA	N-(tert-butyldimethylsilyl)-N-methyl-trifluoroacetamide
NADH	nicotinamide adenine dinucleotide
NSCLC	non-small cell lung cancer
PBMCs	peripheral blood mononuclear cells
PCK1	phosphoenolpyruvate carboxykinase 1 (cytoplasmic isoform)
PCK2	phosphoenolpyruvate carboxykinase 2 (mitochondrial isoform)
PD-1	programmed cell death protein 1

PD-L1	programmed death-ligand 1
PEP	phosphoenolpyruvate
PEPCK	phosphoenolpyruvate carboxykinase
ROS1	ROS proto-oncogene
RT	room temperature
RT-qPCR	quantitative real-time polymerase chain reaction
sgRNA	single-guide-RNA
TAMs	tumor-associated macrophages
TBDMS	tert-butyldimethylsilyl ethers
TCA cycle	tricarboxylic acid cycle (Krebs cycle)
TLR	toll-like receptor
TME	tumor microenvironment

List of figures

List of tables

Zusammenfassung

Tumorzellen weisen einen veränderten Stoffwechsel auf, bei dem eine verstärkte Glukoseaufnahme Wachstum und Proliferation unterstützt. Dadurch entstehen ausgeprägte Gradienten für Glukose und andere essentielle Metaboliten in der Tumormikroumgebung. Sowohl Tumorzellen, als auch umgebende Immunzellen müssen sich diesen Bedingungen anpassen. Verschiedene Tumorzelltypen nutzen dabei unter Glukosemangel das zentrale Gluconeogenese-Enzym Phosphoenolpyruvat-Carboxykinase (PEPCK, PCK1/2), um über Teilschritte der Gluconeogenese Zwischenprodukte aus Nicht-Kohlenhydrat-Vorläufern bereitzustellen.

Makrophagen gehören zu den häufigsten Immunzellpopulationen in soliden Tumoren, wie dem Lungenkrebs. Sie spielen eine Schlüsselrolle in der Immunabwehr durch Phagozytose, Entzündungsaktivierung und die Mobilisierung der adaptiven Immunität. Makrophagen treten als heterogene Subpopulationen in nahezu allen Geweben auf: langlebige, gewebsspezifische Makrophagen können bei Entzündungen oder Erkrankungen wie Atherosklerose, Arthritis, Fibrose oder Tumoren durch aus Monozyten stammende Makrophagen ergänzt werden. In soliden Tumoren fördern Makrophagen häufig die Angiogenese und unterdrücken Anti-Tumor-Immunantworten. Es wurde gezeigt, dass Makrophagen je nach Aktivierungsstatus ihren Stoffwechsel verändern. So sind pro-inflammatorische (M1-artige) Makrophagen eher von Glykolyse abhängig, während anti-inflammatorische (M2-artige) eher auf oxidative Stoffwechselwege zurückgreifen. Noch unklar ist, wie niedrige Glukosespiegel in der Tumormikroumgebung den Stoffwechsel der Makrophagen verändern und ob Gluconeogenese eine Rolle spielt.

In dieser Dissertation konnte gezeigt werden, dass Makrophagen bei niedrigem Glukosegehalt Teilschritte der Gluconeogenese nutzen. Zudem scheint dieser Stoffwechselweg in M2-artigen Makrophagen stärker ausgeprägt. Weiteres zeigen Makrophagen auch bei niedriger Glukoseverfügbarkeit ein konstantes Zytokin-Profil, jedoch eine reduzierte Expression von CD80, eines Oberflächenproteins auf M1-artigen Makrophagen, welches an der Regulation von T-Zellen beteiligt.

Abstract

Cancer cells exhibit a rewired metabolism and enhanced glucose consumption promotes their growth and proliferation. Thus, step gradients emerge for glucose and other essential metabolites in the tumor microenvironment. Tumor cells as well as non-neoplastic cells need to adapt to these conditions. The key gluconeogenesis enzyme, PEPCK (PCK1/2), was shown to support tumor cell survival under low glucose in some cancers, allowing synthesis of glycolytic intermediates for various pathways, from non-carbohydrate precursors.

Macrophages are one of the main infiltrating immune cell types in solid tumors, as lung cancer. As a type of leucocytes, macrophages are indispensable for first line defense via phagocytosis, activation of inflammation and mobilizing adaptive immunity. Macrophages are heterogeneous immune cells, represented as highly diverse subpopulations in almost all tissues of the body: long-lived macrophages are referred to as tissue-resident macrophages, and in case of inflammation or in various inflammatory states, such as atherosclerosis, rheumatoid arthritis, fibrosis, or cancer they may be replenished from bloodstream-derived monocytes. In the context of solid tumors, tumor-associated macrophages are related to promoting angiogenesis as well as suppressing anti-tumor immune response. It has been shown that macrophages alter their metabolism according to their activation state, whereby pro-inflammatory (M1-like) macrophages display high glycolytic dependency, and anti-inflammatory (M2-like) macrophages rely more on oxidative metabolism. It is still unclear how low glucose levels in the tumor microenvironment affect macrophage metabolism and whether gluconeogenesis is involved.

In this dissertation we could show that partial gluconeogenesis is utilized by macrophages when facing low glucose environments. Further, this pathway seems more pronounced in M2-like macrophages, which has not been described before. Furthermore, macrophages maintain their cytokine profile across variable glucose conditions, however M1-related marker CD80, involved in the regulation of T cells, was reduced in acutely glucose-deprived macrophages.

1. Introduction

1.1. Lung cancer

With about 2.2 million new cases world-wide in 2020, lung cancer is the second most common cancer, only exceeded by breast cancer and by causing about 18% of all cancer-related deaths, it is the deadliest of all cancers (2). Presenting symptoms of lung cancer patients are, among others, cough, chest pain, bone pain, dyspnea, hemoptysis, or weight loss, but may vary between individuals (3). Of all types of lung cancer, non-small cell lung cancer (NSCLC) is the most common type, with about 80% to 85% of all cases (4). While smoking is the greatest risk factor for developing NSCLC, 15% of diagnosed patients never smoked (5). The clinical course is highly heterogeneous and depends on stage, histology and molecular features of the disease. Advances in early detection and molecular diagnostics have improved outcomes for selected patients, but the overall burden of disease and the need for improved systemic therapies remain pressing (6). Despite improved treatment options in recent years, the prognosis for NSCLC patients is still very poor, with a 5-year overall survival rate of less than 5 % for patients with metastatic disease (7). Among NSCLC, the most common histological subtypes are adenocarcinoma and squamous cell carcinoma, besides less common subtypes, as large cell carcinoma, and mixed histological subtypes (8).

Classical treatment options such as surgery, radiotherapy, and chemotherapy remain the foundation of NSCLC management. Surgery continues to be the preferred approach for early-stage disease. For resectable NSCLC, complete surgical excision with systematic nodal staging offers the best chance for long-term survival; however, relapse rates highlight the need for effective perioperative systemic strategies. Recent trials have shown that adding neoadjuvant or perioperative systemic therapy can increase pathological response rates and improve event-free survival when combined with surgery, emphasizing the growing importance of multimodal treatment (9). Still, conventional chemotherapy and radiotherapy remain essential for many patients. Platinum-based combination therapies form the backbone for advanced disease and provide disease control in many cases, though often temporary. Radiotherapy also plays a key role for locally advanced tumors, frequently in combination with chemotherapy, and for palliation. The combination of radiotherapy with systemic immune-modulating agents is an active area of research, as synergistic effects on tumor antigens and the microenvironment are expected (10). While surgery, radiotherapy, and chemotherapy aim to target the tumor itself, they affect healthy tissues as well.

Since cancer is increasingly understood as a systemic disease influenced by the tumor microenvironment, individual variability, and genetic background, more comprehensive treatment approaches have become essential. Over the past decades, targeted therapies have further transformed the treatment landscape for patients whose tumors carry genomic alterations. Comprehensive molecular profiling allows the identification of driver oncogenes such as epidermal growth factor receptor (EGFR), Kirsten sarcoma virus (KRAS), ROS proto-oncogene 1 (ROS1), B-rapidly accelerated fibrosarcoma (BRAF), and MET proto-oncogene (MET), among others (11). Selective inhibitors or antibodies directed against these targets can achieve high response rates and prolong progression-free survival (6). However, the development of resistance and relapse still limits long-term success, making additional treatment options necessary (12).

In recent years, immune checkpoint inhibitors have also changed the therapeutic landscape of NSCLC. Programmed death-1 (PD-1) is an inhibitory receptor expressed on activated immune cells, especially T cells, that prevents excessive immune responses. The main ligand, programmed death-ligand 1 (PD-L1) is often expressed on tumor cells and antigen-presenting cells in the tumor microenvironment. When PD-L1 binds to PD-1, inhibitory signals are triggered in the T cells to limit the ability to attack cancer cells (13-15). Antibodies targeting PD-1 or PD-L1, alone or in combination with chemotherapy, have become standard first-line treatments for many patients with advanced disease. Moreover, their use is now being extended into earlier stages, with neoadjuvant and adjuvant checkpoint inhibition showing meaningful improvements in pathological response and event-free survival. Biomarkers such as PD-L1 expression, tumor mutational burden, and certain genomic features can help guide therapy decisions, but none of them reliably predicts treatment benefit (16).

Ongoing research therefore focuses on refining patient selection and on combining immunotherapy with other modalities, such as targeted therapy, radiotherapy, or metabolic modulation, to improve outcomes (9). Although immunotherapy has become a key component of NSCLC treatment, the search for reliable biomarkers remains a central challenge. Wang *et al.* (2023) reviewed current research on predictive biomarkers such as PD-L1 expression, tumor mutational burden, microsatellite instability, and circulating tumor DNA. They concluded that no single marker is sufficient to predict response, and that combinations of biomarkers may be more effective (17). In the neoadjuvant or adjuvant setting, checkpoint inhibitors can reduce recurrence risk of recurrence and improve survival, particularly in tumors with high PD-L1 expression (reviewed in (18)).

Taken together, lung cancer therapy options were greatly expanded over the past years. Surgery, radiotherapy, chemotherapy, targeted agents and immunotherapies are used according to stage and tumor biology. However, tumor relapse and resistance to treatment are frequent. Current research priorities include optimizing perioperative systemic strategies, overcoming resistance to targeted drugs, expanding effective immunotherapy combinations, and ensuring broader access to molecular diagnostics and novel treatments worldwide (10). Despite these recent developments, a large proportion of patients still lacks proper tumor control, thus novel treatment options are required.

1.2. Cancer cell metabolism and the metabolic microenvironment

Cancer cells have a rewired metabolism and depend on high amounts of metabolites. Metabolic rewiring is considered as a fundamental hallmark of cancer, enabling malignant cells to meet their anabolic needs, maintain redox balance and support biomass production (19). The canonical 'Warburg effect' describes the preference of cancer cells for aerobic glycolysis, even in the presence of sufficient oxygen, yielding lactate and generating glycolytic intermediates for anabolic pathways rather than maximal ATP via oxidative phosphorylation (20). This increased glucose uptake promotes growth and proliferation and ensures fuel of glycolysis-branching pathways (21). However, tumor cells outgrow their high demand for nutrients as glucose, and steep gradients emerge (22). Glucose levels can vary also in physiological conditions, across different tissues, as for examples low glucose levels can be found in the alveolar space of the lung (23). In the interstitial fluid of solid tumors, glucose is often reduced (24-26), one the one hand due to increased glucose consumption of the cancer cells, as well as the aberrant tumor vasculature and poor perfusion (27, 28). Not only cancer cells, but also infiltrating leukocytes consume high amounts of glucose, which can lead to further glucose deprivation (29). For example, analysis of tumor interstitial fluid (TIF) in animal models of pancreatic cancer and melanoma, revealed glucose concentrations of only approximately 0.6 mM (25, 30), compared to normal blood glucose levels of 4 mM to 8 mM (31). This is why solid cancers, as lung cancer, may face a tumor microenvironment (TME) that is low in glucose and cancer cells and neighboring, non-neoplastic cells need to adapt to and tolerate a nutrient-deprived TME (25, 29, 32, 33). As well, the increased glucose uptake of cancer cells leads to lactate secretion and microenvironment acidification and consequently tumor acidosis (27, 34, 35). Additionally, the above-mentioned aberrant vasculature prevents efficient perfusion, leaving behind an environment that is low in pH, and hypoxic, which further promotes glycolytic metabolism (27, 34, 35).

It has to be noted, that not all tumor types show reduced glucose levels, as for examples no decrease of glucose was found in tumor tissue of clear cell renal cell carcinoma (ccRCC) patients, compared to normal kidney tissue of patients (32, 36). This highlights the differences in the metabolic TME between tumor types. To compensate for the variable nutrient availability in the respective TME, cancer cells exhibit profound metabolic plasticity and heterogeneity and are capable of using alternative fuels, such as glutamine, fatty acids, or lactate, to shift between glycolysis, oxidative phosphorylation and other metabolic pathways in response to nutrient scarcity (22). Summarized, Figure 1 depicts cancer cells' metabolic flexibility and capability, of using alternative fuels to support proliferation and immunosuppression. In this respect, the (partly) reverse pathway of glycolysis, gluconeogenesis, can be exploited by cancer cells to perpetuate synthesis of glycolytic intermediates and fuel glycolysis branching pathways (37). In fact, the key gluconeogenesis enzyme, phosphoenolpyruvate carboxykinase, PEPCK (PCK1/PCK2), has been shown to support tumor cell adaptation to low glucose conditions in some cancers, as PEPCK/PCK2 allows the synthesis of glycolytic intermediates from non-carbohydrate precursors.

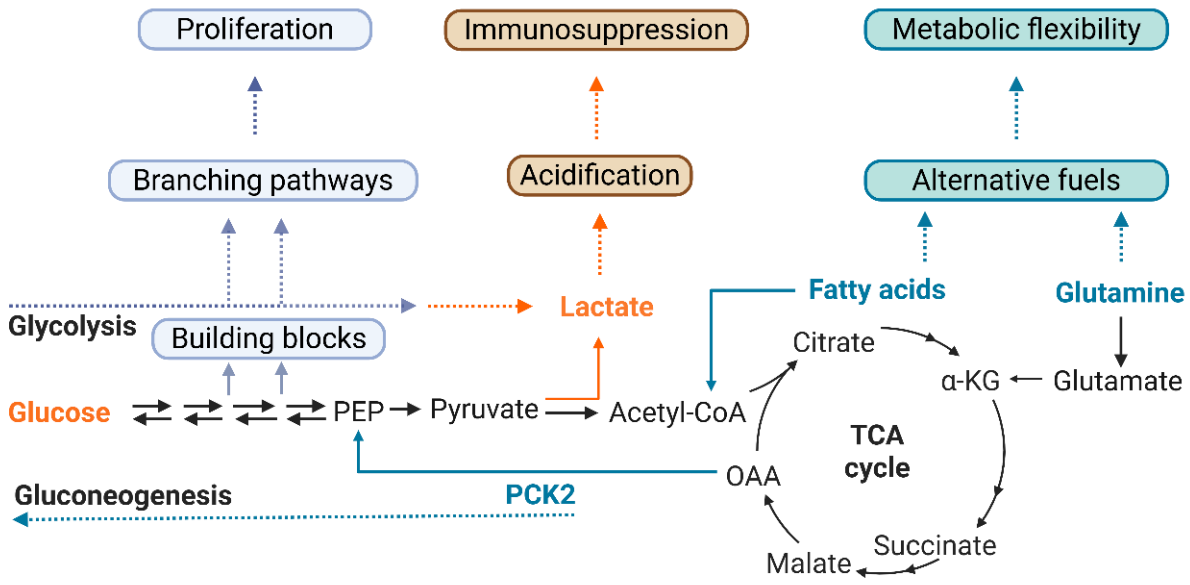

Figure 1: Cancer cell metabolism and adaptation mechanisms to support proliferation, immunosuppression and metabolic flexibility. *(Created with BioRender)*

Metabolites generated via partial gluconeogenesis may be further shunted towards several biosynthesis pathways, including glycerol-phosphate and serine, supporting tumor cell survival (Figure 1) (37, 38). This pathway thus supports metabolic flexibility under glucose deprivation (19).

Other adaptive strategies of cancer cells in response to nutrient deprivation include the activation of autophagy, the scavenging of macromolecules (22), or the activation of salvage pathways, e.g. for ribose (39). Thus, under nutrient-poor conditions, cancer cells are capable of rewiring their metabolism to support proliferation and survival. However, not only cancer cells' metabolism has impact on the metabolic microenvironment of solid tumors. Neighboring non-neoplastic cells, as for examples infiltrating immune cells, not only need to adapt to the described nutrient-scarce conditions, but may impact and shape the TME (32). Furthermore, crosstalk and nutrient competition between tumor cells and stromal or immune cells influences metabolic adaptation of different cell populations residing in the TME (32).

1.3. Tumor immunosurveillance and immunevasion

Cancer cells can be recognized and eliminated by the immune system, however, during tumorigenesis cancer cells evade the immune system by numerous strategies. The core concept here is that newly arising cancer cells are eliminated by the immune system after being identified, before they form a tumor (40-42). However, tumor cells that survive the elimination process persist and eventually avoid being detected by immune cells, thus continue growth and form clinically relevant lesions (40, 42). It has been described that tumor antigens are released upon cancer cell death and taken up by antigen-presenting cells, especially dendritic cells (DCs). DCs travel to the lymph nodes to present the tumor antigens to cluster of differentiation 4 positive ($CD4^+$) helper T cells via major histocompatibility complex class II (MHC-II) receptors, to facilitate the immune response. As well, antigens are presented to $CD8^+$ cytotoxic T cells that in turn proliferate and start to traffic towards the tumor, where the antigens on major histocompatibility complex class I (MHC-I) receptors on the tumor cells are recognized by T cells via T cell receptors to facilitate tumor killing (43, 44). The release of material of dead tumor cells generates even more antigens and amplifies this cycle. However, cancer cells are able to escape this process by reduced antigen presentation, expression of immunosuppressive molecules, as for example PD-L1, as well as recruitment of suppressive cells as for example regulatory T cells (40, 43).

Thus, cancer cells themselves as well as surrounding immune cells shape the tumor microenvironment and tumor progression or elimination is determined by the dynamic interplay between different cells residing in the TME (43, 44). This proposed 'cancer-immunity cycle' also applies to lung cancer, with NSCLC as the most common subtype.

The immune landscape within tumors and the TME is reported to be heterogeneous, first of all between tumor types and subtypes, intra-tumoral concerning spatial distribution, but also within the same disease, between individuals, resulting in a TME challenging to be targeted (45-47).

1.4. Immune cells in non-small cell lung cancer (NSCLC)

In general, ‘hot’ versus ‘cold’ tumors represents a clinically relevant axis in lung and other cancers (48). In NSCLC, inflamed, immune cell- (especially T cell-) infiltrated, ‘hot’ lesions were found to respond more favorably to immune checkpoint blockade compared to ‘cold’ lesions enriched in suppressive myeloid populations (monocytes, macrophages, DCs, and granulocytes) (45, 48). NSCLC, the most common type of lung cancer, contains a broad repertoire of immune cells including $CD8^+$ and $CD4^+$ T cells, regulatory T cells (Tregs), dendritic cells, natural killer (NK) cells, B cells, tumor-associated neutrophils, and abundant tumor-associated macrophages (TAMs), all of which have been assigned to different roles in NSCLC, differentially impacting patient survival, or prognosis, depending on the immune cell type (45). High proportion of $CD8^+$ T cells in the surrounding between cancer nests and the stroma, for example, has been shown to be associated with better survival in a study on stage IV NSCLC patients. High amounts of TAMs however, have been associated with poor prognosis for several types of solid tumors, as for example in breast cancer, bladder cancer, and melanoma (49, 50). Also in NSCLC, high levels of TAMs have been correlated with poor prognosis in a study analyzing 141 tumors (51). However, in contrast to that, high infiltration of TAMs in colorectal cancer has been associated with better prognosis (52). In general, immune cell composition, abundance, and spatial organization differs between tumor types and patients (53, 54). However, not only immune cell type, abundance and localization may modulate the TME, as profound metabolic changes can also affect infiltrating immune cells, potentially shaping their function with impact on disease outcome (25, 55, 56).

1.5. The metabolic TME shapes immune cell metabolism and function

In the past years, the metabolic control of immune cell function came into focus, which may greatly affect anti-tumor immune defense mechanisms. In fact, it has been shown that tumors evade immunity not only through checkpoint upregulation and defective antigen presentation but also, by imposing metabolically hostile conditions - including hypoxia, glucose restriction, and lactate accumulation - that shift the balance toward tolerance (57, 58).

Effector T cells, for example, rely on glycolysis to sustain interferon-gamma (IFN-γ) production; however, within glucose-deprived tumors, reduced mTOR activity and impaired glycolytic flux diminish T cell cytokine output and cytotoxicity, promoting immune dysfunction (55). Tumor-derived lactic acid acidifies the TME and functions as an immunomodulatory metabolite that suppresses lymphocyte infiltration and promotes myeloid cell reprogramming (56, 58). More broadly, nutrient deprivation limits the capacity of T cells and dendritic cells to engage anabolic metabolism, thereby impairing effector differentiation and facilitating immune escape (55, 59).

Similarly, the phenotype of macrophages is closely tied to the metabolic state, and it has been shown that the microenvironment can shift macrophages from a glycolytic, pro-inflammatory program towards oxidative, tissue-repairing, immunosuppressive phenotypes (58-60). Since macrophages are the main focus of this PhD project, the next chapter will outline the roles of macrophages in physiology and disease.

1.6. Macrophages in physiology and disease

Macrophages, as type of leucocytes, are part of the innate immune system and present in almost all tissues of the body. The physiological functions are first line defense via phagocytosis, activation of the adaptive immune response, via antigen presentation to T cells, and the involvement in the initiation of inflammation via cytokine release (61). Macrophages can be distinguished according to their origin, as embryonically or bone-marrow derived, as well as dependent on their localization, as tissue-resident or bloodstream/monocyte-derived macrophages infiltrating various tissues during homeostasis and disease (61). Tissue resident macrophages are long-lived and self-maintaining, with the main function of clearing damaged cells or cell-associated materials of own or foreign origin, to keep tissue homeostasis (61, 62). In case of infection, tissue-resident macrophages may not meet the phagocytic needs and blood-stream derived monocytes need to infiltrate and differentiate in response to predominant disease-related signals (61).

Depending on the course and type of the disease, monocyte-derived macrophages may serve as additional, now tissue-resident macrophages, or die off after disease clearance (61). The above-described mechanism also holds true for the lung, where macrophages show two resident types, namely alveolar and interstitial macrophages, as well as recruited macrophages (63). Alveolar macrophages derived have the primary function to clear the alveoli from pathogens, but they also maintain a non-inflammatory environment in the alveoli and airways, despite constant exposure to inhaled particles and allergens (62, 63).

Interstitial lung macrophages facilitate tissue integrity and shape the immune environment, with inflammatory functions (63). In the case of disease, as for example during inflammation, recruited macrophages from monocytes enter the lung parenchyma, to support resolution of the disease and restoring tissue homeostasis (63).

A very broad classification generally divides macrophages of various tissues into (I) pro-inflammatory, cytotoxic, and anti-tumorigenic M1-like macrophages, activated via interferon-γ (IFNγ), lipopolysaccharide (LPS), or toll-like receptor (TLR) ligands, involved in inflammation; or (II) anti-inflammatory, pro-tumorigenic M-like2 macrophages, activated via interleukin 4 (IL-4), or IL-13, involved in wound healing and tissue repair (64). In this regard, cytotoxic M1-like macrophages are known to be involved in bacterial or viral infection, whereas M2-like macrophages are the main players in tissue repair following infections, as well as parasite infections, or cancer (65). Inflammatory diseases, especially airway diseases, such as fibrosis, asthma, or allergic disorder, are linked to type 2 immune responses, thus M2-like macrophages seem to have the main impact (65). In contrast, M1-like macrophages seem to drive inflammation and insulin resistance in the context of obesity and type 2 diabetes and are reported to be highly involved in autoimmune diseases (65). Still, activation and polarization of macrophages is highly reversible and dependent on time and location. Also, M1- and M2-like macrophages may act opponent or synergistic, depending on the disease setting. It has to be noted, that the categorization into classically and alternatively activated macrophages does not adequately describe the diversity of subtypes, each with distinct physiological functions, according to the origin and niche of the respective population (61, 62, 64).

However, it serves as a reasonable model that mimics the divergent, counteracting phenotypes of pro- and anti-inflammatory functioning macrophages. It is commonly reported that the metabolism of macrophages differs across subpopulations of macrophages (29, 59, 66-68).

1.7. Tumor-associated macrophages

TAMs are activated via IL 4, IL-10, or IL-13, and associated with proliferation, invasion, and metastasis of tumor cells (64). In fact, TAMs are one of the main infiltrating immune cell types in the microenvironment of solid tumors (69-71). They are recruited and reprogrammed by cancer cells to be rendered pro-tumorigenic (M2-like) and suppress anti-tumor immune responses, but promote angiogenesis and tumor cell migration (70-72).

Although initially TAMs were reported to mainly display functions of M2-like macrophages, new data suggest that the complex TME harbors M1- as well as M2-like TAMs (71, 73). In lung cancer specifically, increased infiltration of M2-like TAMs correlates with poor prognosis and therapeutic resistance, while M1-like macrophages are generally associated with better outcomes (74). Beyond the classical M1/M2 dichotomy, single-cell transcriptomic and spatial profiling studies have identified distinct macrophage subpopulations with specialized functions in the tumor microenvironment. Among these, secreted phosphoprotein 1 (SPP1) expression macrophages represent a pro-tumorigenic subset enriched in advanced tumors and metastatic niches; they promote extracellular matrix remodeling, angiogenesis, and tumor cell invasion while contribution to T cell exclusion (75, 76). Macrophage receptor with collagenous structure (MACRO) positive macrophages are associated with an immunosuppressive phenotype, impaired antigen presentation, and resistance to immune checkpoint blockade in lung cancer. In addition, triggering receptor expressed on myeloid cells 2 (TREM2) expressing macrophages define a lipid-associated, metabolically active TAM population that suppresses cytotoxic T cell responses and supports tumor progression by shaping an immunosuppressive microenvironment (77).

These macrophage subsets arise from both tissue-resident and monocyte-derived lineages and exhibit distinct distributions during tumor progression. Collectively, TAM populations display pronounced functional heterogeneity and the factors determining TAM phenotypes are incompletely understood. Potentially, reprogramming of TAMs to a more pro-inflammatory phenotype may enhance anti-tumor immunity and treatment efficacy (78-81).

NSCLC cells have been shown to release M-CSF, that promotes macrophage M2-like polarization (82). Also, tumor cell derived C-C motif ligand 2 (CCL2), known as monocyte chemoattractant protein-1 (MCP-1) favors macrophages' M2-like activation in a model of multiple myeloma (83). A similar mechanism of high secretion of CCL2 was found in NSCLC, and furthermore, blocking MCP-1 has led to reduced tumor growth by reducing M2-like TAMs, shifting the M1/M2 macrophage, in a mouse model (84). Downstream mediators involved in macrophage polarization, seemingly promising for re-shaping macrophages towards an anti-tumor phenotype, are the janus kinase/signal transducers and activators of transcription (JAK/STAT) axis, phosphoinosit-3-kinase/AKT serine/threonine kinase (PI3K/AKT) pathway, as well as nuclear factor kappa B (NF-κB) (85). For example, the PI3Kγ-inhibitor IPI-549 is currently under investigation in clinical trials in combination with chemotherapeutic agents, potentially driving re-polarization from M1-like to M2-like phenotypes in tumor-macrophages (86-88).

Recently, cancer cells have been reported to even more raise the release of several cytokines, as for example IL-8, in response to glucose starvation, resulting in enhanced chemotaxis of macrophages (89). Studies investigating the re-polarization of M2-like to more M1-like, anti-tumor macrophages, are rare and the field is only just emerging. In this respect, inhibition of HDAC6, that is involved in regulating inflammatory responses and activation states in macrophages, lead to an increased M1-like to M2-like macrophage ratio in a recent study (90).

Lactate-driven hypoxia-inducible factor 1 alpha (HIF-1α) activation induces an M2-like, pro-tumoral programs in TAMs, directly linking tumor glycolysis to macrophage polarization (56). Additionally, a recent study has shown that cancer cells' nucleotide metabolism increases extracellular uridine diphosphate (UDP) via cytidine deaminase (CDA), one of the most upregulated metabolic enzymes in tumors resistant to immunotherapy (91). This extracellular UDP lead to an immunosuppressive phenotype of TAMs via the macrophage receptor $P2Y_6$, resulting in reduced T cell infiltration and enhanced resistance to PD-1 immunotherapy, shown by Scolaro *et al*. (91).

Taken together, TAMs occupy a phenotypic spectrum ranging from pro-inflammatory to anti-inflammatory, which is classically shaped by tumor-derived cytokines and other factors, such as lactate (56, 82-91).

1.8. Macrophage Metabolism

Due to the presence of macrophages across different organs throughout the body, they need to adapt to and function in various distinct metabolic microenvironments, requiring high metabolic flexibility to maintain cellular homeostasis, while keeping functionality as phagocytes and mediators of immunity (61, 92, 93). In this respect, immunometabolism has emerged as essential research field that aims to investigate how immune cells manage to sustain energy metabolism for survival and growth, as well as functional integrity, while migrating through and settling in metabolically demanding niches (29). In constant interaction with their environment, plastic macrophages change their activation state, show differential cytokine expression, and even control other, neighboring cells, in response to the surrounding matrix, cells, nutrient availability, growth factors, reactive oxygen species (ROS), or other signaling cues (29). It is known that macrophage activation states are tightly linked to metabolic conditions. As outlined in previous studies, M1-like macrophages have been shown to preferably use glycolysis, whereas M2-like activation is associated with higher oxidative metabolism, fatty acid oxidation, and intact tricarboxylic acid cycle (TCA-cycle, Krebs cycle) activity (Figure 2) (94-99).

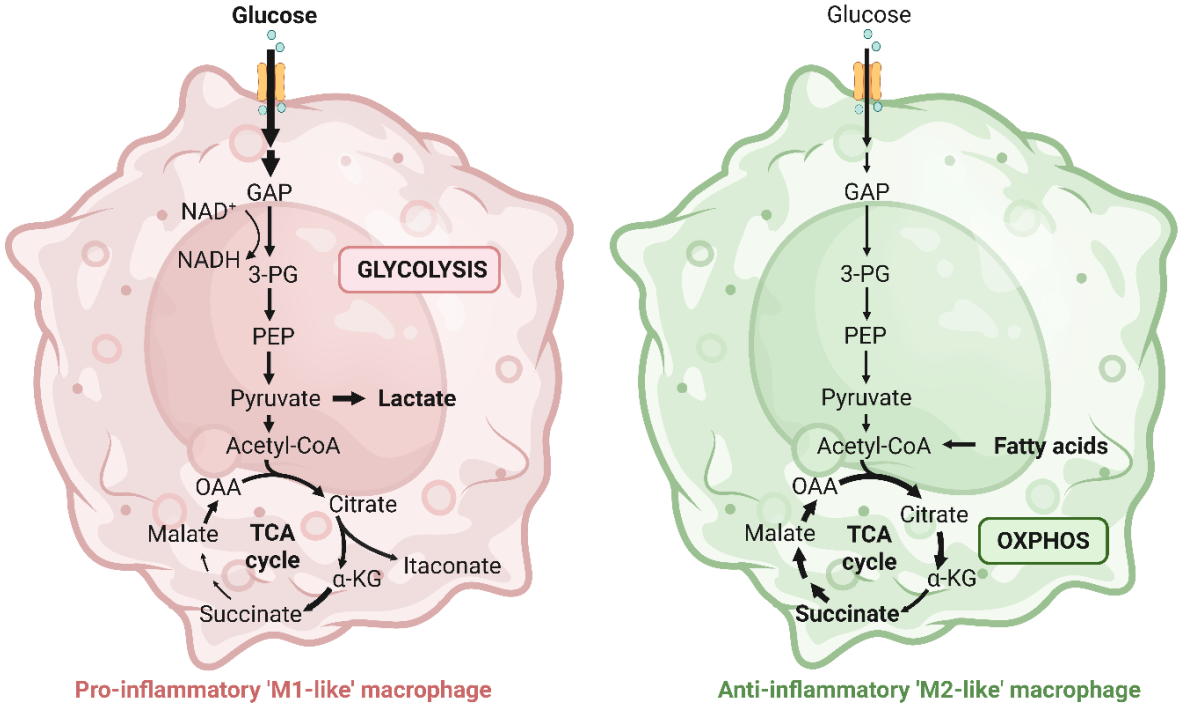

Figure 2: Metabolism of pro-inflammatory ('M1-like') versus anti-inflammatory ('M2-like') macrophages (reviewed in (96-99)). *(Created with BioRender)*

Already around 100 years ago, Otto Warburg observed the well-known 'Warburg effect' of increased utilization of glucose and production of lactate, even in the presence of oxygen, referred to as 'aerobic glycolysis' (20, 100). To date, classically activated M1-like macrophages are referred to as 'Warburg-like', highly glycolytic, with increased glucose uptake via induction of solute carrier family 2 member 1 (SLC2A1, GLUT1), as well as fatty acid synthesis and a truncated TCA cycle (57, 101). Already in 1963, monocytes have been found to preferably use glycolysis upon phagocytosis, in contrast to alveolar macrophages that rather use oxidative phosphorylation (102).

Additionally, glycolysis was found to be associated with pro-inflammatory M1-like macrophages, (103, 104) activated via LPS, and seems to be necessary for the expression of pro-inflammatory IL-1β (96). On the other hand, alternatively activated M2-like macrophages have been reported to rely more on TCA cycle metabolism and oxidative phosphorylation (OXPHOS) for energy providence (57, 101). However, the M1/M2-model describes two extremes of macrophage polarization states with various states in between, and the possibility of macrophages to morph from one into the other phenotype, as well as to incorporate features of more than one subtype at the same time (64, 65).

It is incompletely understood, what deciphers the metabolic state of macrophages and how the adaptation to metabolic microenvironments might influence their phenotype and functions. HIF-1α seems to be a central regulator in this metabolic shift, more specifically, inflammatory stimuli as LPS stabilize HIF-1α even under normoxic conditions, to enable transcription of glycolytic genes and pro-inflammatory effector genes (95). Consistent with these findings, commonly studied glycolytic inhibitor 2-deoxy-glucose (2DG) reduced pro-inflammatory marker CD80 on dendritic cells (94, 95). CD80/CD86 is an important co-stimulatory molecule on antigen-presenting cells, as macrophages and dendritic cells, involved in the stimulation of T cells, thus crucial for tumor cell clearance (94, 95). However, macrophage metabolism is increasingly understood as a spectrum rather than a strict M1–M2 dichotomy. As emphasized in the immunometabolism literature, macrophages may adopt intermediate states and dynamically shift their metabolic configuration depending on nutrient availability and microenvironmental signals, including glucose or glutamine restriction. Thus, glycolysis- and OXPHOS-associated phenotypes should not be viewed as fixed endpoints but as metabolically plastic states adapted to environmental conditions (57, 105-107).

Palmieri *et al.* (2017) demonstrated that glutamine metabolism is a critical determinant of M2-like polarization. Inhibition or genetic deletion of glutamine synthetase (GS) drives M2-like macrophages toward a more M1-like phenotype. Mechanistically, GS-deficient macrophages exhibit reduced intracellular glutamine, succinate accumulation, enhanced glycolytic flux, and stabilization of HIF-1α, thereby reinforcing a pro-inflammatory program. Functionally, supernatants from GS-inhibited macrophages recruited more T cells, as shown in trans-well migration assays, and these macrophages also reduce tumor-cell motility, demonstrated by impaired wound-healing and invasion assays in tumor cells exposed to their conditioned medium (108). Palmieri *et al.* confirmed this *in vivo*, using a 4T1 breast cancer metastasis model. Mice with macrophage-specific GS deletion exhibited reduced lung metastases, increased infiltration of cytotoxic T cells, and features of vascular normalization, indicating that targeting glutamine metabolism can reprogram tumor-associated macrophages toward a more immunostimulatory phenotype (108). These findings suggest that CD80 expression and T cell stimulatory capacity are metabolically regulated, predominantly through glycolysis and HIF-1α–dependent pathways. By shifting macrophages from glutamine-dependent M2-like states toward glucose-driven M1-like states, as demonstrated in the GS inhibition model, it may be possible to enhance anti-tumor immunity by promoting greater co-stimulatory potential at the macrophage-T-cell interface. Downregulation of CD80 could serve as an important checkpoint, as the upregulation could stimulate macrophages towards a more M1-like phenotype that is better capable of tumor killing (94, 95).

In addition, other metabolic cues, such as tumor acidosis and lactic acid accumulation are known to favor M2-like polarization which is why manipulating lactate levels might be able to facilitate a shift towards M1-like activation (85, 109). However, how to potentially render macrophages or other immune cells more pro-inflammatory and anti-tumorigenic in patients remains largely unresolved, and extensive *in vitro* and *in vivo* studies are required to elucidate the underlying mechanisms. As a first step, it is crucial to understand how immune cells adapt to the unstable tumor microenvironment. To date, it is only poorly understood how macrophages adapt to unstable nutrient conditions in the TME, especially glucose deprivation, and how these conditions modulate macrophage metabolism and functions.

1.9. Hypothesis

In our recent study, a high level of PCK2 expression was detected in lung macrophages and lung tumor macrophages (110). As outlined above, PCK2, the initial gluconeogenesis enzyme, was shown to promote metabolic flexibility of tumor cells (37, 38, 111). Thus, we hypothesize that the key enzyme of gluconeogenesis, may support survival and function of TAMs in glucose-limited conditions as well.

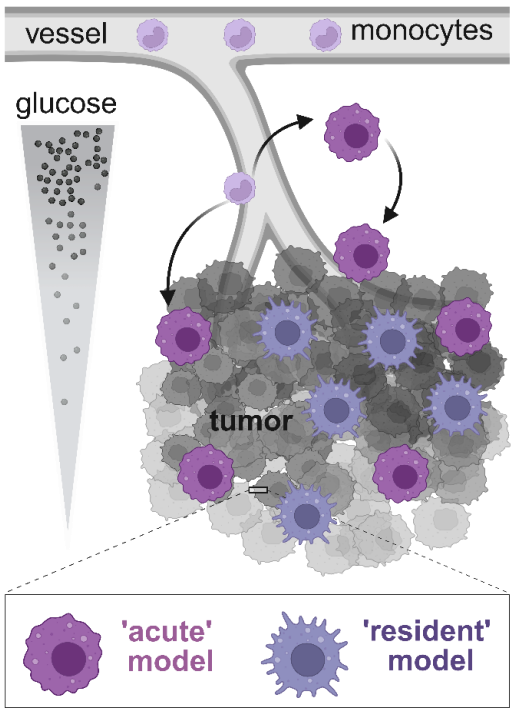

Figure 3: Low glucose conditions in the tumor microenvironment affecting newly infiltrating, monocyte-derived macrophages ('acute' model) and tissue-resident macrophages ('resident' model). *(Created with BioRender)*

Additionally, macrophages' adaptation to the unstable metabolic TME might be time-dependent and differ between macrophage populations; e.g., in newly infiltrating monocytes that are recruited from the blood stream to the tumor site and differentiated into macrophages according to the present signals, or in tissue-resident macrophages already residing in the tumor niche (Figure 3). Thus, we opted for investigating the metabolic as well as functional adaptation of macrophages facing low glucose conditions, as present in the microenvironment of solid tumors.

2. Methods

2.1. Human lung and lung tumor tissue sections of lung cancer patients

Tumor samples from NSCLC patients undergoing surgical resection at the Division of Thoracic and Hyperbaric Surgery, Medical University of Graz. Patients treated with preoperative chemotherapy were excluded. The study protocol was approved by the ethics review board of the Medical University of Graz (EK 17-215 ex 05/06, and EK 34-003 ex 21/22). Signed informed consent was obtained from all patients prior to surgery. NSCLC and non-involved, healthy lung tissue from five patients were used to assess CD68 and PCK2 expression in human tissue on consecutive tissue sections. For detailed experimental protocols for immunohistochemistry (IHC), see method section 2.13.

2.2. Cell culture

Human acute monocytic leukemia THP-1 cell line

The human acute monocytic leukemia cell line, THP-1, was obtained from CLS Cell Lines Service GmbH/Cytion (Eppelheim, DE). Roswell Park Memorial Institute 1640 medium (RPMI 1640, Gibco, Waltham, MA, USA) supplemented with 10% FBS (Bio West, Nuaillé, FR), 100 U/mL penicillin and 100 µg/mL streptomycin (1% P/S, Gibco), and 2 mM L-glutamine (RPMI complete), was used to maintain cells at a cell density of $1x10^6$-$2x10^6$ cells/mL. For differentiation of THP-1 cells to macrophages (THP-1-derived macrophages, THP-1-DMs), cells were treated with 100 nM phorbol-12-myristate-13-acetate (PMA, Sigma-Aldrich, St. Louis, MO, USA) for 48-72h, followed by 24h recovery in RPMI complete. To polarize THP-1-DMs, cell culture media was supplemented with 100 ng/mL lipopolysaccharide (LPS, Sigma-Aldrich) and 20 ng/mL interferon-gamma (IFNγ, Immunotools, Friesoythe, DE) for M1-like, or 20 ng/mL interleukin-4 (IL-4, Immunotools) for M2-like macrophage activation, for 24-72h, or left without supplements for naïve/M0-like macrophages, either along with or prior to high or low glucose treatment.

Human monocyte-derived macrophages from healthy donors

Whole blood of healthy donors was used to isolate peripheral blood mononuclear cells (PBMCs), at the Division of Pharmacology (Medical University of Graz, Graz, AT).

All experiments involving primary cells from human subjects were approved by the Review Board of the Medical University of Graz (EK 17–291 ex 05/06). All volunteers signed an informed consent. After density gradient sedimentation of citrated blood, human monocytes were derived from PBMCs to differentiate into macrophages (monocyte-derived macrophages, MDMs) and characterized as described (112, 113). For differentiation, PBMCs were plated in adhesion medium (RPMI 1640 medium (Gibco) supplemented with 2 mM L-glutamine (Gibco), 1% P/S (Gibco), 1% sodium pyruvate (Sigma-Aldrich), 1% non-essential amino acids (Sigma-Aldrich), 0.5% Hepes (Sigma-Aldrich), and 5% human serum (Sigma-Aldrich) for 1.5 hours. After adhesion, medium was changed to differentiation medium (RPMI 1640 with 2 mM L-glutamine, 1% P/S, 10% fetal bovine serum (FBS, Bio West), and 20 ng/mL macrophage colony stimulating factor (M-CSF, PreproTech, Waltham, MA, USA)), and cells were cultured for 6-8 days. For polarization, MDMs were cultured in normal growth medium (naïve/M0-like) or supplemented with 100 ng/mL lipopolysaccharide (LPS, Sigma-Aldrich) and 20 ng/mL interferon-gamma (IFNγ, Immunotools) for M1-like, or 20 ng/mL interleukin-4 (IL-4, Immunotools) for M2-like macrophage activation. Macrophages were polarized for 24-72h, either simultaneously with or prior to high versus low glucose treatment.

2.3. CRISPR/Cas9 mediated gene editing and PCK2 knockout mice

THP-1 PCK2 CRISPR/Cas9 knock out cells

THP-1 PCK2 CRISPR/Cas9 knock out cells were generated in collaboration with M.A.D., Division of Oncology, Medical University of Graz (Graz, Austria) and according to published protocols (114, 115). Briefly, THP-1 cells were transduced with a pFUCas9mCherry vector for constitutive expression of the Cas9 protein as well as a doxycycline-inducible pFgh1tUTG lentiviral vector carrying sgRNA targeting LacZ (sgLacZ, control cells) or PCK2 (sgPCK2#1 or sgPCK2#2, PCK2 knockout cells). sgRNA sequences are listed in Table 1.

Table 1: CRISPR/Cas9 sgRNA sequences

sgRNA	**Target sequence for sgRNA (5'-3')**
sgPCK2#1	TGCGTATTATGACCCGACTG
sgPCK2#2	GGCACGAGTAGAGAGCAAGA

Transfected THP-1 cells were confirmed by analysis of GFP and mCherry fluorescent proteins. Knockout of PCK2 was induced by adding 1 µg/mL of doxycycline and confirmed by Western blot. Experiments were conducted with polyclonal THP-1 LacZ control cells and two knock out cell lines, THP-1 PCK2 KO#1 and THP-1 PCK2 KO#2, generated with two different guide RNAs, sgPCK2#1 and sgPCK2#2, with a knockout efficiency of more than 80% (Western blot analysis).

PCK2 knockout mice

PCK2 knockout mice were generated by Cyagen (Santa Clara, CA). Experiments that involved PCK2 knockout mice were approved by the Animal Ethics Committee of the Austrian Federal Ministry of Education, Science and Research and carried out in line with the European Community's Council Directive. PCK2 wild type or knockout mice were identified by genotyping PCR after DNA isolation from tail tips, according to standard protocols. Peritoneal macrophages were obtained from sacrificed mice according to previously published protocols (116), before subjection to stable isotopic labeling *ex vivo*. Mice were euthanized via cervical dislocation and macrophages were isolated by injection of isolation buffer (phosphate buffered saline, PBS, containing 0.1 M EDTA) into the peritoneal cavity. Cells were counted using trypan blue (1:1) on a TC20 cell counter (BioRad, Hercules, CA). Intraperitoneal macrophages were cultured in differentiation media (as described above), supplemented with sodium pyruvate (Sigma-Aldrich), non-essential amino acids (Sigma-Aldrich), Hepes (Sigma-Aldrich), 5% human serum (Sigma-Aldrich), and 100 ng/mL murine M-CSF (Preprotech), for one day before flow cytometry analysis or differential glucose treatment and stable isotopic labelling and GC-MS. Identification of isolated cells as macrophages was performed by flow cytometry analysis of macrophage marker CD11b, of adherent cells, resulting in 92.43% ± 1.19% (mean ± SD) cells positive for CD11b.

2.4. Variable glucose treatments

PBMCs were plated onto 12-well plates at a density of 7-9x10^6 cells/well. After adhesion and differentiation, MDMs were washed two times with PBS before treatment. MDMs were treated with RPMI SILAC without glucose, without glutamine (Gibco), supplemented with 1.15 mM arginine and 0.27 mM lysine, 2 mM L-glutamine, 10% dialyzed FBS (Gibco), 0.2 or 10 mM glucose, and antibiotics. Polarization stimuli were added as indicated. THP-1 cells were plated onto 6-well or 12-well plates at a density of 1-2x10^6 cells/well, in normal growth media supplemented with 100 nM PMA for 48-72 hours.

After adhesion, differentiation and polarization, THP-1 derived macrophages were washed two times with PBS before treatment. Cells were treated with RPMI SILAC, supplemented arginine/lysine, 2 mM L-glutamine, 10% dialyzed FBS, 0.2 mM (low) or 10 mM (high) glucose, with or without polarization stimuli, as indicated. Glucose deprivation was applied for 24 or 48 hours with media change after 24 hours. Macrophages received low glucose treatments either along with polarization stimuli (simultaneous treatment), or after a pre-polarization phase (consecutive treatment) of 72 hours, after washing with PBS two times.

2.5. Glucose assay

Cells were subjected to low (0.2 mM) glucose treatments and 50 µL of supernatant media were collected at start of the treatment, after six and after 24 hours. Glucose concentration in the supernatant media was determined with the fluorometric assay of the 'Glucose Assay Kit' (Abcam, Cambridge, UK) according to the manufacturer's protocol. The assay was performed in black 96-well plates with clear optical bottom (Thermo Fisher Scientific, Waltham, MA).

2.6. Stable isotopic tracing

Cells were pre-treated with polarization agents with or without glucose deprivation as described above. Thereafter, 2 mM $^{13}C_5$-glutamine or different concentrations of $^{13}C_6$-glucose (both Cambridge Isotopes, Tewksbury, MA or Sigma-Aldrich), were used as tracers for 24 hours, either with or without a pre-treatment period of 24 hours with the respective unlabeled treatment media. Mouse peritoneal macrophages were differentiated as described above for 24 hours, and thereafter treated with high or low glucose media containing 10% dialyzed FBS for 24 hours, followed by $^{13}C_5$-glutamine tracing in high or low glucose medium for additional 24 hours.

2.7. Gas chromatography – mass spectrometry (GC-MS)

Metabolite extraction from samples was performed according to previously published protocols (117). After treatment and stable isotopic tracing, supernatant media was collected, centrifuged (400 g, 5 min), transferred to new tubes and frozen on liquid nitrogen.

Cells were washed 1x with 0.9% NaCl (Fresenius) and immediately frozen on liquid nitrogen. As extraction buffer, 62.5% methanol (MeOH, UHPLC, for mass spectrometry, Sigma-Aldrich, ice-cold) in H_2O, containing norvaline as internal standard (Sigma-Aldrich), was used.

For metabolite extraction, cells were scraped on ice with extraction buffer, and transferred to micro-centrifuge tubes, and supernatant media was dissolved in extraction buffer. Ice-cold chloroform (for GC-MS, Sigma-Aldrich) was added, samples were vortexed thoroughly, and centrifuged (13,000 rpm, 10 minutes, 4°C) for phase separation. The upper phase comprises polar metabolites, the bottom chloroform phase includes nonpolar metabolites. To measure polar metabolites, the upper phase was evaporated by vacuum centrifugation overnight. Samples were derivatized with 20 µL methoxyamine (MOX) reagent (Thermo Fisher Scientific), vortexed thoroughly for 1-2 minutes and incubated at 37°C for 60 minutes. Then, 30 µL N-(tert-butyldimethylsilyl)-N-methyl-trifluoroacetamide with 1% tert-butyldimethylsilyl ethers (MTBSTFA + 1% TBDMS, Thermo Fisher Scientific) was added as silylation reagent. Samples were vortexed, spinned, and incubated at 60°C for 30 minutes. After spinning, samples were transferred to polypropylene (PP) vials and stored at 4°C until measurement with GC-MS.

For metabolite separation via GC, the Agilent 78901 GC system was used with a DB-35ms column and helium as carrier gas with a flow rate of 1 mL/minute. In split-less mode, 1 µL sample was injected at an inlet temperature of 270°C. Detailed temperature gradients are listed in Table 2. The GC system was coupled with an Agilent 5977A Inert MS system. With an ionization energy of 70 eV, atomic mass units with m/z of 100-650 were measured and isotopologues were corrected for natural abundance with IsoCor (118). Metabolite abundances were normalized to norvaline (internal standard) and the respective protein content.

Table 2: GC-MS temperature gradients

Temperature [°C]	**Gradient**
100	3 minutes hold
300	3.5°C/minute

2.8. Liquid chromatography – mass spectrometry (LC-MS)

Liquid chromatography – mass spectrometry (LC-MS) was performed by our collaborators Thomas Eichmann and Martin Trötzmüller, Core Facility Mass Spectrometry, Medical University of Graz.

^{13}C-Glucose in supernatant media

Media samples (100 µL) were mixed with 400 µL ice-cold methanol under constant shaking (4°C, 10 minutes, 400 rpm). After addition of 300 µL ddH_2O and 900 µL methyl tert-butyl ether (MTBE), samples were further incubated under constant shaking (4°C, 20 minutes, 800 rpm). After centrifugation (13,000 rpm, 10 minutes, 4°C), 800 µL of the upper phase were removed and replaced by 800 µL of an artificial upper phase (MTBE/MeOH/ddH_2O, 9/4/4, v/v/v). After additional incubation and centrifugation, as described above, the complete upper phase was removed and 700 µL of the lower phase were collected and dried using a SpeedVac (Thermo Fisher Scientific).

Metabolites were resolved in 100 µL 70% acetonitrile (1 mM medronic acid) and used for LC-MS analysis. Two empty extractions (sample-free for background control) were injected before and after sample injections. A glucose reference (for level 1 identification) was injected at the start of the sequence. Chromatographic separation was performed on Vanquish systems (Thermo Fisher Scientific) equipped with an ACQUITY UPLC BEH Amide column (2.1 × 150 mm, 1.7 µm; Waters, Milford, MA), using an 18 minutes gradient (400 µL/min) from 97% solvent A (ACN/ddH_2O, 95/5, v/v; 10 mM NH4FA, 10 mM NH3) to 65% solvent B (ddH_2O/ACN, 95/5, v/v; 20 mM NH4FA, 20 mM NH3). The column compartment was kept at 40°C.

For ^{13}C analysis an Orbitrap Eclipse Tribrid mass spectrometer (Thermo Fisher Scientific) equipped with a heated electrospray ionization source (OptaMax NG) was used for detection of the metabolites in negative acquisition mode (MS1: m/z 80-900, resolution 120,000, AGC target 3e5, IT auto). Glucose was identified at level 1 via accurate m/z of the [M-H]- ion (< 5 ppm) and comparison of the retention time (rt) and MS2 spectra (separate MS2 analysis of one sample of each group) to the synthetical reference compound. Isotopic peaks of glucose were manually inspected in Freestyle (1.8 SP2) and peak extraction of regarding isotopes of interest was performed in Skyline (24.1.0.199). Isotopologues were corrected for natural abundance with IsoCor (118).

Lipidomics in THP-1 cells

Lipid extraction was performed according to a modified version of the original extraction protocol (119). Briefly, 5 mL methyl-tert-butyl ether (MTBE) were added to the samples (THP-1 derived macrophages in 2 mL methanol (MeOH) and samples were homogenized for 30 seconds with the Ultra-Turrax tissue homogenizer (IKA Works Inc., Wilmington, N.C., USA). The mixture was incubated in an ice-cooled ultrasound bath for 10 minutes. After addition of 1.3 mL deionized water and 10 minutes of overhead shaking, the mixture was centrifuged for 10 minutes at 1350 g (room temperature (RT).

The upper phase was transferred to a new glass tube. The lower phase was re-extracted (10 minutes overhead shaking) with 2 mL of the upper phase of MTBE/methanol/deionized water (10:3:2.5, v/v/v). The additional upper phase was collected after centrifugation (10 minutes at 1350 g, at RT), combined with the upper phase from the first extraction, evaporated in a vacuum centrifuge (Thermo Fisher Scientific, Waltham, MA, USA) and dissolved in 500 µL chloroform/methanol (1:1, v/v) and stored at −80°C. To 90 µL of the extract, a mixture of internal standards is added for quantification. The solvent was evaporated under a gentle stream of nitrogen and reconstituted in 90 µL injection solvent consisting of isopropanol/chloroform/methanol (90:5:5, v/v/v). The lower aqueous phase was dried using a vacuum centrifuge and the residue was dissolved in 0.3 N NaOH (55°C, 4 hours). Protein content was determined using the Pierce™ BCA reagent (Thermo Fisher Scientific) according to the manufacturer's guidelines. Chromatographic separation was performed as previously described (120).

Briefly, chromatographic separation was performed on a Waters (Waters, Milford, MA, USA) BEH C8 column (100 × 1 mm, 1.7 µm), thermostatted to 50°C in a Dionex Ultimate 3000 RS UHPLC system. Mobile phase A was deionized water containing 1 vol% of 1 M aqueous ammonium formate (final concentration 10 mmol/L) and 0.1 vol% of formic acid as additives. Mobile Phase B was a mixture of acetonitrile/isopropanol 5:2 (v/v) with the same additives. Gradient elution started at 50% mobile phase B, rising to 100% B over 15 minutes; 100% B were held for 10 minutes and the column was re-equilibrated with 50% B for 8 minutes before the next injection. The flow rate was 150 L/minutes, the samples were kept at 8°C and the injection volume was 2 µL. The Orbitrap Velos Pro hybrid mass spectrometer (Thermo Fisher Scientific) was operated in Data Dependent Acquisition (DDA). Every sample was measured in positive polarity mode using a HESI II ion source. Ion source parameters were as follows:

Source Voltage: 4.5 kV; Source Temperature: 275°C; Sheath Gas: 25 arbitrary units; Aux Gas: 9 arbitrary units; Sweep Gas: 0 arbitrary units; Capillary Temperature: 300°C. Automatic gain control target value was set to 106 ions to enter the mass analyzer, with a maximum ion accumulation time of 500 ms. Full scan profile spectra from m/z 320 to 1050 for positive ion mode were acquired in the Orbitrap mass analyzer at a resolution setting of 100,000 at m/z 400. For MS/MS experiments the ten most abundant ions (Top 10) of the full scan spectrum were sequentially fragmented in the ion trap using He as collision gas (CID, Normalized Collision Energy: 50; Isolation Width: 1.5; Activation Q: 0.2; Activation Time: 10) and centroid product spectra at normal scan rate (33 kDa/s) were collected.

LC/MS data were processed using Lipid Data Analyzer (121, 122). Briefly, the algorithm identifies lipids with a 3D algorithm, using the three dimensions m/z, retention time, and intensity to correctly integrate peaks, while also taking into account the isotopic distribution. MS/MS spectra are considered for confirmation of structures by characteristic head group and fatty acyl fragments.

2.9. Quantitative reverse transcription polymerase chain reaction

RNA isolation was done using peqGOLD Total RNA Kit (VWR) according to the manufacturer's instructions. RNA concentration was measured with NanoDrop® (ND-1000, Spectrophotometer, peqLab). 500-1000 ng of isolated RNA was reverse transcribed to cDNA with the qScript cDNA synthesis kit (Quantabio) according to the manufacturer's protocol, in a volume of 20 µL and on the T100TM Thermal Cycler (Bio-Rad).

Table 3: RT-qPCR temperature program

Phase	**Target (°C)**	**Hold**	**°C/s**	**Cycles**	**Mode**
pre-incubation	95	2 min	4.8	1	-
amplification	95 60	5 sec 30 sec	4.8 2.5	45	quantification
melting curve	95 60 95	10 sec 30 sec continuous	4.8 2.5 0.1	1	melting curve
cooling	40	30 sec	2.5	1	-

RT-qPCR was done on the LightCycler 480 (Roche) using QuantiFast SYBR PCR kit (Qiagen) on 384-well plates. cDNA samples were measured in duplicates, along with no-reverse-transcriptase-controls (RT-), and no-template-controls (NTC). The temperature program and primers (Eurofins Genomics) used are listed in Table 3, respectively.

2.10. Western blot

Cells were lysed on ice with RIPA buffer (Sigma-Aldrich) supplemented with protease and phosphatase inhibitors, sonicated (Ultrasonic processor UP50H, Hielscher Ultraonics, Teltow, Germany) three times for 3 seconds, and centrifuged (13,000 rpm, 10 minutes, 4°C). Protein concentration of the supernatant was determined with the BCA Protein Assay Kit (Thermo Fisher Scientific) according to the manufacturer's protocol, measuring absorption at 562 nm. To perform Western blot, 5-10 µg of protein were diluted in RIPA buffer and 1X Laemmli buffer with mercaptoethanol and incubated at 95°C for 10 minutes.

Samples and protein standard (Bio-Rad, Hercules, CA, US) were loaded onto 10% sodium dodecyl sulfate (SDS)-polyacrylamide gels and electrophoresis is run at 180V for 45 minutes. Proteins were transferred to a PVDF membrane (Bio-Rad) at 400 mA for 90 minutes. Membranes were blocked for 1 hour at RT, and incubated with the primary antibody overnight at 4°C. After washing, membranes were incubated with secondary antibodies for 1 hour at RT. Table 4 lists antibodies and blocking conditions. Antibodies were dissolved in Tris-buffered saline (TBS) containing 0.1% Tween 20 (TBST). Chemiluminescence detection was done on ChemiDoc Touch (Bio-Rad). For protein quantification, signal intensities of detected bands were analyzed with the Image Lab Software (Bio-Rad) using the rectangle volume tool and global background subtraction method.

Table 4: Western blot antibodies for immunodetection

Protein	kDa	Blocking	1st antibody	2nd antibody	Detection
PCK2	71	5% BSA	PCK2 (ab187145, Abcam), 1:2000 in 5% BSA-TBST	Anti-rabbit HRP (#7074), 1:3000 in TBST	SuperSignal™ West Pico Chemiluminescent Substrate (Thermo Fisher Scientific)
Beta actin	40	5% milk	Beta-actin (sc-47778, clone C4, Santa Cruz), 1:3000 in 5% milk-TBST	Anti-mouse HRP (#7076), 1:3000 in TBST	

2.11. Fluorescence activated cell sorting analysis

For macrophage-marker analyses, MDMs were cultured, differentiated, polarized and treated as previously described. Cells were harvested with accutase (Sigma-Aldrich) at 37°C for 15-20 minutes, followed by carefully scraping with the plunger of a syringe to remove cells from wells. Cells were stained according to standard protocols of collaborators and our workgroup, or manufacturer's protocols. Reagents and antibodies used for antigen staining are listed in Table 5. To determine dead cells, a viability stain was used along with an unstained control. Unspecific binding was prevented using Fc Block. Isotype controls were included for all fluorophores.

Table 5: FACS reagents

Reagent	**Concentration**	**Company**
Fixation/Permeabilization solution	-	BD Biosciences
Perm/Wash Buffer (10X)	-	BD Biosciences
Zombie Aqua™ Fixable Viability Kit (viability stain)	1:1000	Bio Legend
Intratect® Immunoglobulin G (Fc Block)	1:100	Biotest

After cell harvest and viability stain, cells were subjected to several washing steps and stained with the according antibodies according to established protocols of our group and with the help of collaboration partners. After antigen staining, cells were carefully resuspended in staining buffer consisting of PBS and 2% FBS. The fluorescent signal of cells after antigen staining was measured using CytoFLEX S flow cytometer (Beckman Coulter), with a single-staining strategy using only one fluorophore-conjugated antibody per sample, to avoid spectral overlap and simplify compensation.

To identify the cell population according to size and granularity, cells were gated with forward scatter (FSC) and side scatter (SSC), which reflect cell size and intracellular complexity, respectively, followed by exclusion of duplicate cells and selection of single cells by FSC-height (FSC-H) and -area (FSC-A). This gating strategy ensured that only intact, single cells were included in the analysis. Antibodies and respective isotype controls, including clone information, fluorophore conjugates and suppliers, are listed in Table 6.

Upon analyzing the fluorescent signals, cells positive for CD68 (FITC), CD11b (PE-Cy7), CD80 and CD206 (PE) could be clearly identified as distinct populations based on their respective fluorescence intensity distributions.Isotype control antibodies and viability stain were used to exclude false positive and dead cells, respectively.

Table 6: FACS antibodies

Antigen	Antibody	Concentration	Company	Cat. No.
human CD68	FITC anti-human, CD68	1:25	Bio Legend	333806
human CD80	PE mouse anti-human, CD80	1:10	BD Biosciences	557227
human CD206	PE mouse anti-human, CD206	1:10	BD Biosciences	555954
human CD11b	PE-Cy7 anti-human, CD11b	1:166	Bio Legend	301322
mouse CD11b	PE-Cy7 rat anti-mouse, CD11b	1:10	BD Biosciences	552850
mouse IgG2b	FITC mouse IgG2b, κ Isotype control	1:166	Bio Legend	400310
mouse IgG1	PE mouse IgG1, κ Isotype control	1:10	BD Biosciences	555749
mouse IgG1	PE-Cy7 mouse IgG1, Isotype control	1:166	Bio Legend	406613
rat IgG2b	PE-Cy7 rat IgG2b, κ Isotype control	1:10	BD Biosciences	552849

2.12. PEPCK activity assay

The PEPCK activity assay was performed essentially as described (123). The coupled enzymatic assay measures PEPCK activity in the direction of oxaloacetate (OAA) formation. OAA is further converted to malate, by malate dehydrogenase, which leads to the oxidation of nicotinamide adenine dinucleotide (NADH). THP-1 cells were cultured, differentiated and treated with the respective media for 48 hours, with media change after 24 hours. Cells were washed once with PBS and harvested by scraping.

After centrifugation (400 g, 5 minutes), cells were lysed in ice-cold isolation buffer (10 mM Hepes pH 7.4, 250 mM sucrose, 1 mM EDTA, 1 mM dithiothreitol) and homogenized by sonication with three 5 second pulses followed by centrifugation at 5000 g for 10 minutes.

Protein concentrations in the supernatants were determined using a BCA kit. The reactions were performed in triplicates in 96-well plates (Nunclon Delta Black Microwell SI, Nunc A/S, Roskilde, DK) with a final volume of 200 µL containing 110 mM imidazole-Cl, pH 6.8, 3 mM MnCl2, 13 mM NaF, 10 mM phenylalanine, 1 µM rotenone, 30 mM NaHCO3, 0.15 mM NADH, 6 units/mL malate dehydrogenase, 2 mM phosphoenolpyruvate, and cell homogenate containing 50 µg of protein. Before the experiment the reaction mixture was gassed with 100% CO_2 for 15 minutes. The reaction was initiated with 0.5 mM deoxyguanosine diphosphate (dGDP). The oxidation of NADH by malate dehydrogenase was measured at 355 nm for excitation and 460 nm for emission every 80 seconds for 45 minutes using the CLARIOstar Plus (BMG Labtech, Ortenburg, DE) and MARS Data Analysis Software (BMG Labtech). Control samples lacking HCO_3^-/CO_2 were run simultaneously and this background NADH consumption was subtracted from the consumption in the complete reaction. One unit of PEPCK activity corresponds to the production of 1 µmol product min−1 at 37°C.

2.13. Immunohistochemistry

Human lung tumor and non-involved healthy lung tissue sections of eight NSCLC patients were used to assess the expression of CD68 and PCK2 in consecutive tissue stainings. Table 7 shows NSCLC histology and respective tissues used. Representative samples from patient #1 (NSCLC, squamous cell carcinoma, and healthy lung) and patient #2 (NSCLC, adenocarcinoma, and healthy lung) were used for Figure 16.

After deparaffinization, antigen retrieval, and Fc-receptor block (Intratect/Biotest, Dreieich, DE, human IgG, 100 g/L, 1:100 in PBS), tissue sections were stained with PCK2 rabbit polyclonal antibody (Abcam, ab137580, 1 mg/mL, 1:200 in 0.1% BSA + 0.1% Tween-20 in PBS), or rabbit isotype IgG (Thermo Fisher Scientific, 10500C, 3 mg/mL, 1:600 in 0.1% BSA + 0.1% Tween-20 in PBS), for 90 minutes at RT, or CD68 mouse monoclonal antibody (Santa Cruz, sc-20060, 200 µg/mL, 1:100 in 3% BSA in PBS) or mouse isotype IgG (eBioscience/Invitrogen, 555749, 500 µg/mL, 1:250 in 3% BSA in PBS), for one hour at RT. After protein block with Ultra Vision Protein Block (Epredia, Basel, CH), primary antibody enhancer (Epredia) was applied for 10 minutes and HRP Polymer (Epredia) was added for 15 minutes at RT, before tissue sections were developed with AEC Substrate Kit (Vector lab, Burlingame, CA, USA).

Slides were analyzed in consultation with a lung pathologist (Luka Brcic, Diagnostic and Research Institute for Pathology, Medical University of Graz).

Table 7: Histological subtypes of lung cancer samples from patients used for IHC

Patient	Annotation	Tissues	NSCLC histology
#1	Tumor #1	NSCLC, lung	Squamous cell carcinoma
#2	Tumor #2	NSCLC, lung	Adenocarcinoma
#3	Tumor #3	NSCLC, lung	Adenocarcinoma
#4	Tumor #4	NSCLC, lung	Squamous cell carcinoma
#5	Tumor #5	NSCLC, lung	Adenocarcinoma
#6	Tumor #6	NSCLC, lung	Squamous cell carcinoma
#7	Tumor #7	NSCLC, lung	Squamous cell carcinoma
#8	Tumor #8	NSCLC, lung	Squamous cell carcinoma

2.14. Single-cell RNA sequencing

The extended lung cancer atlas (124), available at CELLxGENE, was used to visualize gene expression levels of selected metabolic enzymes. We used the original annotations to calculate pseudo-bulk gene expression per cell type using the ‘AverageExpression’ function from Seurat v5.1.0 (125), for normal samples (including both healthy normal and tumor-adjacent normal), and tumor samples (including both primary tumors and metastases). The expression values were plotted using the ComplexHeatmap R package v2.18.0 (126). Analyses were performed in R v4.3.2.

2.15. Enzyme-linked immunosorbent assay (ELISA)

THP-1 cells were cultured, differentiated, polarized and treated with low glucose media for 24 hours and media supernatants were centrifuged (450 g, 10 minutes, 4°C) and stored at −80°C until analysis. For cytokine analysis 'DuoSet ELISA Kits' (R&D Systems, Minneapolis, MN, USA) were used for IL-1β, TNFα, IL-10 and TGFβ, according to the manufacturer's protocols, before absorption was measured at 450 nm (cytokine concentration) and 560 nm (background correction). Each experimental condition was performed in duplicate wells.

2.16. Cell count

For cell count, PCK2 wildtype and knockout THP-1-DMs were either polarized towards an M1- or M2-like activation state and subsequently treated with high or low glucose media for 48 hours (media change after 24 hours), as described before. After washing with PBS, cells were detached from cell culture plates with accutase (37°C, 10 minutes) and cell number was determined with the Casy TTC Cell Counter & Analyzer System (Omni Life Science, Bremen, DE).

2.17. Statistics

Data compilation, evaluation and analysis was performed using GraphPad Prism 9 (Boston, MA), or IBM SPSS Statistics 29 (Chicago, IL). Statistical evaluation was performed as applicable with two-sided, unpaired Student's t-test, One-Way ANOVA with Dunnett post-hoc analysis, or Two-Way ANOVA with Tukey post-hoc analysis, as indicated in the respective graphs. Data are represented as mean ± standard error of the mean (SEM). P-values below 0.05 were considered significant.

2.18. Graphs

Graphs showing data were prepared with GraphPad Prism 10 (Boston, MA). Schematic graphs were prepared with PowerPoint (Microsoft 365, Redmond, WA) or BioRender (Toronto, ON).

3. Results

3.1. Macrophage activation and starvation models

Macrophages are versatile immune cells that exhibit vast metabolic flexibility throughout physiology and disease. Still, it is understudied how macrophages might adapt to nutrient-scarce conditions, as for example to low glucose environments. To address our research questions, we analyzed monocyte-derived macrophages (MDMs) obtained from peripheral blood mononuclear cells (PBMCs) of healthy blood donors. Cells were selected from other fractions of PBMCs by adherence to cell culture plates and differentiated using macrophage colony-stimulating factor (M-CSF). Positivity for the macrophage maker CD68 was confirmed using FACS (Figure 4A, left). We also used the human monocytic leukemia THP-1 cell line, derived from the peripheral blood of an acute monocytic leukemia patient, frequently used as a macrophage model, upon differentiation with PMA (127). THP-1 cell to macrophage differentiation was confirmed by analyzing CD68 and CD11b in cells treated with or without PMA (Figure 4A, right). To address the metabolic variations between pro-inflammatory (M1-like) and anti-inflammatory (M2-like) macrophages, we polarized the differentiated MDMs or THP-1 cells with either IFNγ and LPS or IL-4, respectively. For confirming proper macrophage activation, we assessed surface markers CD80 for M1-like, and CD206 for M2-like polarization, in MDMs (Figure 4B), as well as in THP-DMs (Figure 4C). Newly infiltrating, naive monocyte-derived macrophages may face either high or low glucose environments, along with different or no activation stimuli at time of infiltration, depending on the surrounding tissue and microenvironment. Resident macrophages, already activated or not activated, are entering the TME with variable glucose levels after residing in physiological, or high glucose environment, before. Several different scenarios may be applicable for different macrophage activation states, and metabolic microenvironments. Aiming at modeling different physiological conditions, we performed the experiments in macrophages receiving either high (10 mM) or low (0.2 mM) glucose treatment, along with activation stimuli, for 48 hours (‘acute’ model), given that macrophages are known to rapidly increase glycolysis upon LPS stimulation (128). In contrast, variable glucose treatments were applied after a pre-polarization phase of 48 hours (‘resident’ model), as indicated. With this, we intended to mimic newly infiltrated, monocyte-derived macrophages, versus resident macrophages already present in the microenvironment, respectively, where applicable (Figure 4D). MDMs from PBMCs were differentiated and polarized towards (naïve) M0-like, M1-like, or M2-like macrophages, and treated with high (10 mM) or low (0.2 mM) glucose media, as described previously (method section 2.4).

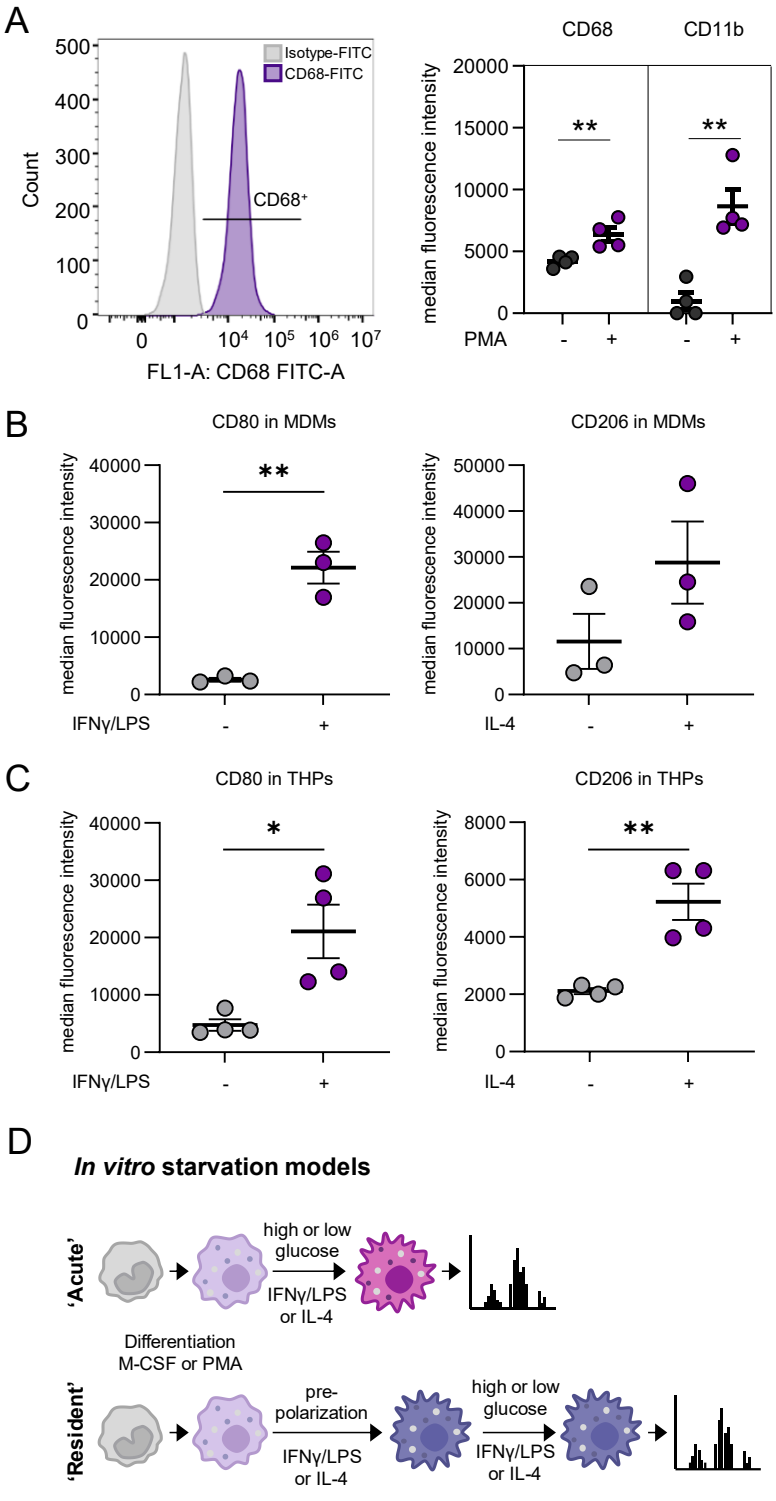

Figure 4: Macrophage differentiation and polarization markers. (A) Representative histogram showing CD68 macrophage marker expression determined by flow cytometry on MDMs compared to isotype control (left) and CD68 and CD11b in PMA-treated vs. non-treated THP-1 cells (right). CD80 and CD206, M1-like and M2-like macrophage markers, respectively, in MDMs (B) and THP-DMs (C). (D) Models of macrophages facing glucose deprivation acutely during (pink) or after (purple) polarization. Adapted from Schindlmaier *et al.* (1).

To clarify, whether macrophages express the initial gluconeogenesis enzyme phosphoenolpyruvate carboxykinase 2 (PCK2), RT-qPCR and Western blot were performed. Levels of mRNA (Figure 5A) and protein (Figure 5B) of PCK2 in differentially activated MDMs, either supplied with high or low glucose, are shown. Interestingly, PCK2 was consistently expressed in MDMs, regardless of macrophage polarization or glucose abundance. Expression of PCK1, the cytosolic isoform, was very low in all conditions tested (Figure 5A).

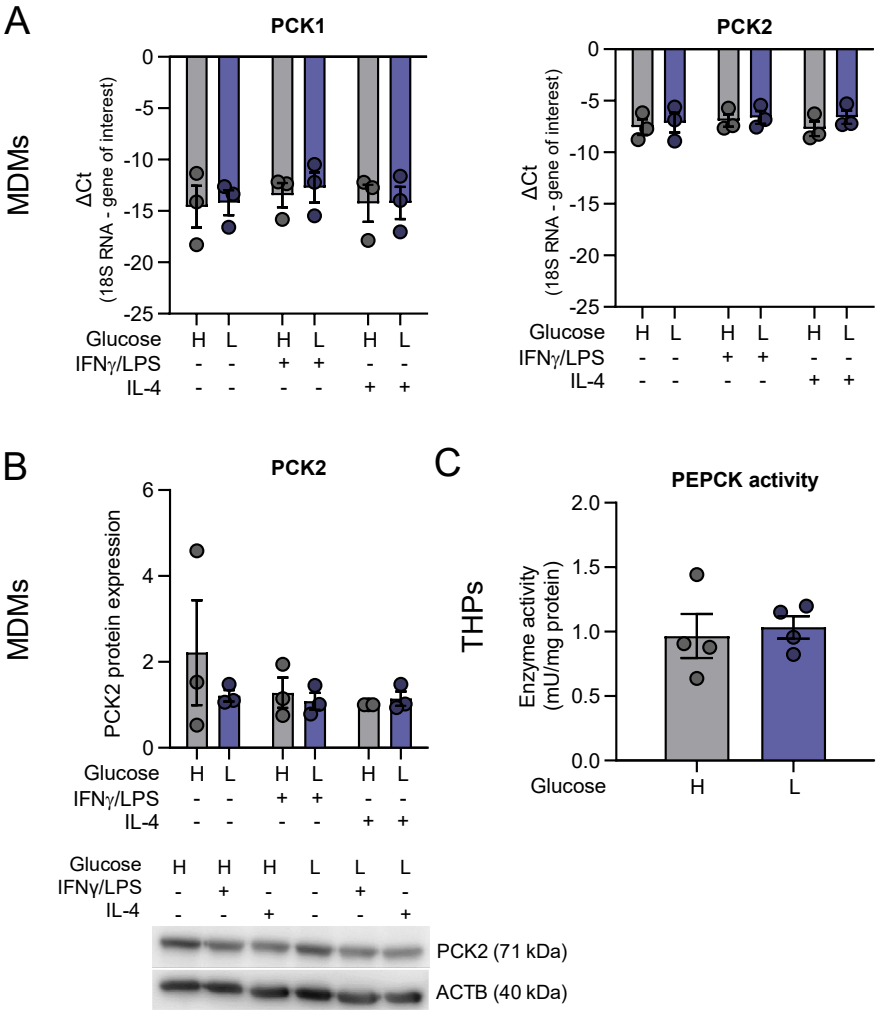

Figure 5: Gluconeogenesis enzyme phosphoenolpyruvate carboxykinase in MDMs and THP-1 derived macrophages. (A) mRNA levels of PCK1 and PCK2 in M0-, M1-, and M2-like pre-polarized MDMs ('resident' model) after treatment with high (H) or low (L) glucose for 48 hours. (B) PCK2 expression in a representative Western blot and β-actin (ACTB) as a loading control in MDMs. Quantification of relative intensities is shown in the bar graph. (C) Activity of PEPCK in PMA-differentiated THP-1 cells after high or low glucose treatment for 48 hours. The data are presented as mean +/- SEM from n=3 different experiments (qPCR and Western blot) or n=4 different experiments (PEPCK activity). Unpaired Student's t-tests were used for group comparisons, which revealed no significant differences. Adapted from Schindlmaier *et al.* (1)

Besides protein and mRNA expression in MDMs, THP-1 cells were utilized to evaluate actual PEPCK activity in macrophages, through a coupled enzymatic assay. Notably, PEPCK activity remained unaffected by glucose levels (Figure 5C). Together these data show that PCK2 is consistently expressed and active in macrophages of different activation states, in high and low glucose conditions.

3.2. Lactate production is reduced in monocyte-derived macrophages under low glucose conditions

In order to assess metabolic adaptations in low glucose treated macrophages, we performed stable isotopic tracing and analyzed polar metabolites by gas chromatography – mass spectrometry (GC-MS). We used $^{13}C_6$-glucose at high (10 mM) or low (0.2 mM) concentrations to monitor glycolysis and the contribution of glucose to central carbon metabolism in acutely glucose-deprived macrophages. As anticipated, under low glucose conditions, glucose was quickly removed from the medium by approximately 95% but it was still detectable after 24 hours (Figure 6A). In order to avoid prolonged glucose deprivation, we replaced high or low glucose media every 24 hours. In the case of stable isotopic tracer experiments, cells were treated with 10 versus 0.2 mM of glucose for 24 hours. Thereafter the medium was changed and the unlabeled glucose was replaced by $^{13}C_6$-glucose at the respective concentration. Polarization stimuli were added simultaneously to high versus low glucose treatment (‘acute’ model). In all MDM subpopulations, unstimulated (naïve, M0-like), IFNγ/LPS stimulated (M1-like), or IL-4 stimulated (M2-like), we observed a significant reduction in lactate release to the medium supernatant under low glucose conditions (Figure 6B). The labeling patterns seen in cells treated with uniformly ^{13}C-labeled glucose are shown in Figure 6C. In comparison to MDMs receiving activation stimuli in high glucose media, MDMs treated with glucose deprivation exhibited significantly lower levels of pyruvate and lactate (Figure 6D) as well as less incorporation of glucose-derived carbons into glycolytic intermediates (Figure 6E and Figure 7B). Similarly, low glucose conditions reduced the time-dependent rise in fractional enrichment of glycolytic intermediates from $^{13}C_6$-glucose (Figure 6F). All of these findings point to a probable reduction in glycolysis in MDMs when glucose levels are low. Basal glycolytic activities in high glucose conditions lightly differed between the different polarization stimuli, with M1-like macrophages showing the highest total levels of pyruvate and by trend also lactate (Figure 6D), in line with previously published studies (96, 97). Under low glucose conditions, glucose contribution to the TCA cycle intermediates α-ketoglutarate (α-KG), succinate, and malate was reduced.

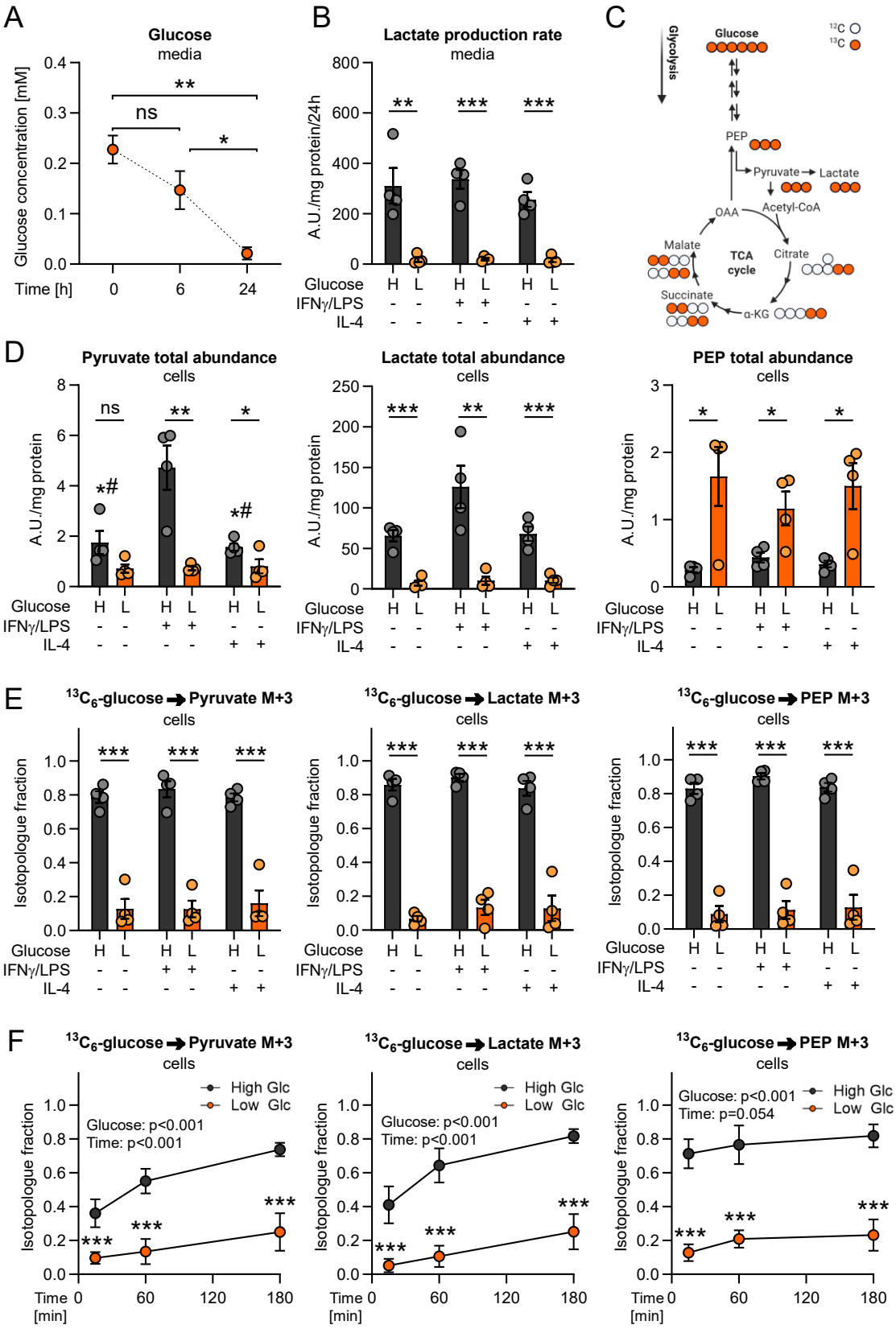

Figure 6: Glucose deprivation modulates glycolysis in monocyte-derived macrophages (MDMs) ('acute' model).

Figure 6 (continued): (A) Glucose concentration in the supernatant of MDMs receiving low glucose treatment. MDMs were treated with medium containing 10% dialyzed FCS supplemented with high (H, 10 mM) or low (L, 0.2 mM) levels of $^{13}C_6$-glucose and at the same time, supplemented with IFNγ/LPS, IL-4 or without stimuli for 24 hours ('acute' model). (B) Lactate production rate measured in the supernatant media. (C) Labeling patterns of intermediates of glycolysis and the TCA cycle in MDMs receiving $^{13}C_6$-labeled glucose. PEP, phosphoenolpyruvate; OAA, oxaloacetate; α-KG, α-ketogultarate. (D) Total abundance of glycolytic intermediates and (E) relative enrichment of fully labeled isotopologues, of pyruvate, lactate, and PEP. (F) Time course of labeling fractions in MDMs acutely treated with $^{13}C_6$-glucose, without polarization stimuli, for 15, 60, or 180 minutes. Data are shown as mean +/- SEM from n=4 independent experiments. Group comparisons were performed using unpaired Student's t-tests. (F) Results from Two-way ANOVA assessing the impact of time and glucose are indicated in the graphs and post-hoc analysis for individual time points was performed using Sidak's test. *p<0.05, **p<0.01, ***p<0.001, n.s., not significant. # vs. IFNγ/LPS-treated cells. Adapted from Schindlmaier et al. (1).

This is demonstrated by the reduced proportions of intermediates formed from (labeled) acetyl-CoA that carry two ^{13}C atoms, designated M+2 (Figure 7A). Malate M+3 labeling and citrate M+3/M+5 labeling suggests that glucose entered the TCA cycle, in part, by malic enzyme or pyruvate carboxylation in high glucose conditions (Figure 7B). Malate M+3 and citrate M+3 fractions were decreased by low glucose treatment (Figure 7B). While malate and succinate remained unaltered, total levels of citrate and α-KG, adjusted to total protein, decreased under low glucose (Figure 7A). These data show that under low glucose conditions, glycolysis and the contribution of glucose to the TCA cycle are reduced in macrophages, irrespective of their polarization status.

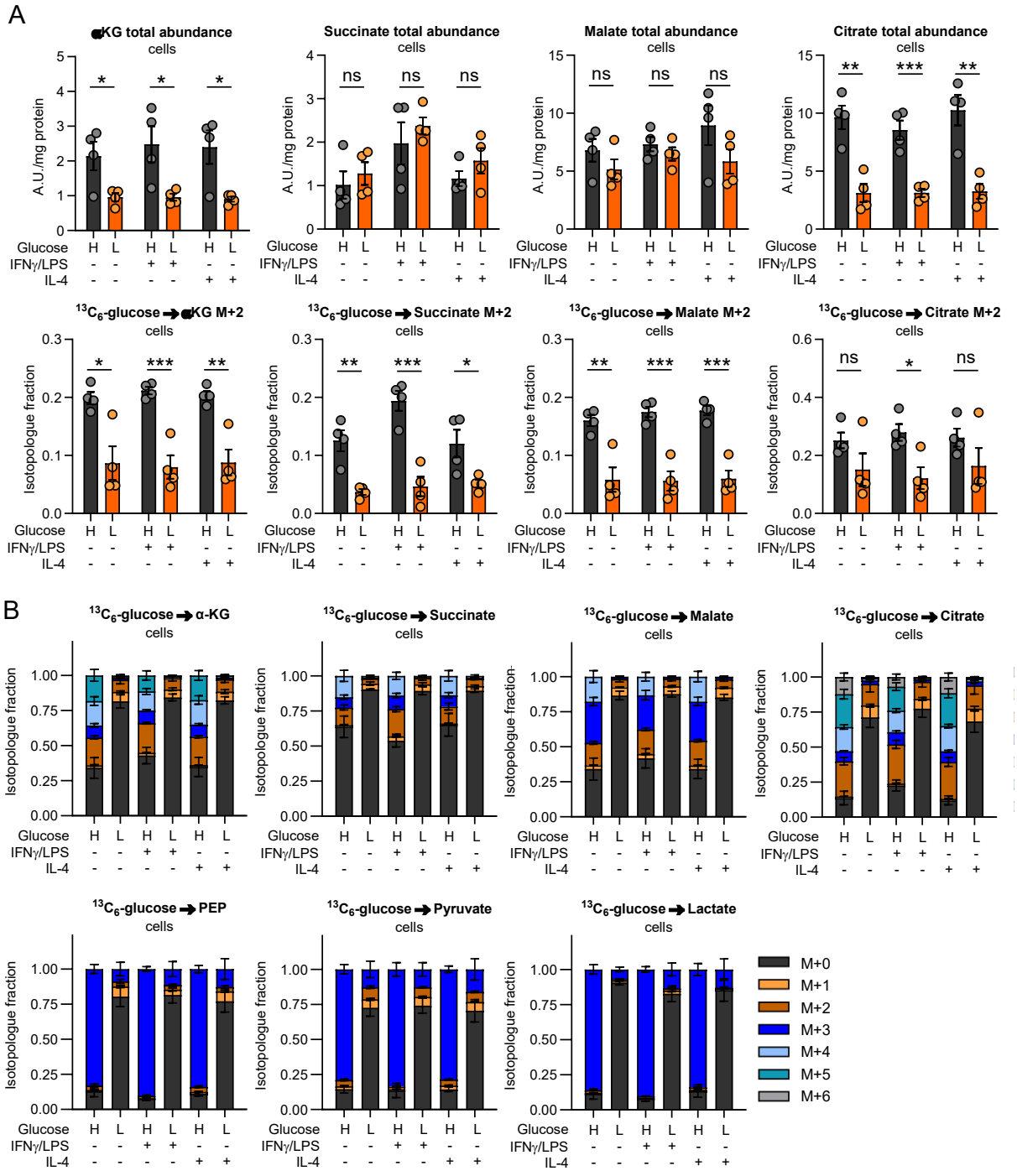

Figure 7: Glucose contribution to the TCA cycle and total abundance of various TCA cycle intermediates are reduced in glucose-deprived MDMs. MDMs were treated high (H, 10 mM) or low (L, 0.2 mM) levels of $^{13}C_6$-glucose along with with IFNγ/LPS or IL-4 or without stimuli at the same time, for 24 hours ('acute' model). (A) Total abundance (top) and M+2 labeled fractions (bottom) of TCA cycle intermediates are shown as mean ± SEM from n=4 independent experiments using MDMs from four different donors. (B) Isotopologue fractions (staggered) of glycolytic and TCA cycle intermediates. Group comparisons were performed using unpaired Student's t-tests. *p<0.05, **p<0.01, ***p<0.001; ns, not significant. Adapted from Schindlmaier *et al.* (1).

3.3. Glucose deprivation activates partial gluconeogenesis in macrophages, along with enhanced glutamine contribution to the TCA cycle

We next differentiated macrophages as described previously and applied $^{13}C_5$-glutamine as an alternative metabolic tracer under either high or low glucose conditions, in parallel with polarization using IFNγ/LPS or IL-4. Glutamine can contribute to the TCA cycle upon conversion to glutamate and α-KG (scheme in Figure 8C). We found that macrophages exposed to glucose limitation exhibited an increased incorporation of glutamine-derived carbon into the TCA cycle. In particular, significantly higher fractions of fully labeled glutamate (M+5), malate (M+4), and succinate (M+4) were detected (Figure 8A). Furthermore, complete labeling of citrate (M+6), resulting from the condensation of fully labeled OAA and acetyl-CoA, was markedly enhanced under low glucose conditions (Figure 8A). However, the total pool sizes of α-KG, malate, and citrate were reduced in glucose-restricted macrophages (Figure 9A). Citrate (M+5) and malate (M+3) labeling were both elevated under low glucose availability (Figure 8A, lower panels; Figure 9C). This suggests that reductive carboxylation, the conversion of α-KG to citrate in a reductive manner, contributes to the incorporation of glutamine-derived carbon into the TCA cycle during glucose deprivation. Taken together these results show that the contribution of glutamine to the TCA cycle is increased under low glucose conditions in both, M1- and M2-like macrophages.

Glucose-limited cancer cells have previously been shown to activate early steps of gluconeogenesis, the reverse pathway of glycolysis, as an adaptive metabolic strategy (33, 37). This pathway enables the regeneration of glycolytic intermediates from the TCA cycle intermediate oxaloacetate, thereby fueling biosynthetic routes branching from glycolysis, even in the absence of glucose. Notably, neutrophils, which share the myeloid lineage with macrophages, can utilize gluconeogenesis to generate glycogen (129). To determine whether macrophages employ (partial) gluconeogenic reactions to adapt to glucose restriction, we assessed the conversion of $^{13}C_5$-glutamine into the glycolytic intermediate phosphoenolpyruvate (PEP). Within the TCA cycle, fully labeled malate generates fully labeled OAA, which is subsequently decarboxylated by the gluconeogenic enzyme PEPCK (PCK2) if it is active in the direction of gluconeogenesis, yielding fully labeled PEP (Figure 8C). Indeed, under low glucose conditions, up to 30% of PEP (M+3) was derived from glutamine (Figure 8B), whereas under high glucose conditions, only about 3% of PEP (M+3) contained ^{13}C from glutamine.

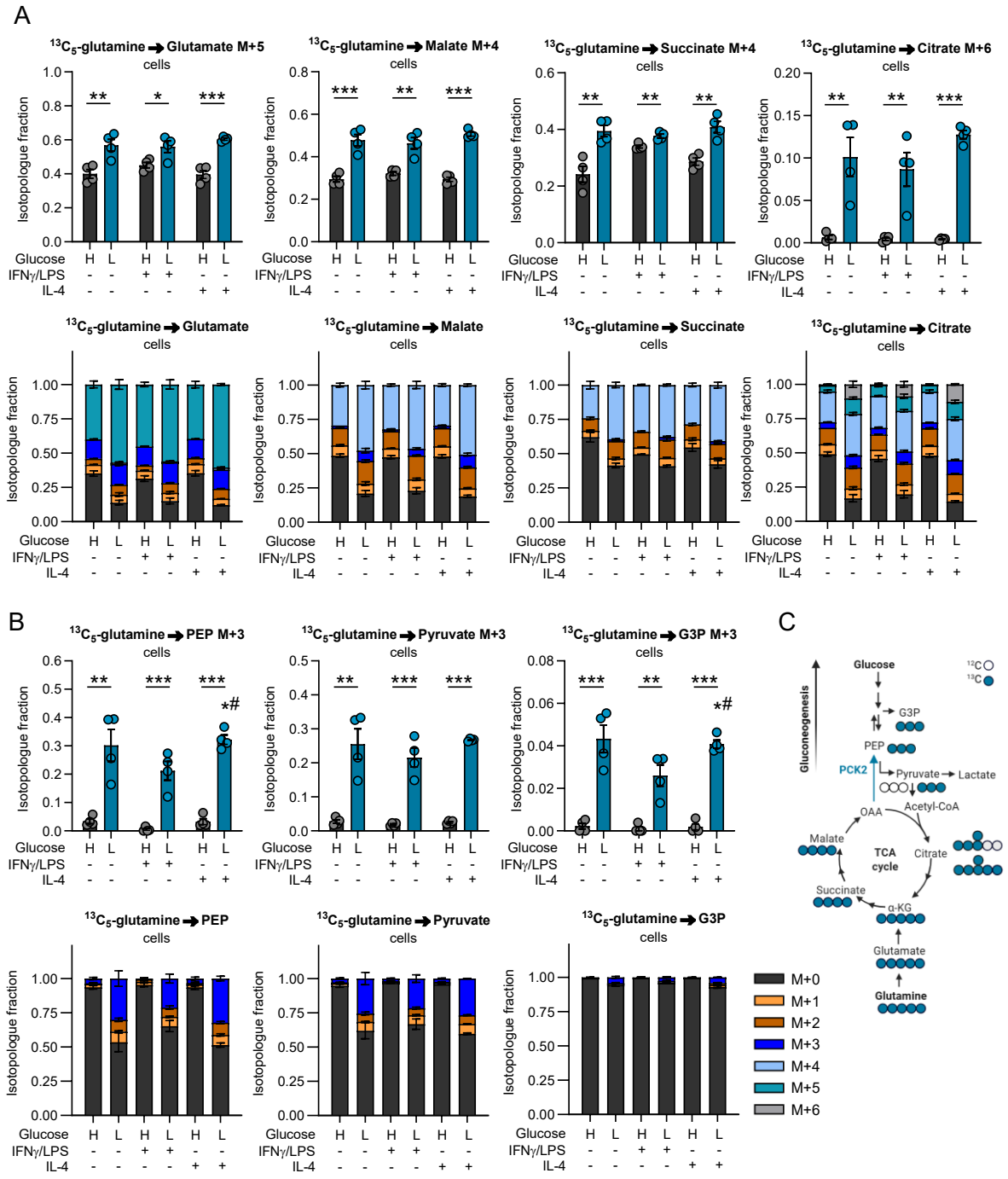

Figure 8: Partial gluconeogenesis in glucose-deprived MDMs ('acute' model). (A, B) MDMs were treated with $^{13}C_5$-glutamine in high (H, 10 mM) or low (L, 0.2 mM) glucose media supplemented with 10% dialyzed FCS and at the same time with IFNγ/LPS or IL-4 or without stimuli for 24 hours ('acute' model). (A) Fractions of fully labeled TCA cycle intermediate or (B) glycolytic/gluconeogenic intermediates and glycerol-3-phosphate (G3P) isotopologues. (A, B) Data are shown as mean +/- SEM from n=4 independent experiments using MDMs from two different donors. Group comparisons were performed using unpaired Student's t-tests. *p<0.05, **p<0.01, ***p<0.001, # vs. IFNγ/LPS-treated cells. (C) Labeling patterns of tricarboxylic acid (TCA) cycle and gluconeogenic/glycolytic intermediates in MDMs receiving $^{13}C_5$-glutamine. Adapted from Schindlmaier *et al.* (1).

PEP was further metabolized to glycerol-3-phosphate (G3P) via partial gluconeogenesis, although the labeled fractions of G3P were lower than the fractions of PEP labeled from glutamine (Figure 8B). Compared to M2-like macrophages, M1-like macrophages show less labeled PEP and G3P from $^{13}C_5$-glutamine (Figure 8B), in our 'acute' model. From PEP to G3P in the direction of gluconeogenesis, PEP is first converted to 2-phosphoglycerate by enolase, then rearranged to 3-phosphoglycerate via phosphoglycerate mutase. Phosphoglycerate kinase phosphorylates 3-phosphoglycerate to 1,3-biphosphoglycerate using ATP, and glyceraldehyde-3-phosphate dehydrogenase reduces it to glyceraldehyde-3-phosphate with NADH. Glyceraldehyde-3-phosphate is rapidly isomerized to dihydroxyacetone phosphate (DHAP) by triose phosphate isomerase, after which glycerol-3-phosphate dehydrogenase reduces DHAP to glycerol-3-phosphate, consuming NADH. This final step links carbohydrate metabolism to lipid synthesis by providing the glycerol backbone for triglycerides and phospholipids (130).

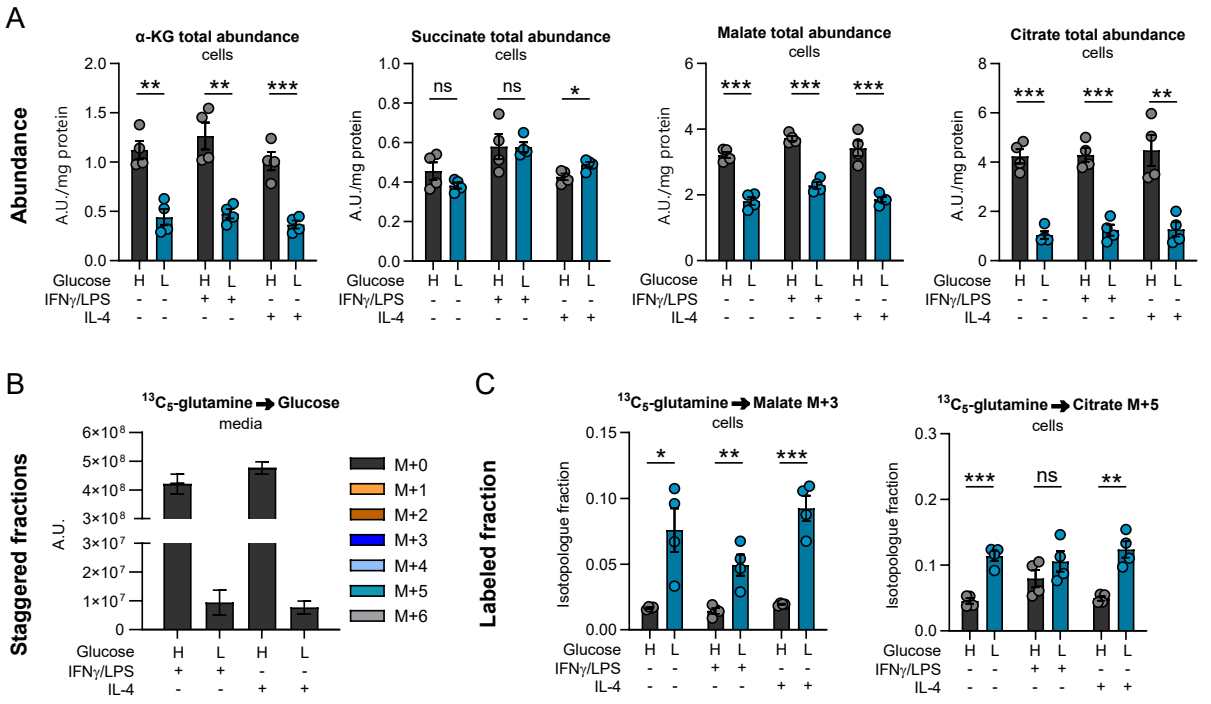

Figure 9: TCA cycle metabolites and supernatant glucose in $^{13}C_5$-glutamine treated cells. MDMs were treated with $^{13}C_5$-glutamine as a tracer in medium containing high (H, 10 mM) or low (L, 0.2 mM) levels of glucose simultaneously with IFNγ/LPS or IL-4 or without stimuli for 24 hours ('acute' model). (A), Total metabolite abundances within cells and (C), citrate M+5 and malate M+3 isotopologe fractions. (B) Relative glucose isotopologue abundance in media supernatants measured by LC-MS. Only unlabeled glucose is found after correction for natural abundance. (A-C) Data are shown as mean ± SEM from n=4 independent experiments using MDMs from two different donors. Group comparisons were performed using unpaired Student's t-tests. *p<0.05, **p<0.01, ***p<0.001; ns, not significant. Adapted from Schindlmaier *et al.* (1).

However, no ^{13}C-labeled glucose was detected in the culture supernatants of glucose-deprived macrophages with LC-MS (collaboration with Thomas Eichmann, Core Facility Mass Spectrometry, Medical University of Graz) (Figure 9B), indicating that gluconeogenesis did not proceed to the formation of glucose.

Upper glycolytic intermediates were not checked in this experimental setup. Thus, the partial gluconeogenesis pathways can be confirmed only up until the level of G3P. A similar pattern, characterized by an increased contribution of glutamine to the TCA cycle and enhanced partial gluconeogenesis, was also observed in the 'resident' macrophage–microenvironment model (Figure 10 and Figure 11A). Here, polarization was started 48 hours prior to low or high glucose treatment and labeling and polarization stimuli were added throughout the experiments ('resident' model).

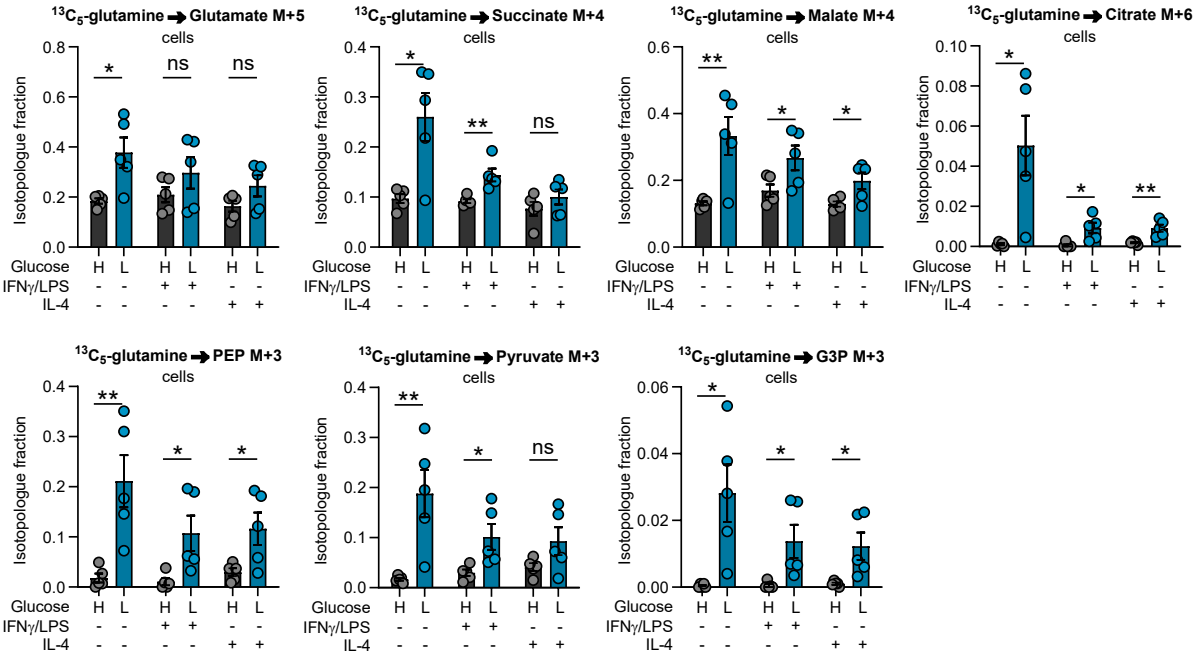

Figure 10: Glucose deprivation induces partial gluconeogenesis in pre-polarized MDMs ('resident' model). Non-activated, IFNγ/LPS or IL-4 activated MDMs were treated with medium containing 10 mM (H) or 0.2 mM (L) glucose, 10% dialyzed FBS, and 2 mM of glutamine for 24 hours. Thereafter glutamine was replaced with $^{13}C_5$-labeled glutamine for additional 24 hours (total glucose deprivation phase of 48 hours). Relative enrichment of fully labeled isotopologues of TCA cycle intermediates, glycolytic/gluconeogenic intermediate PEP, pyruvate and glycerol-3-phosphate (G3P). Data are shown as mean ± SEM from n=5 independent experiments using MDMs from four different donors. Group comparisons were performed using unpaired Student's t-tests. *p<0.05, **p<0.01, ***p<0.001, n.s. not significant; # v.s. IFNγ/LPS-treated cells. Adapted from Schindlmaier *et al.* (1).

Interestingly, although total levels of the glycolytic intermediates pyruvate and lactate were decreased under low glucose conditions, they remained comparable among unpolarized, M1-like, and M2-like macrophages (Figure 11B) in the 'resident' model. Also, in the 'resident' model, no differences in PEP labeling (or partial gluconeogenesis) were found between the different polarization states (Figure 10).

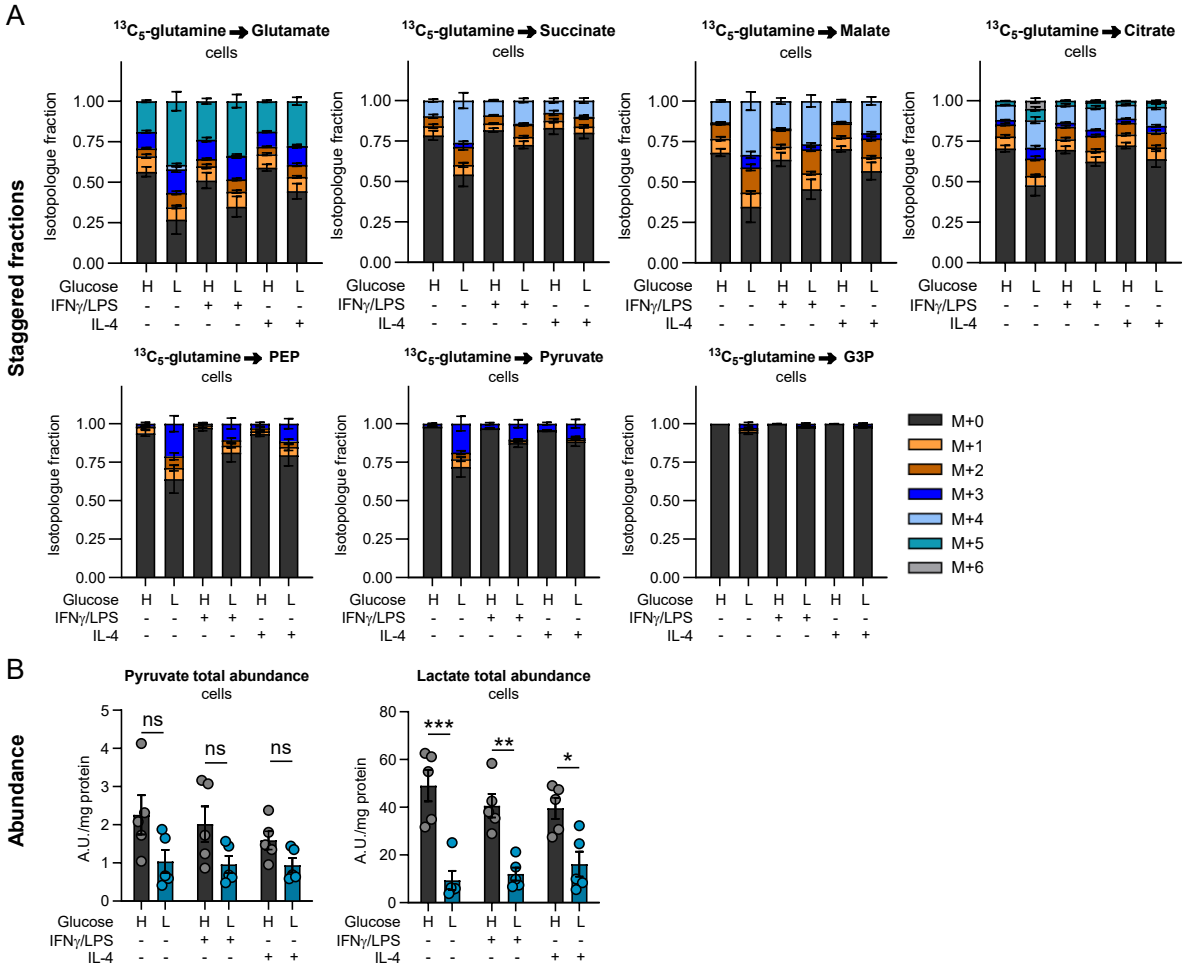

Figure 11: Isotopologue fractions of TCA cycle metabolites and total abundance of pyruvate and lactate in glucose-deprived MDMs ('resident' model). (A-B) Non-activated or IFNγ/LPS or IL-4 activated MDMs were treated with medium containing 10 mM (H) or 0.2 mM (L) glucose, 10% dialyzed FBS, and 2 mM of glutamine for 24 hours. Thereafter glutamine was replaced with $^{13}C_5$-labeled glutamine for additional 24 hours (total glucose deprivation phase of 48 hours). (A) Isotopologue fractions (staggered) of glycolytic and TCA cycle intermediates. (B) Total abundance of lactate and pyruvate. Data are shown as mean ± SEM from n=5 independent experiments using MDMs from four different donors. Group comparisons were performed using unpaired Student's t-tests. *p<0.05, **p<0.01, ***p<0.001, n.s. not significant; # v.s. IFNγ/LPS -treated cells. Adapted from Schindlmaier *et al.* (1).

Together, these findings demonstrate that partial gluconeogenesis is consistently activated in macrophages under glucose-limited conditions, which has not been previously assessed in detail in macrophages, to the best of our knowledge. PEP generated from glutamine is further converted downstream the gluconeogenesis pathway to glycerol-3-phosphate. M+3 labeling of pyruvate was detected upon ^{13}C-glutamine tracing, which may be consistent with a metabolic route involving PCK2-dependent PEP formation from glutamine-derived carbon (Figure 10).

3.4. PCK2 mediates partial gluconeogenesis in human and mouse macrophages

As mentioned above, macrophages robustly expressed PCK2, while PCK1 expression was very low. Cytoplasmic PCK1 would also generate PEP M+3 from $^{13}C_5$-glutamine, thus the labeling patterns are indistinguishable. In the case of PCK1, OAA is generated from TCA-derived malate or aspartate after their transport to the cytosol, since the inner mitochondrial membrane is impermeable to OAA (131). To clarify, whether the activation of early gluconeogenic steps mediated by PCK2, we used CRISPR/Cas9 to knockout (KO) PCK2 in THP-1 cells, and additionally, we derived peritoneal macrophages from PCK2 full body knockout mice (Figure 12A). We generated THP-1 PCK2 knockout cells using a CRISPR/Cas9 approach with two independent guide RNAs (sgPCK2#1 and sgPCK2#2). The inducible knockout was performed together with Theresa Haitzmann in collaboration with Michael Dengler and Vanessa Jäger, Division of Oncology, Department of Internal Medicine, Medical University of Graz. The knockout in polyclonal cells after the induction of gene editing by doxycycline was confirmed using Western blot (Figure 12B). These cells were analyzed under high and low glucose conditions using $^{13}C_5$-glutamine as a tracer. Differentiation into macrophages following PMA treatment was confirmed by cell attachment and expression of the macrophage markers CD68 and CD11b (Figure 4A, right). Western blot analysis revealed an approximate 80% reduction in PCK2 protein in the polyclonal populations by the two different PCK2 gRNA constructs (sgPCK2#1, sgPCK2#2) after doxycycline-induced gene editing (Figure 12B). To address the role of PCK2 in partial gluconeogenesis, we performed $^{13}C_5$-glutamine tracing in our ‘resident’ macrophage model. M1- and M2-like macrophages derived from THP-1 cells transduced with either the non-targeting control (sgLacZ) or PCK2-specific gRNAs (sgPCK2#1, sgPCK2#2) metabolized $^{13}C_5$-glutamine through the TCA cycle under both glucose conditions. Similar to primary macrophages, the proportion of fully ^{13}C-labeled malate (M+4) increased under low glucose conditions.

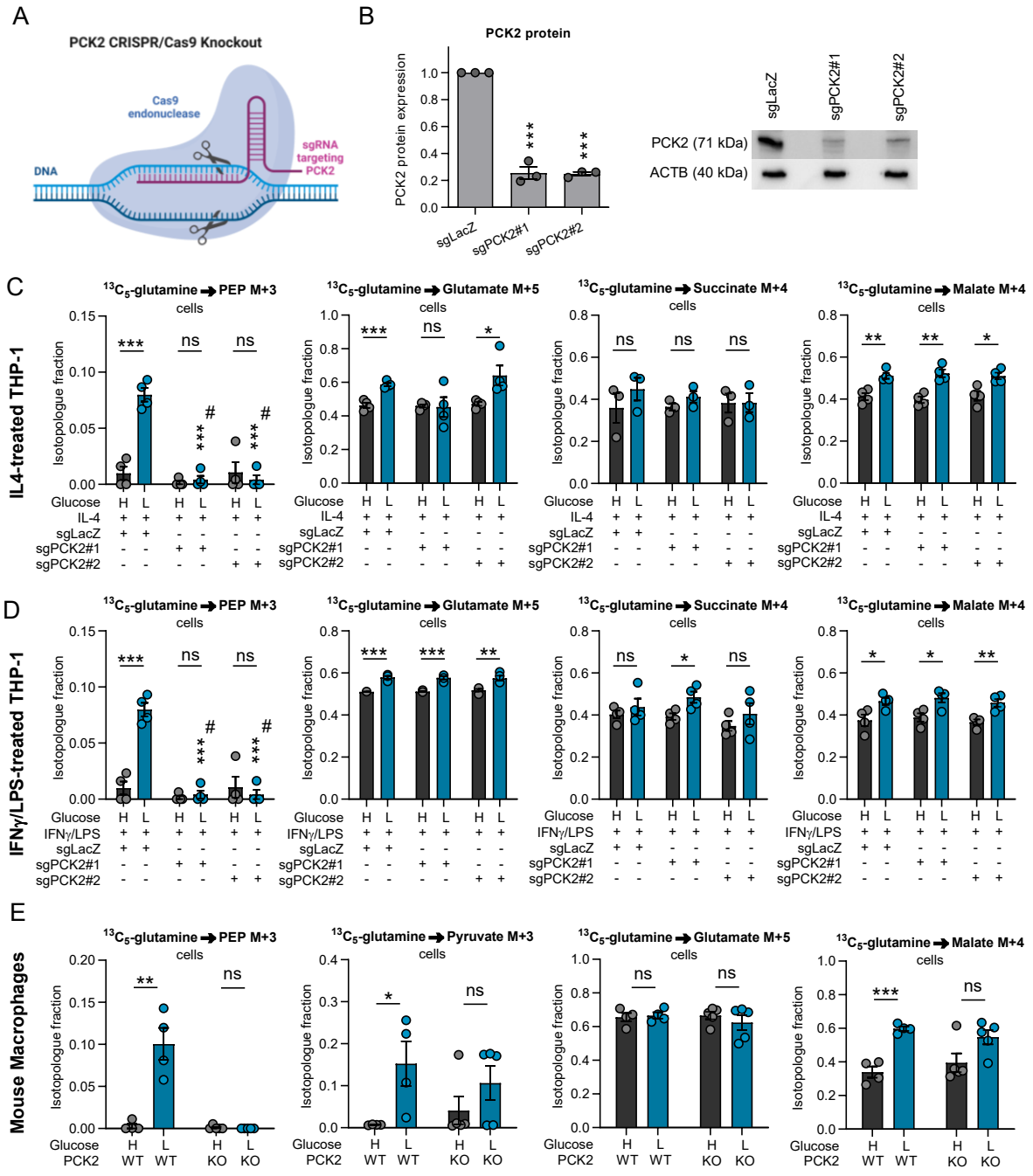

Figure 12: PCK2 mediates partial gluconeogenesis in human and murine macrophages. (A) PCK2 CRISPR/Cas9 knockout scheme (*created with BioRender*). (B) PCK2 protein levels after CRISPR-Cas9 mediated gene editing with guide RNAs targeting either LacZ (control, sgLacZ) or PCK2 (sgPCK2#1, sgPCK2#2). (C-D) Labeling fractions of PEP, pyruvate and TCA cycle intermediates in IL-4 (C) or IFNγ/LPS (D) pre-polarized THP-1 receiving $^{13}C_5$-labeled glutamine. (E) Labeling fractions of TCA cycle intermediates, PEP and pyruvate in peritoneal macrophages from whole body PCK2 WT or KO mice treated with $^{13}C_5$-labeled glutamine in high (H) or low (L) glucose medium. (B-E) Data are shown as mean +/- SEM from four independent experiments; group comparisons were performed using unpaired Student's t-test. *p<0.05, **p<0.01, ***p<0.001. ns, not significant. Adapted from Schindlmaier *et al.* (1).

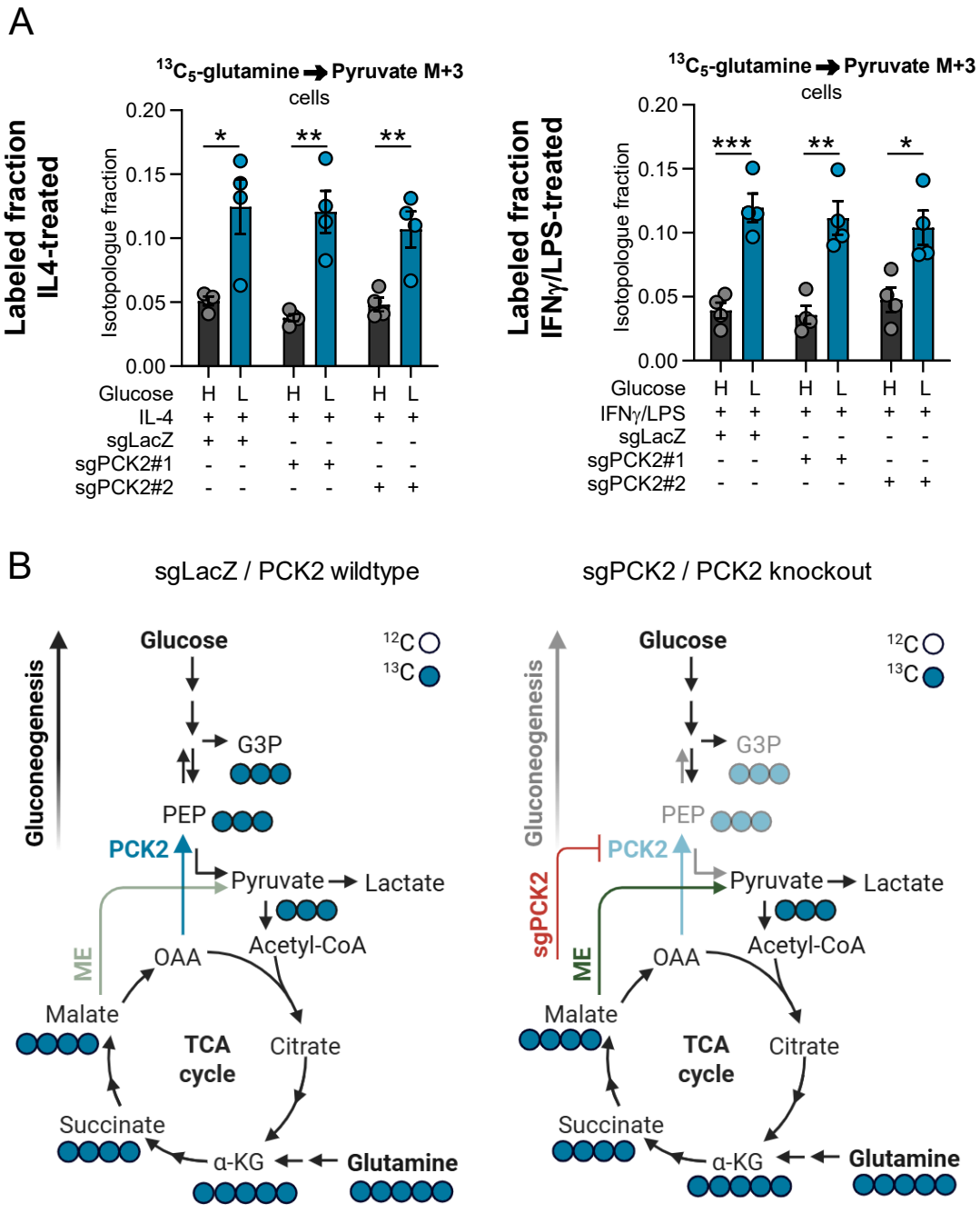

Figure 13: Impact of PCK2 knockout on pyruvate fractions (THPs). (A) Labeled fractions of pyruvate in PCK2 knockout THP-1 cells (sgPCK2#1, sgPCK2#2) or control cells (sgLacZ) pre-polarized with IL-4 (left) or IFNγ/LPS (right) and treated with $^{13}C_5$-glutamine from n=4 independent experiments. H, high glucose; L, low glucose. (B) Labeling patterns from $^{13}C_5$-glutamine entering partial gluconeogenesis and the impact of PCK2 knockout. G3P, glycerol-3-phosphate; PEP, phosphoenolpyruvate; OAA, oxaloacetate; α-KG, α-ketoglutarate; ME, malic enzyme. (A) Data are shown as mean +/- SEM from n=4 independent experiments; group comparisons were performed using unpaired Student's t-test. *p<0.05, **p<0.01, ***p<0.001. ns, not significant. Adapted from Schindlmaier *et al.* (1).

Both M1- and M2-like THP-1–derived macrophages produced PEP (M+3) from labeled glutamine when glucose was limited; however, this pathway was completely abolished in PCK2-deficient cells (Figure 12C, D). These findings confirm that cataplerosis (the export of TCA cycle intermediates) (132) and the initial reactions of gluconeogenesis are mediated by PCK2. Interestingly, the conversion of glutamine-derived carbon to pyruvate remained unaffected by PCK2 deletion (Figure 13A), suggesting the conversion of TCA cycle intermediates to pyruvate occurred via an alternative pathway, such as through malic enzyme activity (Figure 13B).

To further substantiate the involvement of PCK2 in the metabolic adaptation of macrophages to glucose deprivation, we isolated peritoneal macrophages from PCK2 knockout mice. After isolation, macrophages were cultured in differentiation media (method section 2.3) for 24 hours before differential glucose treatment and stable isotopic labelling and GC-MS. These cells also exhibited a shift toward partial gluconeogenesis in response to low glucose, which was completely suppressed in macrophages lacking PCK2 (Figure 12E). This confirms that PCK2 is essential for partial gluconeogenic and contributes to the adaptive metabolic response in primary peritoneal macrophages and in THP-derived macrophages.

3.5. Glucose deprivation does not impact cell number in THP-1 derived PCK2 wildtype or knockout macrophages

As the effects of low glucose availability on macrophage survival remain largely unclear, we aimed to determine whether macrophages derived from THP-1 cells, show impaired survival after high versus low glucose treatment. Additionally, to assess the potential impact of PCK2, we used THP-1 cells to generate polyclonal PCK2 CRISPR/Cas9 knockout macrophages (Figure 14). After pre-polarization towards M1- or M2-like macrophages, we assessed cell numbers of macrophages treated with high or low glucose media for 48 hours, with a medium change after 24 hours (Figure 14). We observed that neither limited glucose availability nor the absence of PCK2 significantly affected the cell numbers of differentially activated THP-1–derived macrophages (Figure 14). These findings indicate a high degree of metabolic adaptability in macrophages exposed to nutrient-restricted conditions resembling those in the tumor microenvironment.

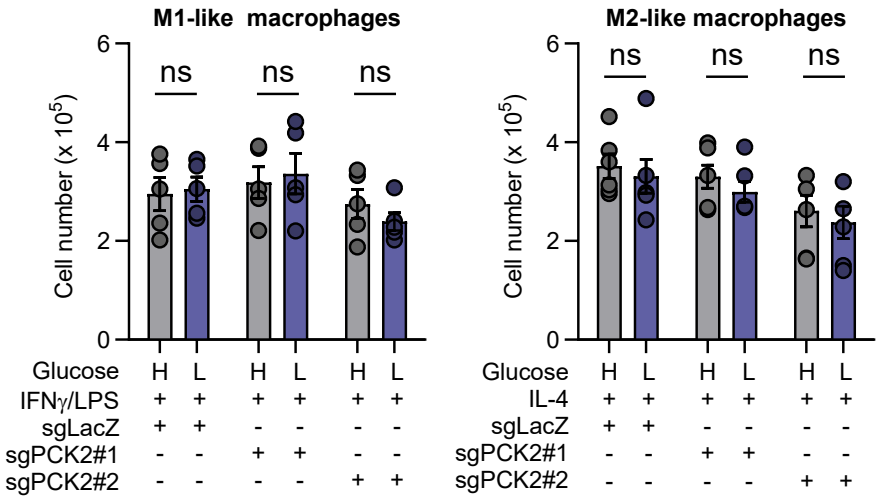

Figure 14: Cell number of M1-like and M2-like THP-1 derived macrophages after high versus low glucose treatment. Cell numbers of M1-like (left) and M2-like (right) THP-1 derived macrophages after variable glucose treatments for 48 hours with media change after 24 hours. Data are shown as mean +/- SEM from n=5 (M1-like) or n=6 (M2-like) independent experiments. Unpaired Student's t-tests were used for group comparisons, which revealed no significant differences. sgLacZ shows THP-1 cells that received guide RNA directed against LacZ, sgPCK#1 and sgPCK#2 depict THP-1 cells that received two different guide RNAs targeting PCK2, respectively.

3.6. Lipid profiles of macrophages are not affected by low glucose treatment or PCK2 knockout

To assess how glucose availability and partial gluconeogenesis observed in macrophages might shape lipid metabolism, liquid chromatography – mass spectrometry (LC-MS) based metabolic profiling was performed in IL-4 activated, M2-like THP-derived macrophages with or without CRISPR/Cas9 knockout of PCK2 (Figure 15). Cells were cultured in high or low glucose media for 48 hours with media change after 24 hours. LC-MS was performed by Martin Trötzmüller, Core Facility Mass Spectrometry, Medical University of Graz. With this approach, total content of cholesterol, triglyceride, sphingomyelin, phosphatidylethanolamine, phosphatidylcholine, and lysophosphatidylcholine were measured (Figure 15). Since especially M2-like and tumor-associated macrophages are associated with enhanced lipid metabolism and storage (133, 134), the impact of low glucose availability on lipid metabolism was assessed in IL-4 activated THP-derived macrophages. Also, our group found that the glycerol-backbone of phospholipids derives from noncarbohydrate precursors in starved lung cancer cells, mediated by PCK2 and partial gluconeogenesis, which is why we assessed lipid species in THP-derived PCK2 wildtype and knockout macrophages (Figure 15).

These lipid species represent major structural and storage lipid species that are tightly linked to membrane composition, cellular signaling, metabolic state and function in macrophages (135). In that respect, lysophosphatidylcholine was even reported to be involved in macrophage polarization and inflammatory responses (136). In our experimental setup, we could not detect significant differences in the measured lipid species, neither under differential glucose treatment, nor in dependence on PCK2 (Figure 15). The treatment duration of 48 hours with a media change of 24 hours could play a role in this respect, as longer periods of glucose starvation might still alter lipid metabolism, which could be assessed in future studies focusing on longer nutrient deprivation.

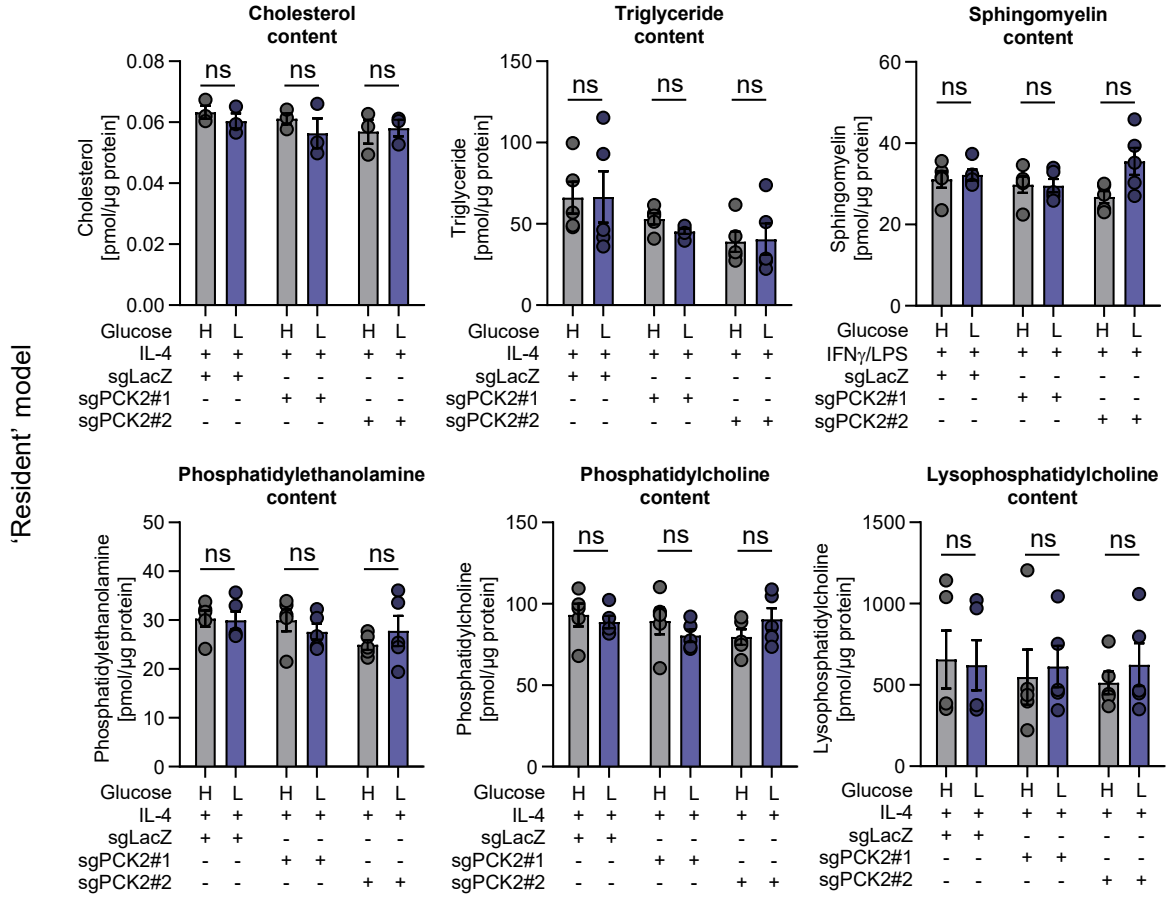

Figure 15: Cholesterol, triglyceride and phospholipid content in glucose-deprived PCK2 wildtype versus knockoud macrophages (THPs). LC-MS in pre-polarized ('resident' model) M2-like THP-derived PCK2 wildtype and CRISPR/Cas9 knockout macrophages in the 'resident' model. Total content of cholesterol, triglyceride, sphingomyelin, phosphatidylethanolamine, phosphatidylcholine, and lysophosphatidylcholine in macrophages treated with high (H, 10 mM) versus low (L, 0.2 mM) glucose media for 48 hours with media change after 24 hours. Data are shown as mean +/- SEM from n=4 independent experiments; group comparisons were performed using unpaired Student's t-test. ns, not significant.

3.7. Immunohistochemistry and single cell RNA sequencing data of human NSCLC and healthy lung suggests relevance of PCK2 in macrophages *in vivo*

Macrophages within the alveolar spaces of the lung and TAMs in lung cancer are likely to experience glucose restriction, necessitating similar metabolic flexibility. We therefore analyzed PCK2 expression in eight paired samples of human non-small cell lung cancer (NSCLC) and corresponding non-tumorous lung tissue (Table 7). Macrophages were identified morphologically and by CD68 positivity in consecutive serial sections. In both tumor and normal lung tissue, macrophages showed consistent PCK2 immunoreactivity (Figure 16A). In line with previous observations (110), bronchial epithelial cells and subsets of tumor cells also expressed PCK2.

We further examined the expression of key metabolic enzymes in macrophages using a published single-cell RNA sequencing dataset of NSCLC and normal lung (124), together with our collaborators Alexander Kirchmair and Zlatko Trajanoski, Biocenter, Institute of Bioinformatics, Medical University of Innsbruck (Figure 16B). The analysis revealed the metabolic gene expression pattern of various different cell types present in normal, healthy tissue as well as NSCLC tissue. Among others, myeloid cells as monocytes and macrophages were particularly interesting for this study. Overall, these cell populations seem to display high metabolic flexibility, compared other immune cells as for example dendritic cells (DCs) or T and B cells, as several metabolic enzymes involved in gluconeogenesis, glutaminolysis, glycolysis, and pyruvate carboxylation, are expressed as well in the healthy lung, as also in the tumor tissue in monocytes and macrophages.

Interestingly, PCK2 expression was consistently detected across multiple macrophage populations in both tissues, while PCK1 transcripts were nearly absent (Figure 16B). Notably, the downstream gluconeogenic enzyme FBP1 was also expressed. Across all macrophage populations, glycolytic genes and malic enzymes (ME1 and ME2) displayed strong expression. Likewise, the glutaminolytic enzyme GLUD1 (glutamate dehydrogenase 1) and pyruvate carboxylase, which catalyzes the interconversion of oxaloacetate and pyruvate, were clearly expressed in macrophages from normal lung, but less prominently in tumor-associated macrophages (Figure 16B). Malic enzyme or pyruvate carboxylase expression are in line with the observed malate (M+3) and citrate (M+3) labeling patterns in $^{13}C_6$-glucose–treated macrophages under high glucose conditions (Figure 7B).

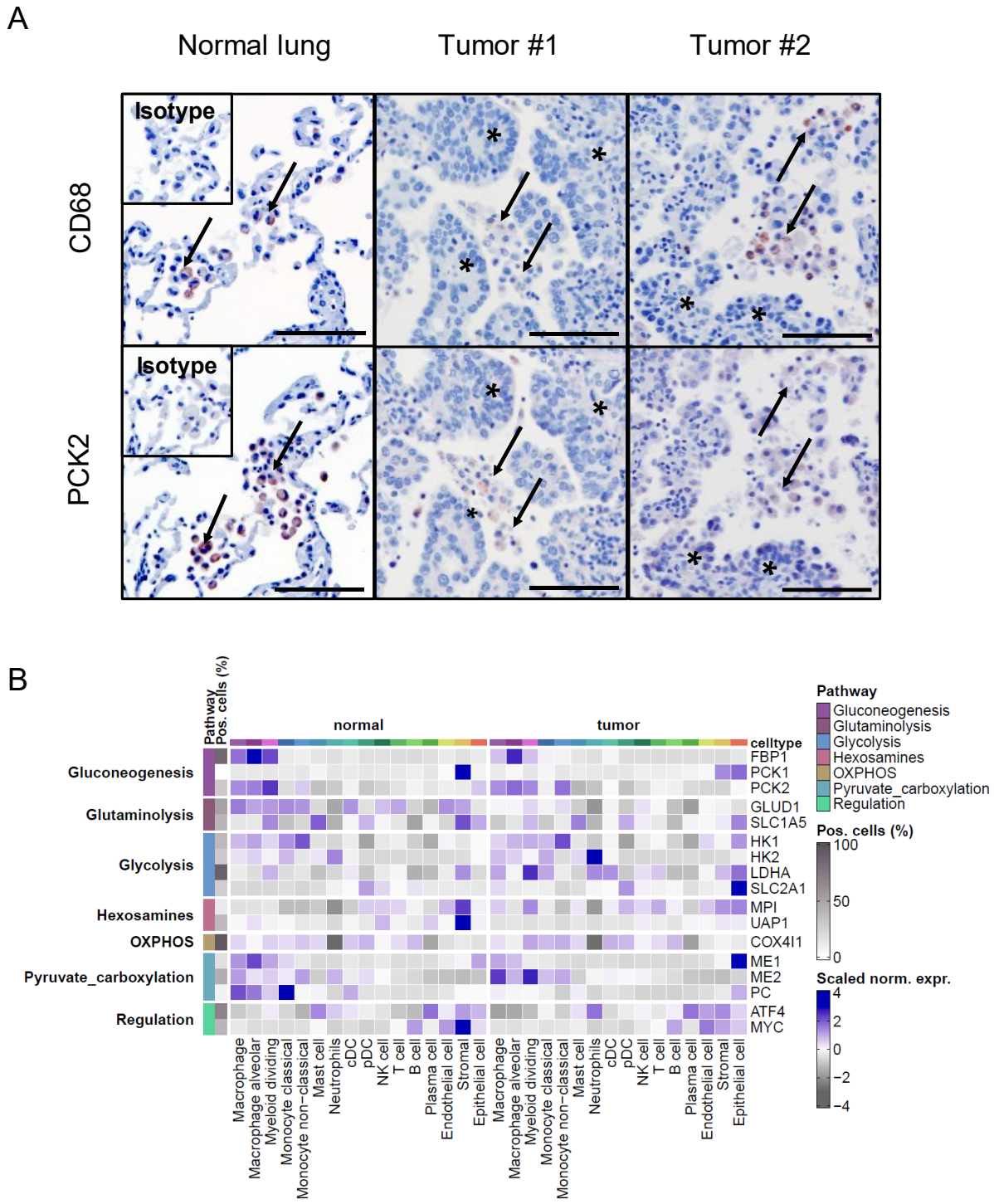

Figure 16: PCK2 is expressed in human lung and lung cancer macrophages along with glycolytic genes. (A) Representative immunohistochemistry staining of PCK2 and CD68 (macrophage marker) performed on consecutive slides from a normal human lung, a lung squamous cell carcinoma (Tumor#1) or a lung adenocarcinoma (Tumor#2). Arrows: Macrophages, asterisks: tumor cell nests. Scale bar: 100 µm. (B) Expression of gluconeogenesis, glycolysis and glutaminolysis genes in different subsets of macrophages from human non-small cell lung cancers or non-involved normal lung determined by single cell RNA sequencing (124). Adapted from Schindlmaier *et al.* (1).

Taken together, these results indicate that both normal and tumor-associated lung macrophages exhibit a high degree of metabolic flexibility, enabling them to adapt to nutrient-restricted microenvironments such as those found in solid tumors.

3.8. Low glucose conditions reduce the expression of M1-like macrophage marker CD80, but do not affect cytokine production

Next, we examined macrophage phenotypes and functions under varying glucose conditions. The surface markers CD80 (M1-like) and CD206 (M2-like) were analyzed in MDMs exposed to high (10 mM) or low (0.2 mM) glucose, either during activation for 48 hours (‘acute’ model) or following a 48-hour pre-polarization phase (‘resident’ model) (Figure 4D). In MDMs subjected to simultaneous activation and glucose variation, but not in pre-polarized M1-like macrophages, CD80 expression was significantly reduced under low glucose conditions (Figure 17A), indicating that successful M1-like polarization depends on glucose availability, consistent with previous findings (128). In contrast, CD206, the M2-like marker, remained unchanged between high and low glucose conditions (Figure 17A). Expression of M1- and M2-associated cytokines did not differ significantly between glucose conditions (Figure 17B, MDMs). Interestingly, vascular endothelial growth factor (VEGFA), a pro-angiogenic mediator typically released by tumor-associated macrophages, was significantly upregulated in non-polarized and M2-like MDMs under low glucose conditions on mRNA level (Figure 17C). Similarly, the expression of GLUT1 (SLC2A1), the primary glucose transporter in macrophages, was increased in response to low glucose, possibly reflecting an adaptive mechanism to limited glucose availability (Figure 17C).

To explore the underlying mechanisms of the observed impairment in M1-like activation, we next investigated the involvement of mechanistic target of rapamycin (mTOR) signaling and endoplasmic reticulum (ER) stress, both known regulators of pro-inflammatory macrophage function (137-140). Indeed, flow cytometric analysis revealed that treatment with Tunicamycin (an ER stress inducer) or Torin1 (an inhibitor of mTORC1 and mTORC2) significantly reduced CD80 expression in MDMs under high glucose conditions (Figure 17D).

In addition, glutaminase activity was inhibited using CB839, given the enhanced contribution of glutamine to the TCA cycle observed under low glucose conditions. Also, as mentioned before, since oxidative metabolism has been reported to be rather a feature of M2-like macrophages, we hypothesized that inhibition of an enzyme involved in glutamine metabolism might lead to a less pronounced M2-like activation.

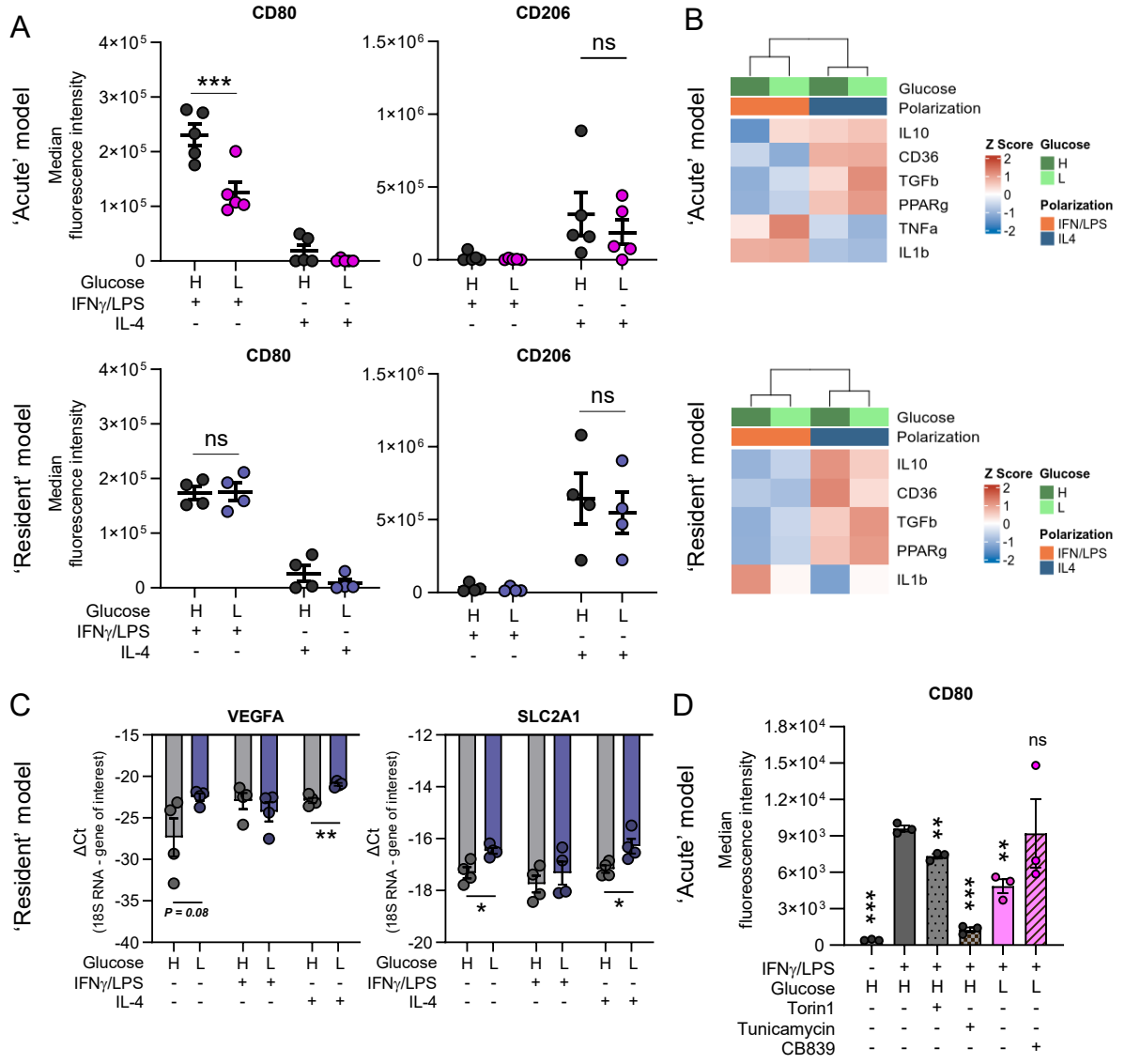

Figure 17: Low glucose treatment leads to reduced M1-like macrophage marker CD80, modulates VEGFA and SLC2A1, while M1- or M2-related cytokines are unaltered. (A) Flow cytometry measurement of macrophage markers CD80 and CD206 in MDMs after high (H) vs. low (L) glucose treatment. (B) Mean cytokine mRNA levels in MDMs treated with high (H) or low (L) concentrations of glucose, from n=3 ('acute' model) or n=4 ('resident' model) independent experiments using MDMs from three different donors in each model. Heatmaps of scaled expression data, based on hierarchical clustering, were generated using the R package 'ggplot2´ (R version 4.3.1) (126). (C) mRNA expression of GLUT1 (SLC2A1) and VEGFA in 'resident' MDMs treated for 48 hours with high (H) vs. low (L) glucose, from n=4 independent experiments using MDMs from three different donors. (D) Expression of CD80 on 'acute' MDMs, treated with high (H) vs. low (L) glucose, as well as Torin1, Tunicamycin, or CB839. Data are shown as mean +/- SEM from n=5 experiments/donors ('acute' model, A), n=4 experiments/donors ('resident' model, A), or n=3 experiments/donors (D). (A, C, D) Group comparisons were performed using unpaired Student's t-tests. *p<0.05, **p<0.01, ***p<0.001. (D) Significance values are in comparison to the control condition high (H) glucose + IFNγ/LPS. Adapted from Schindlmaier et al. (1).

In fact, under low glucose conditions, glutaminase inhibition restored CD80 expression (Figure 17D). These findings indicate that enhanced glutamine metabolism under glucose deprivation contributes to the regulation of the M1-like marker CD80, whereas mTOR inhibition or ER stress induction disrupts CD80 expression even in glucose-replete environments. Since cytokine expression on mRNA levels seemed not to be influenced by variable glucose conditions, we assessed actual cytokine secretion in THP-1–derived macrophages using ELISA (Figure 18).

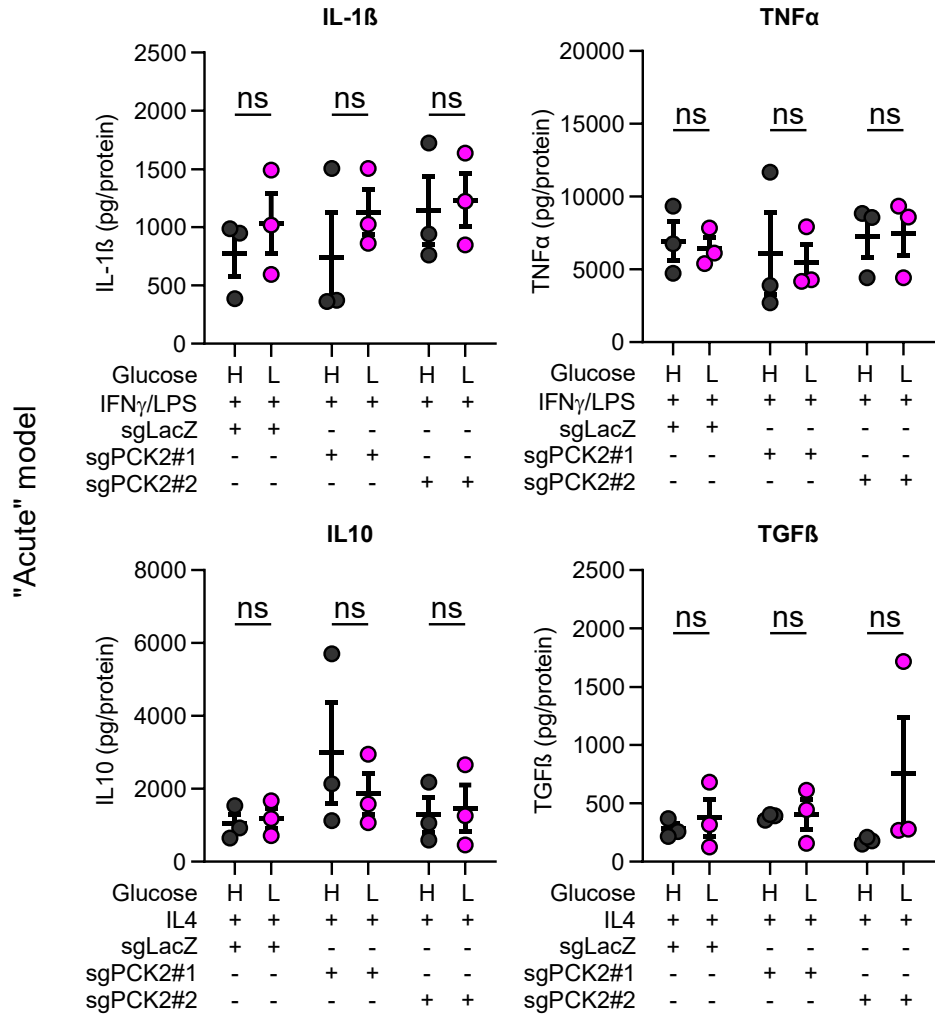

Figure 18: Impact of PCK2 knockout on cytokine secretion to the supernatant media. Secretion of IL-1β, TNFα, IL-10 and TGFβ were determined in macrophages derived from PCK2 knockout THP-1 cells (sgPCK2#1, sgPCK2#2) or control cells (sgLacZ), treated with high (H) vs. low (L) glucose media, simultaneously with activation stimuli IFNγ/LPS or IL-4 ('acute' model), for 24 hours (M1-related cytokines), or 48 hours (M2-related cytokines). Photometrical determination of cytokine secretion in the supernatant media was performed from n=3 independent experiments. Data are shown as mean ± SEM. Group comparisons were performed by unpaired Student's t-tests and showed no significant differences. Adapted from Schindlmaier *et al. (*1).

To also study the potential impact on PCK2 in this respect, we used macrophages differentiated from the PCK2 wildtype versus knockout THP-1 cells. However, not only cytokine mRNA expression (Figure 17B, in MDMs), but also cytokine secretion to the supernatant media (Figure 18) was unaffected by glucose concentration or PCK2 expression. This once more underpins the high metabolic flexibility of macrophages upon variable glucose conditions, as they still maintain cytokine expression and release, that are major features in both M1- and M2-like macrophages, ensuring proper immune response, even in nutrient-poor conditions.

4. Discussion

In this dissertation, we assessed the impact of low glucose conditions on macrophage metabolism, phenotype, and function, by using stable isotopic labeling and GC-MS and various gene expression analyses. To date, it is still poorly understood how different immune cells adapt to nutrient deprivation, as present in the TME. In the context of solid cancer, cancer cells themselves are capable of various adaptation mechanisms, involving metabolic adaptation to the harsh TME. Here, we found that macrophages induce partial gluconeogenesis, mediated by PCK2, when glucose is limited. M1- and M2-like macrophages reduce glycolytic activity and enhance glutamine usage within the TCA cycle, when treated with low-glucose media. Besides these profound metabolic changes, we found no alterations in phospholipid or cholesterol metabolism, in response to glucose deprivation or PCK2 expression. While macrophages maintained M1- and M2-related cytokine expression and release upon variable glucose treatments, M1-related CD80 surface marker expression was reduced in our model of 'acute' glucose deprivation and macrophage activation. In our 'resident' model, we found enhanced expression of VEGF on mRNA level, only in M2-like macrophages.

Our group and others showed that cancer cells can use partial gluconeogenesis mediated via PCK2 to ensure formation of glycolytic intermediates from non-carbohydrate precursors (37, 38, 111). Apart from that, neutrophils have been shown to as well use steps of gluconeogenesis and glycogenesis, supporting their effector functions (129). Until very recently, partial gluconeogenesis or activity of the initial gluconeogenesis enzyme PCK2 in macrophages has not been investigated, highlighting the research gap that this dissertation attempted to fill.

Dong et al. reported that PCK2 is upregulated in Kupffer cells, the resident macrophages of the liver, following pro-inflammatory stimulation, and that PCK2 overexpression resulted in increased expression of inflammatory markers (141). Ko et al. showed that myeloid-specific deletion of PCK2 enhanced lactate production and promoted a more pro-inflammatory phenotype (142). In that study, glucose production from non-carbohydrate labeled precursors (i.e., complete gluconeogenesis) was not detected in macrophages, and glycerol synthesis via glyceroneogenesis (partial gluconeogenesis) was minimal; however, gluconeogenesis was assessed only under high glucose (10 mM) conditions (142). Very recent studies have also reported gluconeogenic activity to the level of fructose-6-phosphate or glucose-6-phosphate formation in macrophages (143, 144).

Fan et al. demonstrated incorporation of ^{13}C from fully labeled ^{13}C-glutamine into fructose-6-phosphate and fructose-1,6-phosphate in human MDMs, which was increased after treatment of macrophages with glucan particles from yeast, indicating gluconeogenic activity up to the level of sugar phosphates (143). However, low glucose conditions were not investigated in that study.

More recently, Jeroundi et al. reported that macrophages can synthesize glycogen from non-carbohydrate precursors as they found glycogen being labeled from $^{13}C_5$-glutamine and $^{13}C_3$-lactic acid, indicating glyconeogenesis from both of these precursors in macrophages in a medium containing low glucose (< 0.1 g/L ~ < 0.6 mM) (144). These findings were more pronounced in pro-inflammatory, M1-like macrophages in their study (144). Also, they found that glycogenolysis seems to support M1-like cytokine secretion (e.g., TNFα, IL-6) and phagocytosis in M2-like macrophages, as they found no alterations in these functional readouts after low glucose treatments, however after inhibition of the glycogenolysis enzyme glycogen phosphorylase, both cytokine secretion and phagocytosis were impaired (144). Culturing macrophages in a glucose-low (and glutamine-low) medium for three days, after culture in a glucose- and glutamine-replete medium for two days, did not impact classical M1- or M2-related markers (144), in line with our study. These studies demonstrate macrophages' ability to use some steps of gluconeogenesis. However, the contribution of PCK2 to partial gluconeogenesis under different concentrations of glucose remained elusive.

To study our hypothesis, that the key enzyme of gluconeogenesis, phosphoenolpyruvate carboxykinase 2 (PCK2) may support survival and functions of TAMs in glucose-limited conditions, we established the differentiation and M1- versus M2-like activation of monocytes to macrophages from different sources, such as PBMCs from human blood donors, the monocyte-like THP-1 cell line, and from murine peritoneal macrophages, according to established protocols and together with collaboration partners. The establishment of proper macrophage models was confirmed by according macrophage differentiation and polarization markers and accompanying cytokine expression widely studied for the pro-inflammatory M1-like, and the anti-inflammatory M2-like phenotype. However, the M1- and M2-like macrophage populations mark only the extreme ends of the spectrum, as various heterogeneous subpopulations of macrophages, varying across tissues upon physiological conditions, as well as additionally altered in the context of diseases, are reported and more and more studied in the field (63, 85, 93, 106).

However, in the scope of this PhD thesis, we wanted to assess the two major phenotypes, namely pro-inflammatory, potentially anti-tumorigenic as well as anti-inflammatory, pro-tumorigenic macrophages, both relevant and present in the microenvironment of solid tumors. Assessing different macrophage subpopulations is beyond the scope of this PhD project and should be addressed in future studies.

Our study revealed metabolic adaptations of macrophages to low glucose availability, characterized by reduced lactate production indicating reduced glycolysis, as well as enhanced glutamine consumption and glutamine contribution to the TCA cycle, in both M1- and M2-like macrophage models. Additionally, macrophages are capable of performing initial steps of gluconeogenesis in glucose-limited conditions. These findings confirm high metabolic flexibility of macrophages in response to nutrient deprivation. We demonstrate that low glucose conditions induce partial gluconeogenesis from glutamine as a carbon source across both distinct macrophage polarization states, the pro-inflammatory M1-like as well as the anti-inflammatory M2-like model. The observed induction of partial gluconeogenesis under low glucose conditions cannot be explained with modulation of the initial gluconeogenesis enzyme, as we found no difference in PCK2 expression or activity in our high versus low glucose treatment. Thus, the observed enhanced activity in the partial gluconeogenesis pathway may be mediated rather by changes in the product and substrate concentrations. Our carbon tracing experiments indicate that this partial gluconeogenesis proceeds at least to the level of G3P as ^{13}C-labeled carbons, arising from fully ^{13}C-labeled glutamine gave rise to fully ^{13}C-labeled G3P, directing the gluconeogenesis pathway. This indicates, that this adaptation supports the generation of glycolytic intermediates from non-glucose precursors when glucose is limited, rather than being a source of glucose production per se, as we could not find labeled glucose produced by macrophages from glutamine.

Thus, after assessing glycolysis and TCA cycle metabolism using GC-MS, we aimed at investigating whether glucose availability or PCK2-dependent partial gluconeogenesis impact lipid metabolism. Since the observed partial gluconeogenesis pathway was more pronounced in the M2-like macrophages, we assessed lipid metabolism only in M2-like, more TAM-like macrophages. After LC-MS based lipidomics in IL-4 activated, M2-like macrophages from THP-1 cells with or without PCK2 knockout, no significant changes were found in our experimental setup of 48 hours of glucose deprivation.

Neither glucose availability, nor PCK2 KO altered lipid metabolism in our experimental setting as we did not detect differences in lipid levels in PCK2 knockout versus wildtype cells, yet the partial gluconeogenesis pathway was blocked. Potentially, glucose may be re-routed to glycerol-phosphate formation in PCK2 knockout and low glucose conditions, even if its availability is limited. These findings suggest that at least after rather short-term glucose restriction, lipid metabolism is not altered, however prolonged glucose limitation might show differential results and could be addressed in future experiments. Exploring the role of PCK2-dependent glycerol-3-phosphate metabolism in macrophages under different nutrient conditions in future studies, may therefore provide additional insights into the metabolic regulation of macrophage effector functions and the role of PCK2.

Additionally, upper glycolysis and thus downstream pathways branching from PCK2 dependent gluconeogenesis, depending on cellular context or nutrient availability, were not addressed within this project, as we focused on (lower) glycolysis, TCA cycle and lipid metabolism. Further investigation of upper glycolytic intermediates, for example with an LC-MS approach, might shed more light on the further usage of non-carbohydrate precursors used in the partial gluconeogenesis pathway in macrophages. Concerning the metabolic differences between M1- and M2-like phenotypes, we observed elevated levels of the glycolytic intermediate pyruvate in pro-inflammatory macrophages in the ‘acute’ model, along with trends towards increased lactate, consistent with previous reports describing a glycolytic preference in M1-like macrophages (96, 97). These metabolic alterations were relatively modest, suggesting that M1-like polarization may induce only transient or context-specific increases in glycolytic activity. The less pronounced accumulation of glycolytic intermediates in the ‘resident’ model compared to the ‘acute’ model supports this explanation.

The mediation of the robust activation of the partial gluconeogenesis pathway by PCK2 was confirmed in two knockout models, in the CRISPR/Cas9 mediated PCK2 knockout in the monocyte-like THP-1 cells, as well as the peritoneal macrophages of PCK2 full body knockout mice. Despite robust activation of the PCK2-mediated pathway under low glucose conditions, knockout of PCK2 along with low glucose treatments did not impair the survival of THP-derived macrophages, neither after M1- or M2-like activation, once more suggesting high metabolic flexibility and adaptability of macrophages in various metabolic niches. One potential compensatory mechanism could involve the mobilization of intracellular glycogen stores. Indeed, recent work has demonstrated that glycogen synthesis from glucose or glutamine, as well as glycogen breakdown, are dynamically regulated in macrophages (144).

Alternatively, macrophages may rely primarily on oxidative phosphorylation to meet their energy needs, when glucose levels are low, switching to glutamine as an alternative energy fuel. The latter is supported by the observed greater contribution of glutamine to the TCA cycle and conversion of glutamine to acetyl-CoA (yielding M+6 citrate), under glucose deprivation. The functional relevance of partial gluconeogenesis in macrophages is likely context dependent and its role in regulation macrophage behavior *in vivo* remains to be determined.

To approach the *in vivo* relevance, we as a first step analyzed PCK2 expression in human lung and lung tumor macrophages using immunohistochemistry of human lung and lung tumor tissues, and publicly available single-cell RNA sequencing data from NSCLC and matched non-tumor lung tissue. Macrophages in both, healthy lung and tumor tissue, consistently expressed PCK2, whereas the cytosolic isoform PCK1 was rather absent. Also, the expression of downstream gluconeogenic enzymes, glycolytic genes, malic enzymes, and glutaminolytic enzymes further supports the metabolic flexibility of macrophages in the human lung and also in lung tumors. This data support that the metabolic flexibility of macrophages, and also PCK2 and partial gluconeogenesis have physiological relevance in human macrophage populations.

After the metabolic studies in macrophages of different sources and activation states, we wanted to assess the potential impact of glucose-deprivation on macrophage phenotype and cytokine expression, aiming to approximate also potential functional changes. Besides the impact on macrophage metabolism, glucose deprivation led to a marked reduction in the expression of CD80 in pro-inflammatory M1-like macrophages, in our ‘acute’ model. This finding is in line with literature suggesting that glucose is necessary for full M1-like polarization (128). CD80 is a key co-stimulatory molecule expressed by M1-like macrophages and plays a central role in Tcell activation and the crosstalk between innate and adaptive immunity (145). This finding is supported by reduced levels of CD80 on dendritic cells, after treatment with 2-deoxy-glucose (2DG), a widely studied glycolytic inhibitor (94, 146).

While our data demonstrate clear effects of glucose availability on macrophage metabolism and CD80, the broader context-dependent impact of glucose levels on immune function remains incompletely understood. Identifying glucose-dependent metabolic alterations that mechanistically link nutrient availability to CD80 regulation or other macrophage phenotypes will probably require more analyses of glycolytic and branching pathways (147). Taken together, CD80 surface expression, as shown by our study, and other M1-linked functions might be impaired in macrophages entering glucose-deprived environments, such as the tumor microenvironment (94, 96).

In contrast, already established polarization states seem to not be disturbed by subsequent variation of glucose levels, as no changes were found in CD80 in our 'resident' model. Notably, inhibition of glutaminase reversed the reduction of CD80 under low glucose conditions, suggesting that enhanced glutaminolysis and glutamine anaplerosis contribute to the observed phenotype. However, the precise (metabolic) mechanisms underlying this effect remain unclear and need further investigation in future studies. By screening various M1- and M2-related genes in high and low glucose conditions, we could not find significant alterations, neither on mRNA level nor in secreted cytokines. Thus, macrophages seem to maintain their functional cytokine secretion across different nutrient conditions and expression of activation-associated genes is undisturbed.

Glucose availability can vary both locally, for example within the tumor microenvironment, and systemically in response to dietary intake and hormonal regulation. A limitation of our study is that the experimental model of 'acute' versus 'resident' macrophage–microenvironment interactions does not fully recapitulate the complexity of metabolic conditions encountered *in vivo* across different tissues and disease states. Furthermore, the glucose concentrations used in this study (0.2 mM versus 10 mM) were chosen to model glucose deprivation but could only be precisely controlled at the start of the experiment. As glucose was rapidly consumed, media were replaced every 24 hours to avoid prolonged complete glucose depletion. Maintaining glucose concentrations within a narrow and constant range would require a continuous-flow culture system; however, such an approach was not feasible in the context of ^{13}C tracer experiments due to the excessive tracer consumption it would entail.

Moreover, our high (10 mM) and low (0.2 mM) glucose concentrations cannot fully reflect the glucose gradient present in the tumor microenvironment, as glucose levels may lie in between those values, or might be even fully depleted in the TME (24, 26, 148). Future studies could also focus on completely depleting glucose, or approaching the various nutrient conditions with concentration gradients better reflecting the *in vivo* conditions. In addition, deprivation of other metabolites frequently reduced in the TME, as for example glutamine or both, glucose and glutamine, could provide more insight in macrophages' adaptation to poor nutrient availability. Additionally, although hypoxia and tumor cell acidification were not assessed in this PhD project, recent work of the group has shown that cancer cells are still capable of adaptation via partial gluconeogenesis under hypoxic conditions (Konrad *et al.*, in press). In this context, it has been reported that PCK2 is regulated by hypoxia, more specifically, expression of PCK2 is increased via hypoxia inducible factor 1 alpha (HIF-1α) (149). This axis could be assessed in macrophages in future experiments.

In summary, our data indicate that macrophages adapt to low glucose conditions by reducing glycolytic activity, enhancing glutamine-dependent anaplerosis of the TCA cycle, and activating initial steps of gluconeogenesis via PCK2. These findings highlight the remarkable metabolic plasticity of macrophages and their availability to sustain energetic and biosynthetic demands in challenging metabolic niches, as the microenvironment of solid tumors. Moreover, the robust expression of PCK2 in macrophages from human lung and lung tumor tissue suggests a potential role for this pathway in macrophage populations *in vivo*.

Taken together, this PhD project adds an important piece to the puzzle of macrophages residing in a low glucose metabolic microenvironment, as the microenvironment of solid tumors and the above-mentioned studies support our finding, that macrophages are capable of PCK2-mediated partial gluconeogenesis. Overall, this PhD thesis contributes to a deeper understanding of how metabolic cues shape macrophage metabolism and function, as this study sheds light on how macrophages, major tumor infiltrating immune cells, adapt to different glucose conditions. The understanding of how variable nutrient conditions affect immune cells and may potentially impact immune cell survival and function provides the basis for future pre-clinical and clinical studies addressing diseases involving the immune system. As cancer is a systemic disease with enormous involvement of the immune system, understanding metabolism on a systemic, but also cell-specific level is indispensable for new treatment approaches. Thought far, the understanding of how different types of cells behave in the tumor environment might enable us to find strategies to influence this environment, creating conditions that are unfavorable for the tumor and favorable for patients.

Bibliography

1. Schindlmaier K, Haitzmann T, Bubalo V, Konrad B, Jelwan J, Bluemel G, et al. Metabolic adaptation of glucose-deprived macrophages involves partial gluconeogenesis. Proc Natl Acad Sci U S A. 2025;122(44):e2419568122.

2. Sung H, Ferlay J, Siegel RL, Laversanne M, Soerjomataram I, Jemal A, et al. Global Cancer Statistics 2020: GLOBOCAN Estimates of Incidence and Mortality Worldwide for 36 Cancers in 185 Countries. CA: A Cancer Journal for Clinicians. 2021;71(3):209-49.

3. Spiro SG, Gould MK, Colice GL, American College of Chest P. Initial evaluation of the patient with lung cancer: symptoms, signs, laboratory tests, and paraneoplastic syndromes: ACCP evidenced-based clinical practice guidelines (2nd edition). Chest. 2007;132(3 Suppl):149S-60S.

4. Vanhove K, Graulus GJ, Mesotten L, Thomeer M, Derveaux E, Noben JP, et al. The Metabolic Landscape of Lung Cancer: New Insights in a Disturbed Glucose Metabolism. Front Oncol. 2019;9:1215.

5. Couraud S, Zalcman G, Milleron B, Morin F, Souquet PJ. Lung cancer in never smokers--a review. Eur J Cancer. 2012;48(9):1299-311.

6. Hendriks LEL, Remon J, Faivre-Finn C, Garassino MC, Heymach JV, Kerr KM, et al. Non-small-cell lung cancer. Nat Rev Dis Primers. 2024;10(1):71.

7. Arbour KC, Riely GJ. Systemic Therapy for Locally Advanced and Metastatic Non-Small Cell Lung Cancer: A Review. JAMA. 2019;322(8):764-74.

8. Herbst RS, Heymach JV, Lippman SM. Lung cancer. N Engl J Med. 2008;359(13):1367-80.

9. Forde PM, Spicer J, Lu S, Provencio M, Mitsudomi T, Awad MM, et al. Neoadjuvant Nivolumab plus Chemotherapy in Resectable Lung Cancer. N Engl J Med. 2022;386(21):1973-85.

10. Thai AA, Solomon BJ, Sequist LV, Gainor JF, Heist RS. Lung cancer. Lancet. 2021;398(10299):535-54.

11. Friedlaender A, Perol M, Banna GL, Parikh K, Addeo A. Oncogenic alterations in advanced NSCLC: a molecular super-highway. Biomark Res. 2024;12(1):24.

12. Reck M, Frost N, Peters S, Fox BA, Ferrara R, Savai R, et al. Treatment of NSCLC after chemoimmunotherapy - are we making headway? Nat Rev Clin Oncol. 2025;22(11):806-30.

13. Freeman GJ, Long AJ, Iwai Y, Bourque K, Chernova T, Nishimura H, et al. Engagement of the PD-1 immunoinhibitory receptor by a novel B7 family member leads to negative regulation of lymphocyte activation. J Exp Med. 2000;192(7):1027-34.

14. Dong H, Zhu G, Tamada K, Chen L. B7-H1, a third member of the B7 family, co-stimulates T-cell proliferation and interleukin-10 secretion. Nature Medicine. 1999;5(12):1365-9.

15. Sharpe AH, Pauken KE. The diverse functions of the PD1 inhibitory pathway. Nat Rev Immunol. 2018;18(3):153-67.

16. Li H, van der Merwe PA, Sivakumar S. Biomarkers of response to PD-1 pathway blockade. Br J Cancer. 2022;126(12):1663-75.

17. Wang X, Qiao Z, Aramini B, Lin D, Li X, Fan J. Potential biomarkers for immunotherapy in non-small-cell lung cancer. Cancer Metastasis Rev. 2023;42(3):661-75.

18. Lazzari C, Spagnolo CC, Ciappina G, Di Pietro M, Squeri A, Passalacqua MI, et al. Immunotherapy in Early-Stage Non-Small Cell Lung Cancer (NSCLC): Current Evidence and Perspectives. Curr Oncol. 2023;30(4):3684-96.

19. Hanahan D. Hallmarks of Cancer: New Dimensions. Cancer Discov. 2022;12(1):31-46.

20. DeBerardinis RJ, Chandel NS. We need to talk about the Warburg effect. Nature Metabolism. 2020;2:127-9.

21. DeBerardinis RJC, Navdeep S. Fundamentals of cancer metabolism. Science Advances. 2016;2(5).

22. Pavlova NN, Zhu J, Thompson CB. The hallmarks of cancer metabolism: Still emerging. Cell Metab. 2022;34(3):355-77.

23. Woods PS, Kimmig LM, Meliton AY, Sun KA, Tian Y, O'Leary EM, et al. Tissue-Resident Alveolar Macrophages Do Not Rely on Glycolysis for LPS-induced Inflammation. Am J Respir Cell Mol Biol. 2020;62(2):243-55.

24. Sullivan MR, Danai LV, Lewis CA, Chan SH, Gui DY, Kunchok T, et al. Quantification of microenvironmental metabolites in murine cancers reveals determinants of tumor nutrient availability. Elife. 2019;8.

25. Ho PC, Bihuniak JD, Macintyre AN, Staron M, Liu X, Amezquita R, et al. Phosphoenolpyruvate Is a Metabolic Checkpoint of Anti-tumor T Cell Responses. Cell. 2015;162(6):1217-28.

26. Gullino PM, Clark SH, Grantham FH. The Interstitial Fluid of Solid Tumors. Cancer Research. 1964;24:780–94.

27. Vaupel P. Tumor microenvironmental physiology and its implications for radiation oncology. Semin Radiat Oncol. 2004;14(3):198-206.

28. Martin JD, Fukumura D, Duda DG, Boucher Y, Jain RK. Reengineering the Tumor Microenvironment to Alleviate Hypoxia and Overcome Cancer Heterogeneity. Cold Spring Harb Perspect Med. 2016;6(12).

29. Buck MD, Sowell RT, Kaech SM, Pearce EL. Metabolic Instruction of Immunity. Cell. 2017;169(4):570-86.

30. Nwosu ZC, Ward MH, Sajjakulnukit P, Poudel P, Ragulan C, Kasperek S, et al. Uridine-derived ribose fuels glucose-restricted pancreatic cancer. Nature. 2023;618(7963):151-8.

31. Postprandial blood glucose. American Diabetes Association. Diabetes Care. 2001;24(4):775-8.

32. Reinfeld BI, Madden MZ, Wolf MM, Chytil A, Bader JE, Patterson AR, et al. Cell-programmed nutrient partitioning in the tumour microenvironment. Nature. 2021;593(7858):282-8.

33. Grasmann G, Mondal A, Leithner K. Flexibility and Adaptation of Cancer Cells in a Heterogenous Metabolic Microenvironment. Int J Mol Sci. 2021;22(3).

34. Corbet C, Feron O. Tumour acidosis: from the passenger to the driver's seat. Nat Rev Cancer. 2017;17(10):577-93.

35. Romero-Garcia SL-G, Jose Sullivan; B´ez-Viveros, José Luis; Aguilar-Cazares, Dolores; Prado-Garcia, Heriberto. Tumor cell metabolism. Cancer Biology and Therapy. 2011;12:939-48.

36. Siska PJ, Beckermann KE, Mason FM, Andrejeva G, Greenplate AR, Sendor AB, et al. Mitochondrial dysregulation and glycolytic insufficiency functionally impair CD8 T cells infiltrating human renal cell carcinoma. JCI Insight. 2017;2(12).

37. Leithner K, Hrzenjak A, Trotzmuller M, Moustafa T, Kofeler HC, Wohlkoenig C, et al. PCK2 activation mediates an adaptive response to glucose depletion in lung cancer. Oncogene. 2015;34(8):1044-50.

38. Leithner K, Triebl A, Trotzmuller M, Hinteregger B, Leko P, Wieser BI, et al. The glycerol backbone of phospholipids derives from noncarbohydrate precursors in starved lung cancer cells. Proc Natl Acad Sci U S A. 2018;115(24):6225-30.

39. Skinner OS, Blanco-Fernandez J, Goodman RP, Kawakami A, Shen H, Kemeny LV, et al. Salvage of ribose from uridine or RNA supports glycolysis in nutrient-limited conditions. Nat Metab. 2023;5(5):765-76.

40. Kroemer G, Chan TA, Eggermont AMM, Galluzzi L. Immunosurveillance in clinical cancer management. CA Cancer J Clin. 2024;74(2):187-202.

41. Tsai CH, Chuang YM, Li X, Yu YR, Tzeng SF, Teoh ST, et al. Immunoediting instructs tumor metabolic reprogramming to support immune evasion. Cell Metab. 2023;35(1):118-33 e7.

42. Roerden M, Spranger S. Cancer immune evasion, immunoediting and intratumour heterogeneity. Nat Rev Immunol. 2025;25(5):353-69.

43. Kunimasa K, Goto T. Immunosurveillance and Immunoediting of Lung Cancer: Current Perspectives and Challenges. Int J Mol Sci. 2020;21(2).

44. Yang K, Halima A, Chan TA. Antigen presentation in cancer - mechanisms and clinical implications for immunotherapy. Nat Rev Clin Oncol. 2023;20(9):604-23.

45. Lim JU, Lee E, Lee SY, Cho HJ, Ahn DH, Hwang Y, et al. Current literature review on the tumor immune micro-environment, its heterogeneity and future perspectives in treatment of advanced non-small cell lung cancer. Transl Lung Cancer Res. 2023;12(4):857-76.

46. Lu Q, Luo J, Tung CH, Wang X, Zhao Z. Quantitative profiling of intratumor immune heterogeneity identifies loss of immune diversity as a hallmark of cancer progression. NPJ Precis Oncol. 2025;10(1):39.

47. Qian J, Olbrecht S, Boeckx B, Vos H, Laoui D, Etlioglu E, et al. A pan-cancer blueprint of the heterogeneous tumor microenvironment revealed by single-cell profiling. Cell Res. 2020;30(9):745-62.

48. Wang L, Geng H, Liu Y, Liu L, Chen Y, Wu F, et al. Hot and cold tumors: Immunological features and the therapeutic strategies. MedComm (2020). 2023;4(5):e343.

49. Mantovani A, Marchesi F, Malesci A, Laghi L, Allavena P. Tumour-associated macrophages as treatment targets in oncology. Nat Rev Clin Oncol. 2017;14(7):399-416.

50. Bingle L, Brown NJ, Lewis CE. The role of tumour-associated macrophages in tumour progression: implications for new anticancer therapies. J Pathol. 2002;196(3):254-65.

51. Koukourakis MI, Giatromanolaki A, Kakolyris S, O'Byrne KJ, Apostolikas N, Skarlatos J, et al. Different patterns of stromal and cancer cell thymidine phosphorylase reactivity in non-small-cell lung cancer: impact on tumour neoangiogenesis and survival. British Journal of Cancer. 1998;77(10):1696-703.

52. Zhang QW, Liu L, Gong CY, Shi HS, Zeng YH, Wang XZ, et al. Prognostic significance of tumor-associated macrophages in solid tumor: a meta-analysis of the literature. PLoS One. 2012;7(12):e50946.

53. Gentles AJ, Newman AM, Liu CL, Bratman SV, Feng W, Kim D, et al. The prognostic landscape of genes and infiltrating immune cells across human cancers. Nat Med. 2015;21(8):938-45.

54. Thorsson V, Gibbs DL, Brown SD, Wolf D, Bortone DS, Ou Yang TH, et al. The Immune Landscape of Cancer. Immunity. 2018;48(4):812-30 e14.

55. Chang CH, Qiu J, O'Sullivan D, Buck MD, Noguchi T, Curtis JD, et al. Metabolic Competition in the Tumor Microenvironment Is a Driver of Cancer Progression. Cell. 2015;162(6):1229-41.

56. Colegio OR, Chu NQ, Szabo AL, Chu T, Rhebergen AM, Jairam V, et al. Functional polarization of tumour-associated macrophages by tumour-derived lactic acid. Nature. 2014;513(7519):559-63.

57. O'Neill LA, Pearce EJ. Immunometabolism governs dendritic cell and macrophage function. J Exp Med. 2016;213(1):15-23.

58. Pearce EL, Pearce EJ. Metabolic pathways in immune cell activation and quiescence. Immunity. 2013;38(4):633-43.

59. Geeraerts X, Bolli E, Fendt SM, Van Ginderachter JA. Macrophage Metabolism As Therapeutic Target for Cancer, Atherosclerosis, and Obesity. Front Immunol. 2017;8:289.

60. Sanin DE, Matsushita M, Klein Geltink RI, Grzes KM, van Teijlingen Bakker N, Corrado M, et al. Mitochondrial Membrane Potential Regulates Nuclear Gene Expression in Macrophages Exposed to Prostaglandin E2. Immunity. 2018;49(6):1021-33 e6.

61. Park MD, Silvin A, Ginhoux F, Merad M. Macrophages in health and disease. Cell. 2022;185(23):4259-79.

62. Wynn TA, Chawla A, Pollard JW. Macrophage biology in development, homeostasis and disease. Nature. 2013;496(7446):445-55.

63. Aegerter H, Lambrecht BN, Jakubzick CV. Biology of lung macrophages in health and disease. Immunity. 2022;55(9):1564-80.

64. Orecchioni M, Ghosheh Y, Pramod AB, Ley K. Macrophage Polarization: Different Gene Signatures in M1(LPS+) vs. Classically and M2(LPS-) vs. Alternatively Activated Macrophages. Front Immunol. 2019;10:1084.

65. Shapouri-Moghaddam A, Mohammadian S, Vazini H, Taghadosi M, Esmaeili SA, Mardani F, et al. Macrophage plasticity, polarization, and function in health and disease. J Cell Physiol. 2018;233(9):6425-40.

66. Liu PS, Ho PC. Determining Macrophage Polarization upon Metabolic Perturbation. Methods Mol Biol. 2019;1862:173-86.

67. Hobson-Gutierrez SA, Carmona-Fontaine C. The metabolic axis of macrophage and immune cell polarization. Dis Model Mech. 2018;11(8).

68. Viola A, Munari F, Sanchez-Rodriguez R, Scolaro T, Castegna A. The Metabolic Signature of Macrophage Responses. Front Immunol. 2019;10:1462.

69. Pansy K, Uhl B, Krstic J, Szmyra M, Fechter K, Santiso A, et al. Immune Regulatory Processes of the Tumor Microenvironment under Malignant Conditions. Int J Mol Sci. 2021;22(24).

70. Chanmee T, Ontong P, Konno K, Itano N. Tumor-associated macrophages as major players in the tumor microenvironment. Cancers (Basel). 2014;6(3):1670-90.

71. Pan Y, Yu Y, Wang X, Zhang T. Tumor-Associated Macrophages in Tumor Immunity. Front Immunol. 2020;11:583084.

72. Sarode P, Schaefer MB, Grimminger F, Seeger W, Savai R. Macrophage and Tumor Cell Cross-Talk Is Fundamental for Lung Tumor Progression: We Need to Talk. Front Oncol. 2020;10:324.

73. van Vlerken-Ysla L, Tyurina YY, Kagan VE, Gabrilovich DI. Functional states of myeloid cells in cancer. Cancer Cell. 2023;41(3):490-504.

74. Jackute J, Zemaitis M, Pranys D, Sitkauskiene B, Miliauskas S, Vaitkiene S, et al. Distribution of M1 and M2 macrophages in tumor islets and stroma in relation to prognosis of non-small cell lung cancer. BMC Immunol. 2018;19(1):3.

75. Li X, Lian J, Lu H. The role of SPP1(+)TAMs in cancer: Impact on patient prognosis and future therapeutic targets. Int J Cancer. 2025;157(9):1763-71.

76. Wang J, Wang Y, Liu Y, Yang R. SPP1(+) macrophages in tumor immunosuppression: mechanisms and therapeutic implications. Front Immunol. 2025;16:1711015.

77. Khantakova D, Brioschi S, Molgora M. Exploring the Impact of TREM2 in Tumor-Associated Macrophages. Vaccines (Basel). 2022;10(6).

78. Zilionis R, Engblom C, Pfirschke C, Savova V, Zemmour D, Saatcioglu HD, et al. Single-Cell Transcriptomics of Human and Mouse Lung Cancers Reveals Conserved Myeloid Populations across Individuals and Species. Immunity. 2019;50(5):1317-34 e10.

79. Casanova-Acebes M, Dalla E, Leader AM, LeBerichel J, Nikolic J, Morales BM, et al. Tissue-resident macrophages provide a pro-tumorigenic niche to early NSCLC cells. Nature. 2021;595(7868):578-84.

80. Zhu R, Huang J, Qian F. The role of tumor-associated macrophages in lung cancer. Front Immunol. 2025;16:1556209.

81. DeNardo DG, Ruffell B. Macrophages as regulators of tumour immunity and immunotherapy. Nat Rev Immunol. 2019;19(6):369-82.

82. Lu CS, Shiau AL, Su BH, Hsu TS, Wang CT, Su YC, et al. Oct4 promotes M2 macrophage polarization through upregulation of macrophage colony-stimulating factor in lung cancer. J Hematol Oncol. 2020;13(1):62.

83. Xu R, Li Y, Yan H, Zhang E, Huang X, Chen Q, et al. CCL2 promotes macrophages-associated chemoresistance via MCPIP1 dual catalytic activities in multiple myeloma. Cell Death Dis. 2019;10(10):781.

84. Fridlender ZG, Kapoor V, Buchlis G, Cheng G, Sun J, Wang LC, et al. Monocyte chemoattractant protein-1 blockade inhibits lung cancer tumor growth by altering macrophage phenotype and activating CD8+ cells. Am J Respir Cell Mol Biol. 2011;44(2):230-7.

85. Gao J, Liang Y, Wang L. Shaping Polarization Of Tumor-Associated Macrophages In Cancer Immunotherapy. Front Immunol. 2022;13:888713.

86. Hong DS, Postow M, Chmielowski B, Sullivan R, Patnaik A, Cohen EEW, et al. Eganelisib, a First-in-Class PI3Kgamma Inhibitor, in Patients with Advanced Solid Tumors: Results of the Phase 1/1b MARIO-1 Trial. Clin Cancer Res. 2023;29(12):2210-9.

87. Mognol GP, Ghebremedhin A, Varner JA. Targeting PI3Kgamma in cancer. Trends Cancer. 2025;11(5):462-74.

88. Evans CA, Liu T, Lescarbeau A, Nair SJ, Grenier L, Pradeilles JA, et al. Discovery of a Selective Phosphoinositide-3-Kinase (PI3K)-gamma Inhibitor (IPI-549) as an Immuno-Oncology Clinical Candidate. ACS Med Chem Lett. 2016;7(9):862-7.

89. Puschel F, Favaro F, Redondo-Pedraza J, Lucendo E, Iurlaro R, Marchetti S, et al. Starvation and antimetabolic therapy promote cytokine release and recruitment of immune cells. Proc Natl Acad Sci U S A. 2020;117(18):9932-41.

90. Noonepalle SKR, Gracia-Hernandez M, Aghdam N, Berrigan M, Coulibaly H, Li X, et al. Cell therapy using ex vivo reprogrammed macrophages enhances antitumor immune responses in melanoma. J Exp Clin Cancer Res. 2024;43(1):263.

91. Scolaro T, Manco M, Pecqueux M, Amorim R, Trotta R, Van Acker HH, et al. Nucleotide metabolism in cancer cells fuels a UDP-driven macrophage cross-talk, promoting immunosuppression and immunotherapy resistance. Nat Cancer. 2024;5(8):1206-26.

92. Lavin Y, Merad M. Macrophages: gatekeepers of tissue integrity. Cancer Immunol Res. 2013;1(4):201-9.

93. Lavin Y, Winter D, Blecher-Gonen R, David E, Keren-Shaul H, Merad M, et al. Tissue-resident macrophage enhancer landscapes are shaped by the local microenvironment. Cell. 2014;159(6):1312-26.

94. Kelly B, O'Neill LA. Metabolic reprogramming in macrophages and dendritic cells in innate immunity. Cell Res. 2015;25(7):771-84.

95. Corcoran SE, O'Neill LA. HIF1alpha and metabolic reprogramming in inflammation. J Clin Invest. 2016;126(10):3699-707.

96. Tannahill GM, Curtis AM, Adamik J, Palsson-McDermott EM, McGettrick AF, Goel G, et al. Succinate is an inflammatory signal that induces IL-1beta through HIF-1alpha. Nature. 2013;496(7444):238-42.

97. Mills EL, Kelly B, Logan A, Costa ASH, Varma M, Bryant CE, et al. Succinate Dehydrogenase Supports Metabolic Repurposing of Mitochondria to Drive Inflammatory Macrophages. Cell. 2016;167(2):457-70 e13.

98. Vats D, Mukundan L, Odegaard JI, Zhang L, Smith KL, Morel CR, et al. Oxidative metabolism and PGC-1beta attenuate macrophage-mediated inflammation. Cell Metab. 2006;4(1):13-24.

99. Huang SC, Everts B, Ivanova Y, O'Sullivan D, Nascimento M, Smith AM, et al. Cell-intrinsic lysosomal lipolysis is essential for alternative activation of macrophages. Nat Immunol. 2014;15(9):846-55.

100. Vander Heiden MG, Cantley LC, Thompson CB. Understanding the Warburg Effect: The Metabolic Requirements of Cell Proliferation. Science. 2009;324(5930):1029-33.

101. Kieler M, Hofmann M, Schabbauer G. More than just protein building blocks: how amino acids and related metabolic pathways fuel macrophage polarization. FEBS J. 2021;288(12):3694-714.

102. Oren R, Farnham AE, Saito K, Milofsky E, Karnovsky ML. Metabolic patterns in three types of phagocytizing cells. Journal of Cell Biology. 1963;17(3):487-501.

103. Newsholme P, Curi R, Gordon S, Newsholme EA. Metabolism of glucose, glutamine, long-chain fatty acids and ketone bodies by murine macrophages. Biochemical Journal. 1986;239(1):121-5.

104. O'Neill LA, Hardie DG. Metabolism of inflammation limited by AMPK and pseudo-starvation. Nature. 2013;493(7432):346-55.

105. Liu PS, Wang H, Li X, Chao T, Teav T, Christen S, et al. alpha-ketoglutarate orchestrates macrophage activation through metabolic and epigenetic reprogramming. Nat Immunol. 2017;18(9):985-94.

106. Geeraerts X, Fernandez-Garcia J, Hartmann FJ, de Goede KE, Martens L, Elkrim Y, et al. Macrophages are metabolically heterogeneous within the tumor microenvironment. Cell Rep. 2021;37(13):110171.

107. Diskin C, Palsson-McDermott EM. Metabolic Modulation in Macrophage Effector Function. Front Immunol. 2018;9:270.

108. Palmieri EM, Menga A, Martin-Perez R, Quinto A, Riera-Domingo C, De Tullio G, et al. Pharmacologic or Genetic Targeting of Glutamine Synthetase Skews Macrophages toward an M1-like Phenotype and Inhibits Tumor Metastasis. Cell Rep. 2017;20(7):1654-66.

109. Noe JT, Rendon BE, Geller AE, Conroy LR, Morrissey SM, Young LEA, et al. Lactate supports a metabolic-epigenetic link in macrophage polarization. Science Advances. 2021;7(46).

110. Smolle E, Leko P, Stacher-Priehse E, Brcic L, El-Heliebi A, Hofmann L, et al. Distribution and prognostic significance of gluconeogenesis and glycolysis in lung cancer. Mol Oncol. 2020;14(11):2853-67.

111. Mendez-Lucas A, Hyrossova P, Novellasdemunt L, Vinals F, Perales JC. Mitochondrial phosphoenolpyruvate carboxykinase (PEPCK-M) is a pro-survival, endoplasmic reticulum (ER) stress response gene involved in tumor cell adaptation to nutrient availability. J Biol Chem. 2014;289(32):22090-102.

112. Rittchen S, Jandl K, Lanz I, Reiter B, Ferreiros N, Kratz D, et al. Monocytes and Macrophages Serve as Potent Prostaglandin D(2) Sources during Acute, Non-Allergic Pulmonary Inflammation. Int J Mol Sci. 2021;22(21).

113. Hartnell A, Heinemann A, Conroy DM, Wait R, Sturm GJ, Caversaccio M, et al. Identification of selective basophil chemoattractants in human nasal polyps as insulin-like growth factor-1 and insulin-like growth factor-2. J Immunol. 2004;173(10):6448-57.

114. Kueh AJ, Herold MJ. Using CRISPR/Cas9 Technology for Manipulating Cell Death Regulators. Methods Mol Biol. 2016;1419:253-64.

115. Aubrey BJ, Kelly GL, Kueh AJ, Brennan MS, O'Connor L, Milla L, et al. An inducible lentiviral guide RNA platform enables the identification of tumor-essential genes and tumor-promoting mutations in vivo. Cell Rep. 2015;10(8):1422-32.

116. De Jesus A, Pusec CM, Nguyen T, Keyhani-Nejad F, Gao P, Weinberg SE, et al. Optimized protocol to isolate primary mouse peritoneal macrophage metabolites. STAR Protoc. 2022;3(4):101668.

117. Lorendeau D, Rinaldi G, Boon R, Spincemaille P, Metzger K, Jager C, et al. Dual loss of succinate dehydrogenase (SDH) and complex I activity is necessary to recapitulate the metabolic phenotype of SDH mutant tumors. Metab Eng. 2017;43(Pt B):187-97.

118. Millard P, Delepine B, Guionnet M, Heuillet M, Bellvert F, Letisse F. IsoCor: isotope correction for high-resolution MS labeling experiments. Bioinformatics. 2019;35(21):4484-7.

119. Matyash V, Liebisch G, Kurzchalia TV, Shevchenko A, Schwudke D. Lipid extraction by methyl-tert-butyl ether for high-throughput lipidomics. J Lipid Res. 2008;49(5):1137-46.

120. Triebl A, Hartler J, Trotzmuller M, H CK. Lipidomics: Prospects from a technological perspective. Biochim Biophys Acta Mol Cell Biol Lipids. 2017;1862(8):740-6.

121. Hartler J, Trotzmuller M, Chitraju C, Spener F, Kofeler HC, Thallinger GG. Lipid Data Analyzer: unattended identification and quantitation of lipids in LC-MS data. Bioinformatics. 2011;27(4):572-7.

122. Hartler J, Triebl A, Ziegl A, Trotzmuller M, Rechberger GN, Zeleznik OA, et al. Deciphering lipid structures based on platform-independent decision rules. Nat Methods. 2017;14(12):1171-4.

123. Stark R, Pasquel F, Turcu A, Pongratz RL, Roden M, Cline GW, et al. Phosphoenolpyruvate cycling via mitochondrial phosphoenolpyruvate carboxykinase links anaplerosis and mitochondrial GTP with insulin secretion. J Biol Chem. 2009;284(39):26578-90.

124. Salcher S, Sturm G, Horvath L, Untergasser G, Kuempers C, Fotakis G, et al. High-resolution single-cell atlas reveals diversity and plasticity of tissue-resident neutrophils in non-small cell lung cancer. Cancer Cell. 2022;40(12):1503-20 e8.

125. Hao Y, Stuart T, Kowalski MH, Choudhary S, Hoffman P, Hartman A, et al. Dictionary learning for integrative, multimodal and scalable single-cell analysis. Nat Biotechnol. 2024;42(2):293-304.

126. Gu Z, Eils R, Schlesner M. Complex heatmaps reveal patterns and correlations in multidimensional genomic data. Bioinformatics. 2016;32(18):2847-9.

127. Park EK, Jung HS, Yang HI, Yoo MC, Kim C, Kim KS. Optimized THP-1 differentiation is required for the detection of responses to weak stimuli. Inflamm Res. 2007;56(1):45-50.

128. Lauterbach MA, Hanke JE, Serefidou M, Mangan MSJ, Kolbe CC, Hess T, et al. Toll-like Receptor Signaling Rewires Macrophage Metabolism and Promotes Histone Acetylation via ATP-Citrate Lyase. Immunity. 2019;51(6):997-1011 e7.

129. Sadiku P, Willson JA, Ryan EM, Sammut D, Coelho P, Watts ER, et al. Neutrophils Fuel Effective Immune Responses through Gluconeogenesis and Glycogenesis. Cell Metab. 2021;33(2):411-23 e4.

130. Chandel NS. Navigating metabolism. Cold Spring Harbor, New York: Cold Spring Harbor Laboratory Press; 2015.

131. Stark R, Kibbey RG. The mitochondrial isoform of phosphoenolpyruvate carboxykinase (PEPCK-M) and glucose homeostasis: has it been overlooked? Biochim Biophys Acta. 2014;1840(4):1313-30.

132. Inigo M, Deja S, Burgess SC. Ins and Outs of the TCA Cycle: The Central Role of Anaplerosis. Annu Rev Nutr. 2021;41:19-47.

133. Marelli G, Morina N, Portale F, Pandini M, Iovino M, Di Conza G, et al. Lipid-loaded macrophages as new therapeutic target in cancer. J Immunother Cancer. 2022;10(7).

134. Masetti M, Carriero R, Portale F, Marelli G, Morina N, Pandini M, et al. Lipid-loaded tumor-associated macrophages sustain tumor growth and invasiveness in prostate cancer. J Exp Med. 2022;219(2).

135. O'Neill LA, Kishton RJ, Rathmell J. A guide to immunometabolism for immunologists. Nat Rev Immunol. 2016;16(9):553-65.

136. Qin X, Qiu C, Zhao L. Lysophosphatidylcholine perpetuates macrophage polarization toward classically activated phenotype in inflammation. Cell Immunol. 2014;289(1-2):185-90.

137. Palombo R, Passacantilli I, Terracciano F, Capone A, Matteocci A, Tournier S, et al. Inhibition of the PI3K/AKT/mTOR signaling promotes an M1 macrophage switch by repressing the ATF3-CXCL8 axis in Ewing sarcoma. Cancer Lett. 2023;555:216042.

138. Chen S, Chen L, Ye L, Jiang Y, Li Q, Zhang H, et al. PP2A-mTOR-p70S6K/4E-BP1 axis regulates M1 polarization of pulmonary macrophages and promotes ambient particulate matter induced mouse lung injury. J Hazard Mater. 2022;424(Pt C):127624.

139. Byles V, Covarrubias AJ, Ben-Sahra I, Lamming DW, Sabatini DM, Manning BD, et al. The TSC-mTOR pathway regulates macrophage polarization. Nat Commun. 2013;4:2834.

140. Yang F, Liu Y, Ren H, Zhou G, Yuan X, Shi X. ER-stress regulates macrophage polarization through pancreatic EIF-2alpha kinase. Cell Immunol. 2019;336:40-7.

141. Dong H, Feng Y, Yang Y, Hu Y, Jia Y, Yang S, et al. A Novel Function of Mitochondrial Phosphoenolpyruvate Carboxykinase as a Regulator of Inflammatory Response in Kupffer Cells. Front Cell Dev Biol. 2021;9:726931.

142. Ko CW, Counihan D, Wu J, Hatzoglou M, Puchowicz MA, Croniger CM. Macrophages with a deletion of the phosphoenolpyruvate carboxykinase 1 (Pck1) gene have a more proinflammatory phenotype. J Biol Chem. 2018;293(9):3399-409.

143. Fan TW, Daneshmandi S, Cassel TA, Uddin MB, Sledziona J, Thompson PT, et al. Polarization and beta-Glucan Reprogram Immunomodulatory Metabolism in Human Macrophages and Ex Vivo in Human Lung Cancer Tissues. J Immunol. 2022;209(9):1674-90.

144. Jeroundi N, Roy C, Basset L, Pignon P, Preisser L, Blanchard S, et al. Glycogenesis and glyconeogenesis from glutamine, lactate and glycerol support human macrophage functions. EMBO Rep. 2024.

145. Burke KP, Chaudhri A, Freeman GJ, Sharpe AH. The B7:CD28 family and friends: Unraveling coinhibitory interactions. Immunity. 2024;57(2):223-44.

146. Jantsch J, Chakravortty D, Turza N, Prechtel AT, Buchholz B, Gerlach RG, et al. Hypoxia and hypoxia-inducible factor-1 alpha modulate lipopolysaccharide-induced dendritic cell activation and function. J Immunol. 2008;180(7):4697-705.

147. Buescher JM, Antoniewicz MR, Boros LG, Burgess SC, Brunengraber H, Clish CB, et al. A roadmap for interpreting (13)C metabolite labeling patterns from cells. Curr Opin Biotechnol. 2015;34:189-201.

148. Vecchio E, Caiazza C, Mimmi S, Avagliano A, Iaccino E, Brusco T, et al. Metabolites Profiling of Melanoma Interstitial Fluids Reveals Uridine Diphosphate as Potent Immune Modulator Capable of Limiting Tumor Growth. Front Cell Dev Biol. 2021;9:730726.

149. Vincent EE, Sergushichev A, Griss T, Gingras MC, Samborska B, Ntimbane T, et al. Mitochondrial Phosphoenolpyruvate Carboxykinase Regulates Metabolic Adaptation and Enables Glucose-Independent Tumor Growth. Mol Cell. 2015;60(2):195-207.